UNIVERSIDADE DA BEIRA INTERIOR
Engenharia

Robust Controller Design for an Autonomous Underwater Vehicle

Carlos Hugo Ribeiro Mendes

Dissertação para obtenção do Grau de Mestre em
Engenharia Aeronáutica
(Ciclo de estudos integrado)

Orientador: Prof. Doutor Kouamana Bousson

Covilhã, Outubro de 2017

Dedication

To my parents for all the support and dedication.

”A dream is your creative vision for your life in the future. You must break out of your current comfort zone and become comfortable with the unfamiliar and the unknown.”

-Denis Waitley

Acknowledgments

First and foremost, I would like to thank my supervisor, Professor Kouamana Bousson, for providing me guidance and support throughout this work.

I would like to express my deep gratitude to both of my co-supervisors, Tiago Rebelo and Cristiano Bentes, and all the engineers at CEiiA, who provided outstanding support during my Internship at CEiiA.

My special thanks to my parents, Carlos and Maria, to my brothers, Cátia and Pedro, and to my girlfriend, Mafalda, for the unconditional love, patience and support.

Finally, thank to my friends who kept me sane during periods of great frustration.

Resumo

É visível, a nível mundial, um aumento considerável do interesse em Veículos Autónomos Subaquáticos (*Autonomous Underwater Vehicles* - AUV). O que torna esta tecnologia tão atraente é a capacidade de operar sem intervenção humana. Contudo, a ausência do ser humano restringe a operação do AUV ao seu sistema de controlo, computação e capacidades de detecção.
Desta forma, conceber um controlo robusto é obrigatório para viabilizar o AUV.

Motivado por este facto, esta tese tem como objetivo apresentar, discutir e avaliar duas soluções de controlo linear, a propor a um AUV desenvolvido por um consórcio liderado pelo CEiiA. Para que o projeto do controlador seja possível, o modelo dinâmico deste veículo e respectivas considerações são primeiramente abordados.

Com a finalidade de possibilitar a operação do veículo, torna-se essencial a elaboração de leis de *guidance* adequadas. Para este efeito são apresentados algorítmos de *Waypoint following* e *Station keeping*, e de *path following*.

Para a projeção dos controladores é derivada uma versão linear do modelo dinâmico, considerando um único ponto operacional. Através da separação do modelo linear em três subsistemas são criados quatro controladores Proporcional Integral Derivativo (PID) para cada grau de liberdade (*Degree Of Freedom* - DOF) do veículo. É também projetado um Regulador Linear Quadrático (LQR), baseado na separação do modelo linear em dois subsistemas, longitudinal e lateral. É ainda apresentada uma lei de alocação de controlo para distribuir o sinal de saída dos controladores pelos diferentes atuadores. Esta provou melhorar a manobrabilidade do veículo. Os resultados finais apresentam um desempenho sólido para ambos os métodos de controlo. No entanto, neste trabalho, o LQR provou ser mais rápido do que o PID.

Palavras-chave

Veículo Autónomo Subaquático; Controlo Robusto; Proportional Integral Derivativo (PID); Regulador Linear Quadrático (LQR); Simulação.

Abstract

Worldwide there has been a surge of interest in Autonomous Underwater Vehicles (AUV). The ability to operate without human intervention is what makes this technology so appealing. On the other hand, the absence of the human narrows the AUV operation to its control system, computing, and sensing capabilities. Therefore, devising a robust control is mandatory to allow the feasibility of the AUV.

Motivated by this fact, this thesis aims to present, discuss and evaluate two linear control solutions being proposed for an AUV developed by a consortium led by CEiiA. To allow the controller design, the dynamic model of this vehicle and respective considerations are firstly addressed.

Since the purpose is to enable the vehicle's operation, devising suitable guidance laws becomes essential. A simple waypoint following and station keeping algorithm, and a path following algorithms are presented.

To devise the controllers, a linear version of the dynamic model is derived considering a single operational point. Then, through the decoupling of the linear system into three lightly interactive subsystems, four Proportional Integral Derivative controllers (PIDs) are devised for each Degree Of Freedom (DOF) of the vehicle. A Linear Quadratic Regulator (LQR) design, based on the decoupling of the linear model into longitudinal and lateral subsystems is also devised. To allocate the controller output throughout the actuators, a control allocation law is devised, which improves maneuverability of the vehicle. The results present a solid performance for both control methods, however, in this work, LQR proved to be slightly faster than PID.

Keywords

Autonomous Underwater Vehicle; Robust Control; Proportional Derivative Integral Derivative (PID); Linear Quadratic Regulator (LQR); Simulation.

Contents

List of Figures

List of Acronyms

AOSN	Autonomous Oceanographic Sampling System
AUV	Autonomous Underwater Vehicle
CEiiA	Centre of Engineering and Product Development
CFD	Computational Fluid Dynamics
COA	Circle Of Acceptance
DOF	Degree-of-Freedom
DSV	Deep Submersible Vehicle
DVL	Doppler Velocity Log
EMEPC	Estrutura de Missão para a Extensão da Plataforma Continental
GNC	Guidance, Navigation and Control
HOSM	High Order Sliding Mode
INS	Inertial Navigation System
IMU	inertial measurement units
LHP	Left Half Plane
LOS	Line Of Sight
LQG	Linear Quadratic Gaussian
LQR	Linear Quadratic Regulator
LOS	Line Of Sight
LTI	Linear Time Invariant
MIMO	Multiple Input Multiple Output
NED	North-East-Down
NN	Neural Networks
ODEs	ordinary differential Equations
PID	Proportional Integral Derivative
POC	Proof Of Concepts
RHP	Right Half Plane
ROV	Remotely Operated Vehicle
SISO	Single Input Single Output
SNAME	Society of Naval Architects and Marine Engineers
SMC	Sliding Mode Control
SPURV	Self-Propelled Underwater Research Vehicle
TTT	Time To Targe
UBI	University of Beira Interior
UUV	Unmanned Underwater Vehicle

Nomenclature

0_b	Origin of the body-fixed frame
0_n	Origin of the inertial frame
$\{b\}$	Body frame
$\{n\}$	Inertial frame
A_L	Longitudinal system matrix
A_{L_a}	Longitudinal system matrix with integral states
A_H	Lateral system matrix
B	Buoyancy force
B_H	Input Lateral matrix
B_L	Input Longitudinal matrix
B_{L_a}	Input Longitudinal matrix with integral states
C_A	Coriolis and centripetal effects due to added mass
C_{RB}	Coriolis and centripetal forces acting on the rigid body
D	Hydrodynamic damping matrix
d_k	Planar (xy) distance to the waypoint
d_u	Complementary planar distance (xy) to the waypoint
e_z	Depth error
f_B^b	Buoyancy force vector in the body fixed frame
f_B^n	Buoyancy force vector in the inertial frame
f_g^b	Gravitational force vector in the body fixed frame
f_g^n	Gravitational force vector in the inertial frame
g	Restoring force vector
I_b	Body's Inertia tensor
J	Transformation matrix
K	Torque applied to vehicle along the x axis
k_u	Upper limit of the reference surge speed
k_w	Upper limit of the reference heave speed
L	Mapping matrix
M	Torque applied to vehicle along the y axis
M_A	Added mass matrix
M_RB	Rigid body inertia matrix
N	Torque applied to vehicle along the z axis
Q_{La}	Longitudinal state weighting matrix
Q_H	Lateral state weighting matrix
r_B^b	Centre of buoyancy vector with respect to body fixed frame
R_b^n	Rotation Matrix for converting linear velocities from body to inertial coordinates
r_g^b	Centre of gravity vector with respect to body fixed frame
R_H	Input Lateral matrix
R_{La}	Longitudinal control weighting matrix
S	Skew-symmetric matrix
s	Along the track distance

T	Transformation Matrix for converting angular velocities from body to inertial coordinates
U	Control vector
u	Surge
u_{cmI}	Lower limit of the transitional speed for vertical common mode
u_{cmS}	Upper limit of the transitional speed for vertical common mode
u_d	Desired surge speed
u_{dmI}	Lower limit of the transitional speed for vertical differential mode
u_{dmS}	Upper limit of the transitional speed for vertical differential mode
v	Sway
W	Weight
w	Heave
W_{cm}	Weight of the vertical common mode
w_d	Desired heave speed
W_{dm}	Weight of the vertical differential mode
X	Force applied to vehicle along the x axis
x	Position along the x axis
x_b	x-coordinate of the body-fixed frame
x_k	x-coordinate of the waypoint k
x_n	x-coordinate of the inertial reference frame
Y	Force applied to vehicle along the y axis
y	Position along the y axis
y_b	y-coordinate of the body-fixed frame
y_k	y-coordinate of the waypoint k
y_n	y-coordinate of the inertial reference frame
Z	Force applied to vehicle along the z axis
z	Position along the z axis
z_b	z-coordinate of the body-fixed frame
z_k	z-coordinate of the waypoint k
z_n	z-coordinate of the inertial reference frame

Greek Letters

α	Angle of attack
β	Side-slip angle
Δ	Lookahead distance
ε_z	Acceptance depth error
η	Position and Euler angles vector
θ	Pitch Euler angle
Θ_{nb}	Euler Attitude vector
θ_r	Reference pitch angle
ν	Linear and angular velocities vector
ρ_{cm}	Steepness of the transitional speed for common mode
ρ_{dm}	Steepness of the transitional speed for differential mode
ρ_k	Radius of the Waypoint's planar (xy) Circle Of Acceptance
ρ_u	Radius of surge's Circle Of Acceptance

τ	Force and Torque state vector
τ_A	Vector due to hydrodynamic added mass
τ_{rb}	Vector of external forces and moments about the origin acting as an input to the rigid body
ϕ	Roll Euler angle
ψ_{LA}	Lookahead reference angle
ψ_r	Yaw reference angle

Chapter 1

Introduction

The ocean plays a significant role in the human life. It is the central engine of energy and chemical balance that sustains humanity [1]. The ability to understand and to predict the ocean depends upon our ability to understand the processes within it. However, the rough environment is the biggest stumbling block in the ocean's data acquisition.

The first knowledge of the oceans came from a direct observation made from vessels, later airplanes, and finally from instruments placed in the water. However, these techniques only work on the surface [1], which falls short of what underwater exploration is all about. According to Steinar Ellefmo [2]: *"There are large unexplored ocean areas, and there is an enormous amount we do not know about them. We actually know more about the moon than the seafloor"*. Underwater vehicles (UV) are perfect for the job since they provide a window to the oceans' deep secrets. Figure 1.1 divides UVs into two categories: manned vehicles and Unmanned Underwater Vehicle (UUV). UUVs are subdivided in Remotely Operated Vehicles (ROVs), Autonomous Underwater Vehicles (AUVs), and hybrid vehicles, which can be autonomous or remotely operated [3].

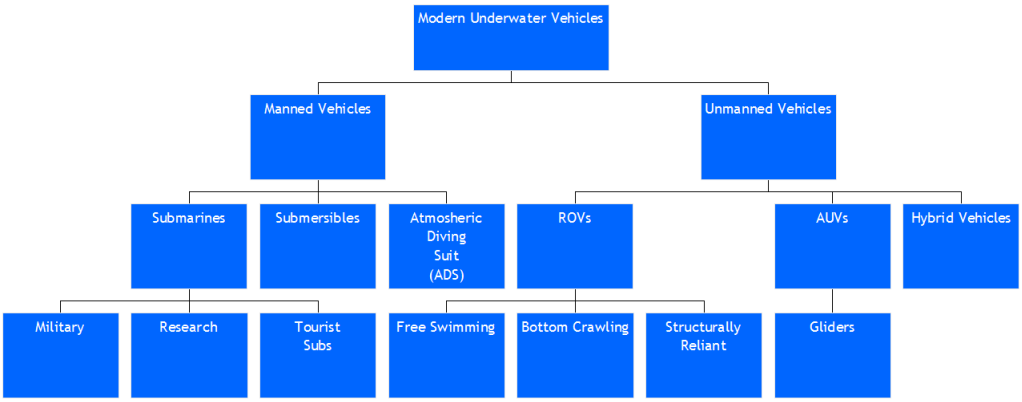

Figure 1.1: Underwater vehicle class division.

Manned underwater vehicles are human occupied, and despite the ability to perform complex missions, they are still limited to low endurance, due to human physical and psychological limitation. Doing an analogy with space exploration, citing Mark Henderson: *"Human beings are poorly designed for the job. They need food, water and oxygen (...) Mechanical probes have none of these shortcomings. They can fly further and faster(...)* " [4].

Remotely operated vehicles are tethered vehicles that draw power from the surface vessel and, as the name suggests, are remotely operated. They are used for routine inspection and maintenance tasks. However, the operation range is limited by the size of the umbilical cable, and as the cable size rises the drag upon itself and the signal delay increases as well, making it difficult to maneuver, requiring a skilled pilot for the task [1].

In contrast, autonomous underwater vehicles are systems that carry their power supplies and are fully autonomous, releasing the vehicle from the surface vessel and therefore eliminating the costly handling gear, which a tether entails. However, the absence of a human operator narrows AUV operations to its control system, computing, and sensing capabilities. Robustness in control is mandatory to allow the feasibility of such tool [5].

The AUV concept started to be studied in the 60s [6]. The SPURV, Self-Propelled Underwater Research Vehicle, developed at the University of Washington, is the first reported AUV [7]. In the following decades (1970 to 2000) advances outside the AUV community greatly affected the AUV development [6]. The small low-power computers enabled the guidance and control algorithms implementation on autonomous platforms. Proof Of Concepts (POC) prototypes were tested and evolved to the first generation of operational systems able to accomplish predefined objectives. Autonomous Oceanographic Sampling System (AOSN) is an example of that [8]. In this decade, the AUV technology commercialization is becoming a near reality [6]. Currently, there are different solutions for different applications. Marport's AUV *SQX-500*, *Girona 500* from University Of Girona Center for Research Underwater Robotics (figure 1.2) and SeaBED from Woods Hole Oceanographic Institution (figure 1.3) are examples of multiple body AUVs.

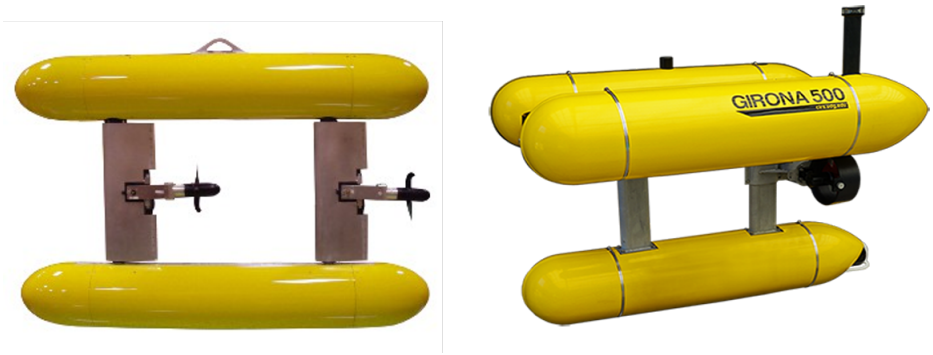

Figure 1.2: SQX-500 AUV (left) and Girona 500 AUV (right) (adapted from [9][9]).

Figure 1.3: Seabed AUV (adapted from [9]).

In May 2009, Portugal submitted a proposal to the United Nations to expand the continental shelf beyond the 200 nautical miles from the coastline [10]. Having tools for exploration and monitoring is therefore essential. In that sense, CEiiA (Centre of Engineering and Product Development), in collaboration with other partners, preceding actual and forthcoming demands,

started to develop an AUV [11].

1.1 The AUV

CEiiA is a non-profit organization, located in Porto, Portugal. In September 2015, a consortium led by CEiiA started the development of a lightweight AUV (figure 1.4) with the main goal to reinforce the national capacity for mobile autonomous deep-sea exploration and monitoring [11]. Capable of a NDD[1] of 3000 meters, the AUV follows a double-hull configuration.

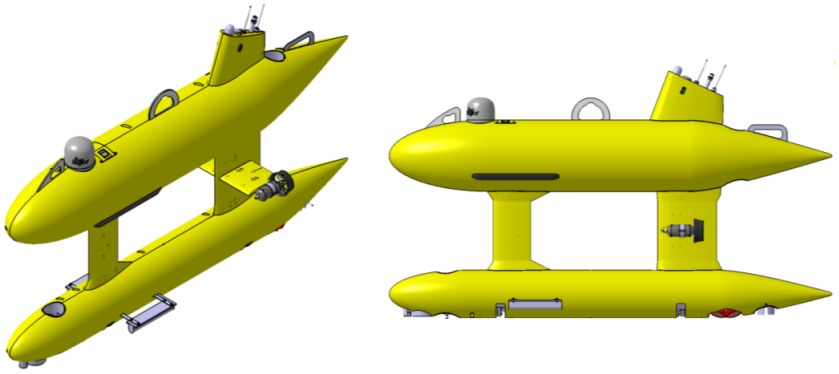

Figure 1.4: 3D model of the developed AUV at CEiiA (courtesy of CEiiA).

Payload

The vehicle's payload is distributed by both hulls. The batteries are on the lower hull and the necessary dry systems and sensors on the upper hull. For the purpose of navigation, the AUV is equipped with the following sensors:

- *Depth Cell* - This system allows the determination of the vehicle's depth, based on pressure values;
- *Doppler Velocity Log* (DVL) - This device uses the Doppler principle [13] to determine the velocity of the vehicle;
- *Magnetometer* - This device determines the magnetic north;
- *Inertial Navigation System* (INS) - Through inertial measurement units (IMU), *accelerometers* and *gyroscopes*, this system calculates the current position, with the knowledge of the initial position;
- *Underwater Altimeter* - This device sends acoustic signals towards seafloor, and captures the "reflected" signal. The time between measurements, and knowing the speed of sound in water, the vehicle altitude is calculated.

For the propulsive system, the AUV has four identical thrusters. Two are placed on the vertical plane and the other two on the horizontal plane. The vertical thrusters are located in both of the hulls: the forward thruster is embedded in the lower body and the aft thruster on the

[1] Nominal Diving Depth - the diving depth for the unrestricted operation of the submersible [m] [12].

upper. The horizontal thrusters, as can be seen in the figure 1.4, are located in the aft horizontal fairing.

Mission

According to [11], the system was mainly designed to comply with three missions scenarios:

1. Data download and water column profiling, figure 1.5;
2. Resource exploration and mapping, figure 1.6;
3. High resolution habitat mapping, figure 1.7.

With respect to operational scenario, the AUV mission is divided into:

1. *Dive* - In traditional submarines, the dive maneuver is accomplished through ballast tanks. By the ”in hail” of water, negative buoyancy is achieved, allowing the dive. For this AUV, these compartments do not exist, and the scenario of using the vertical thrusters to reach the depth goal is nonviable, concerning energetic consumption. Therefore, the AUV carries an extra mass in the bow, allowing the descending movement, with nose down attitude. By reaching the predefined operational depth, the extra mass is released, and the residual buoyancy is achieved. Through this stage, it is possible to accomplish mission scenario (1).
2. *Data acquisition* - During this stage, mission scenarios (2) and (3) can be performed.
3. *Ascent* - Although the residual buoyancy will always bring the AUV to the surface, and to avoid energy wasting to speed up the ascent, the AUV carries an extra mass in the stern. When the data acquisition is over, the mass is released and the ascent will begin. Given the fact that the center of buoyancy is aft the center of gravity, the ascent will happen with nose down attitude. Therefore, on the surface, the GPS, global positioning system, which is located in the upper hull’s vertical fin, is above the water line, ensuring the continuous position transmitting.

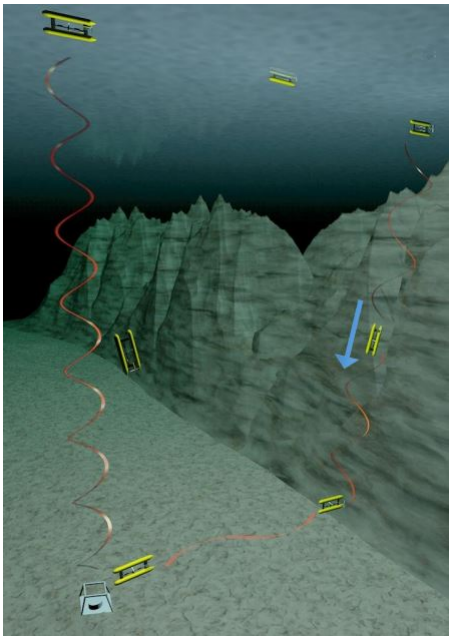

Figure 1.5: Ascent and descend scenario (courtesy of CEiiA).

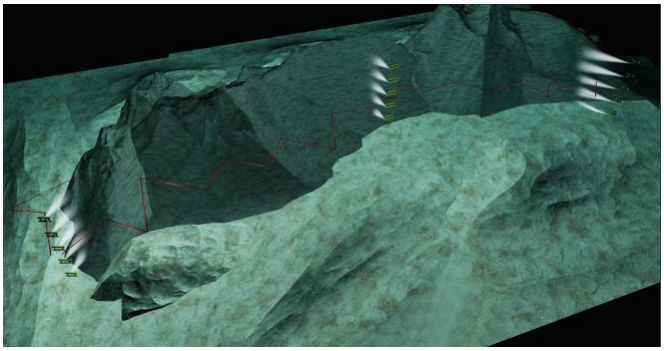

Figure 1.6: Resource exploration and mapping (courtesy of CEiiA).

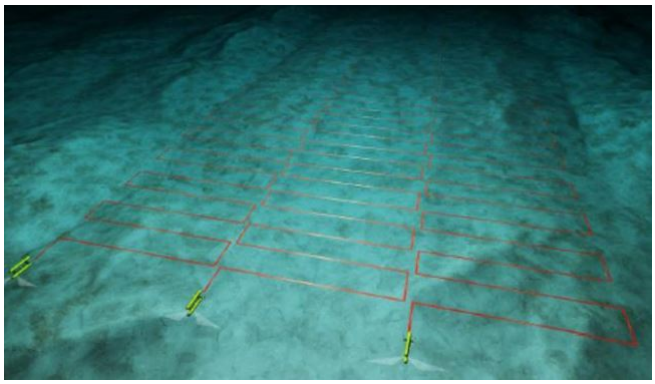

Figure 1.7: High resolution habitat mapping (courtesy of CEiiA).

1.2 AUV Motion Control Techniques Overview

1.2.1 Dynamics

The dynamic model is essential to design the motion control algorithms [14]. The dynamics can be divided into kinematics and kinetics [15]. A brief description will be hereby presented to introduce the general concepts of the AUV dynamic model.

1.2.1.1 Reference Frames and Terminology

To derive the equations of motion that describe the AUV kinematics, the definition of two reference frames is mandatory. The notation that will be used from now on is the one defined [16] by SNAME[2], with slight differences, as in [15].
As seen in figure 1.8, the chosen reference frames are:

- The body-fixed $\{b\}$, the non-inertial frame, composed by the axes $\{x_b,y_b,z_b\}$, and the 0_b is chosen, for simplicity, to coincide with the Center of Gravity (CG) of the AUV.
- The local NED (North-East-Down) $\{n\}$, the inertial reference frame, composed by the orthonormal axes $\{x_n,y_n,z_n\}$, the origin is represented by 0_n.

The CG and the Center of Buoyancy (CB), which is the hydrostatic buoyancy center, are defined with respect to the 0_b, and are represented by:

[2]Society of Naval Architects and Marine Engineers.

$$\mathbf{r}_g^b = \begin{bmatrix} x_g & y_g & z_g \end{bmatrix}^T ; \qquad \mathbf{r}_B^b = \begin{bmatrix} x_B & y_B & z_B \end{bmatrix}^T$$

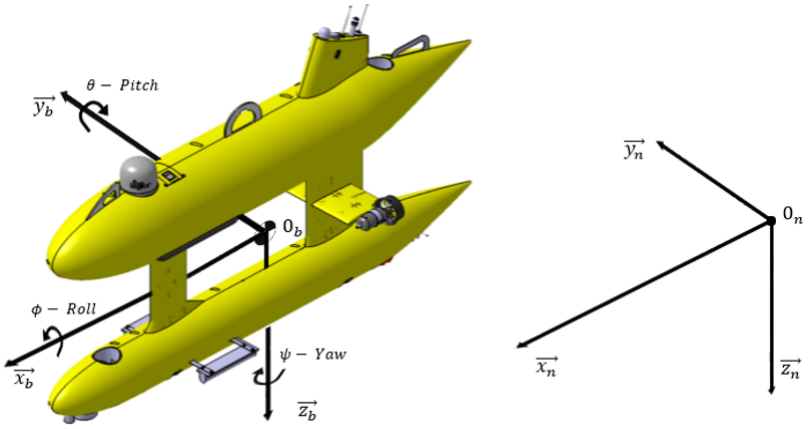

Figure 1.8: Body-fixed and local NED reference frames.

Therefore, to determine the position and orientation of the vehicle, six independent coordinates are needed, namely $(x, y, z, \phi, \theta, \psi)$, which are expressed in the inertial frame, $\{n\}$. For linear and angular velocity, the six coordinates are (u, v, w, p, q, r), and (X, Y, Z, K, M, N) for control forces/moments, both expressed in the non-inertial frame, $\{b\}$. The six motion components can be expressed as in table 1.1, or, in the vector form, as:

- η=$\begin{bmatrix} x & y & z & \phi & \theta & \psi \end{bmatrix}^T$ expressed in the $\{n\}$ frame;
- ν=$\begin{bmatrix} u & v & w & p & q & r \end{bmatrix}^T$ expressed in the $\{b\}$ frame;
- τ=$\begin{bmatrix} X & Y & Z & K & M & N \end{bmatrix}^T$ expressed in the $\{b\}$ frame.

Table 1.1: SNAME notation for underwater vehicles.

Terminology	*Forces and Moments*	*Linear and Angular Velocities*	*Position and Euler angles*
Motion along x_b direction (Surge)	*X*	*u*	*x*
Motion along y_b direction (Sway)	*Y*	*v*	*y*
Motion along z_b direction (Heave)	*Z*	*w*	*z*
Rotation along x_b axis (Roll)	*K*	*p*	ϕ
Rotation along y_b axis (Pitch)	*M*	*q*	θ
Rotation along z_b axis (Yaw)	*N*	*r*	ψ

1.2.1.2 Kinematic Equations

Kinematics deal with the geometrical aspects of motion and relates the velocities with positions [14]. To transform linear velocities from the body-fixed frame to the inertial coordinate frame, a transformation matrix, J, is defined, resulting in the kinematic equation [15]:

$$\dot{\eta} = J(\eta)\nu \quad (1.1)$$

where:

$$J(\eta) = \begin{bmatrix} R_b^n(\Theta_{nb}) & 0_{3\times3} \\ 0_{3\times3} & T_\Theta(\Theta_{nb}) \end{bmatrix} \quad (1.2)$$

where $R_b^n(\Theta_{nb})$ represents the rotation matrix that allows the linear velocity transformation, from b to n frame, and is defined by [15]:

$$R_b^n(\Theta_{nb}) = \begin{bmatrix} cos(\psi)cos(\theta) & cos(\psi)sin(\theta)sin(\phi) - sin(\psi)cos(\phi) & cos(\psi)sin(\theta)cos(\phi) + sin(\psi)sin(\phi) \\ sin(\psi)cos(\theta) & sin(\psi)sin(\theta)sin(\phi) + cos(\psi)cos(\phi) & sin(\psi)sin(\theta)cos(\phi) - cos(\psi)sin(\phi) \\ -sin(\theta) & cos(\theta)sin(\phi) & cos(\theta)cos(\phi) \end{bmatrix} \quad (1.3)$$

The $T_\Theta(\Theta_{nb})$ represents the Euler attitude transformation matrix and is defined as [15]:

$$T_\Theta(\Theta_{nb}) = \begin{bmatrix} 1 & sin(\phi)tan(\theta) & cos(\phi)tan(\theta) \\ 0 & cos(\phi) & -sin(\phi) \\ 0 & sin(\phi)/cos(\theta) & cos(\phi)/cos(\theta) \end{bmatrix} \quad (1.4)$$

Equation 1.4 produces a singularity in pitch, $\theta = \pm 90°$. Since the vehicle will operate at around $\theta_{max} \approx \pm 25°$, Euler representation can still be used. In alternative, the quaternion representation can be used, as shown in [17].

1.2.1.3 Kinetics

Rigid-Body Equations

Kinetics address the relationship between motion and forces. By applying Newton's law in the body-fixed frame $\{b\}$, it is possible to express the rigid-body equation as [15]:

$$M_{rb} \cdot \dot{\nu} + C_{rb}(\nu) \cdot \nu = \tau_{rb} \quad (1.5)$$

where M_{rb} represents the rigid-body mass matrix, C_{rb} the rigid-body Coriolis force, and τ_{rb} the external forces and moments action on the vehicle.
The rigid-body mass matrix is defined as [15]:

$$\begin{aligned} M_{rb} &= \begin{bmatrix} m \cdot I_{3\times 3} & -m \cdot S(r_g^b) \\ m \cdot S(r_g^b) & I_b \end{bmatrix} \\ &= \begin{bmatrix} m & 0 & 0 & 0 & m \cdot z_g & -m \cdot y_g \\ 0 & m & 0 & -m \cdot z_g & 0 & m \cdot x_g \\ 0 & 0 & m & m \cdot y_g & -m \cdot x_g & 0 \\ 0 & -m \cdot z_g & m \cdot y_g & I_x & -I_{xy} & -I_{xz} \\ m \cdot z_g & 0 & -m \cdot x_g & -I_{yx} & I_y & -I_{yz} \\ -m \cdot y_g & m \cdot x_g & 0 & -I_{zx} & -I_{zy} & I_z \end{bmatrix} \end{aligned} \quad (1.6)$$

where m is the mass of the vehicle, $I_{3\times 3}$ is a 3 x 3 identity matrix; $S(r_g^b)$ is the skew-symmetric matrix of r_g^b, which represents the location of the vehicle's CG, with respect to the body-fixed frame, ($r_g^b = [x_g \quad y_g \quad z_g]^T$); and I_b represents the body's inertia tensor.

The Coriolis and centripetal matrix, C_{rb}, is defined as [15]:

$$C_{rb}(\nu) = \begin{bmatrix} 0_{3\times3} & -m \cdot S(\nu_1) - m \cdot S(\nu_2) \cdot S(r_g^b) \\ m \cdot S(\nu_1) + m \cdot S(r_g^b) \cdot S(\nu_2) & -S(I_b \cdot \nu_2) \end{bmatrix}$$

$$= \begin{bmatrix} 0 & 0 & 0 \\ 0 & 0 & 0 \\ 0 & 0 & 0 \\ -m(y_g q + z_g r) & m(y_g p + w) & m(z_g p - v) \\ m(x_g q - w) & -m(z_g r + x_g p) & m(z_g q + u) \\ m(x_g r + v) & m(y_g r - u) & -m(x_g p + y_g q) \end{bmatrix} \quad (1.7)$$

$$\begin{bmatrix} m(y_g q + z_g r) & -m(x_g q - w) & -m(x_g r + v) \\ -m(y_g p + w) & m(z_g r + x_g p) & -m(y_g r - u) \\ -m(z_g p - v) & -m(z_g q + u) & m(x_g p + y_g q) \\ 0 & -I_{yz} q - I_{xz} p + I_z r & I_{yz} r + I_{xy} p - I_y q \\ I_{yz} q + I_{xz} p - I_z r & 0 & -I_{xz} r - I_{xy} q + I_x p \\ -I_{yz} r - I_{xy} p + I_y q & I_{xz} r + I_{xy} q - I_x p & 0 \end{bmatrix}$$

where $\nu_1 = [u \quad v \quad w]^T$, and $\nu_2 = [p \quad q \quad r]^T$.

The external forces and moments acting on the vehicle, τ_{rb}, can be decomposed in [14]:

$$\tau_{rb} = \tau + \tau_A + \tau_D + \tau_R \quad (1.8)$$

- τ - Vector of forces and torques created by the surfaces/thrusters. Usually treated as the control input, and defined as:

  $$\tau = L \cdot U \quad (1.9)$$

  where, L represents the mapping matrix and U the force vector representing the thrust of each thruster.

- τ_A - The vector due to the hydrodynamic *added mass*. In fluid mechanics, an accelerating or decelerating body must move some volume of the surrounding fluid with it. The mass representative of this volume is called the *added mass*. The added mass vector is defined as [15]:

  $$\tau_A = -M_A - C_A(\nu)\nu \quad (1.10)$$

  where M_A is the added mass matrix, expressed as [15]:

  $$M_A = -\begin{bmatrix} X_{\dot{u}} & X_{\dot{v}} & X_{\dot{w}} & X_{\dot{p}} & X_{\dot{q}} & X_{\dot{r}} \\ Y_{\dot{u}} & Y_{\dot{v}} & Y_{\dot{w}} & Y_{\dot{p}} & Y_{\dot{q}} & Y_{\dot{r}} \\ Z_{\dot{u}} & Z_{\dot{v}} & Z_{\dot{w}} & Z_{\dot{p}} & Z_{\dot{q}} & Z_{\dot{r}} \\ K_{\dot{u}} & K_{\dot{v}} & K_{\dot{w}} & K_{\dot{p}} & K_{\dot{q}} & K_{\dot{r}} \\ M_{\dot{u}} & M_{\dot{v}} & M_{\dot{w}} & M_{\dot{p}} & M_{\dot{q}} & M_{\dot{r}} \\ N_{\dot{u}} & N_{\dot{v}} & N_{\dot{w}} & N_{\dot{p}} & N_{\dot{q}} & N_{\dot{r}} \end{bmatrix} \quad (1.11)$$

  where, for example, the term $X_{\dot{u}}$ represents the hydrodynamic added mass force X along the x-axis due to an acceleration $\dot{u}$ in the x direction [16]. For the Coriolis and centripetal

forces due to added mass [15]:

$$C_A(\nu) = \begin{bmatrix} 0 & 0 & 0 & 0 & -a_3 & a_2 \\ 0 & 0 & 0 & a_3 & 0 & -a_1 \\ 0 & 0 & 0 & -a_2 & a_1 & 0 \\ 0 & -a_3 & a_2 & 0 & -b_3 & b_2 \\ a_3 & 0 & -a_1 & b_3 & 0 & -b_1 \\ -a_2 & a_1 & 0 & -b_2 & b_1 & 0 \end{bmatrix} \quad (1.12)$$

Where:

$$\begin{aligned} a_1 &= X_{\dot{u}}u + X_{\dot{v}}v + X_{\dot{w}}w + X_{\dot{p}}p + X_{\dot{q}}q + X_{\dot{r}}r \\ a_2 &= Y_{\dot{u}}u + Y_{\dot{v}}v + Y_{\dot{w}}w + Y_{\dot{p}}p + Y_{\dot{q}}q + Y_{\dot{r}}r \\ a_3 &= Z_{\dot{u}}u + Z_{\dot{v}}v + Z_{\dot{w}}w + Z_{\dot{p}}p + Z_{\dot{q}}q + Z_{\dot{r}}r \\ b_1 &= K_{\dot{u}}u + K_{\dot{v}}v + K_{\dot{w}}w + K_{\dot{p}}p + K_{\dot{q}}q + K_{\dot{r}}r \\ b_2 &= M_{\dot{u}}u + M_{\dot{v}}v + M_{\dot{w}}w + M_{\dot{p}}p + M_{\dot{q}}q + M_{\dot{r}}r \\ b_3 &= N_{\dot{u}}u + N_{\dot{v}}v + N_{\dot{w}}w + N_{\dot{p}}p + N_{\dot{q}}q + N_{\dot{r}}r \end{aligned}$$

- τ_D - The vector due to lift, drag, skin friction, etc; defined as [15]:

$$\tau_D = -D(\nu)\nu \quad (1.13)$$

with $D(\nu)$ being the hydrodynamic damping matrix. If moving with low speed, it is common to use a quadratic approximation [17]:

$$D(\nu) = D_l + D_q(\nu) \quad (1.14)$$

where:

$$D_l = \begin{bmatrix} X_u & X_v & X_w & X_p & X_q & X_r \\ Y_u & Y_v & Y_w & Y_p & Y_q & Y_r \\ Z_u & Z_v & Z_w & Z_p & Z_q & Z_r \\ K_u & K_v & K_w & K_p & K_q & K_r \\ M_u & M_v & M_w & M_p & M_q & M_r \\ N_u & N_v & N_w & N_p & N_q & N_r \end{bmatrix} \quad (1.15)$$

and:

$$D_q(\nu) = - \begin{bmatrix} X_{u|u|}\,|\,u\,| & X_{v|v|}\,|\,v\,| & X_{w|w|}\,|\,w\,| & X_{p|p|}\,|\,p\,| & X_{q|q|}\,|\,q\,| & X_{r|r|}\,|\,r\,| \\ Y_{u|u|}\,|\,u\,| & Y_{v|v|}\,|\,v\,| & Y_{w|w|}\,|\,w\,| & Y_{p|p|}\,|\,p\,| & Y_{q|q|}\,|\,q\,| & Y_{r|r|}\,|\,r\,| \\ Z_{u|u|}\,|\,u\,| & Z_{v|v|}\,|\,v\,| & Z_{w|w|}\,|\,w\,| & Z_{p|p|}\,|\,p\,| & Z_{q|q|}\,|\,q\,| & Z_{r|r|}\,|\,r\,| \\ K_{u|u|}\,|\,u\,| & K_{v|v|}\,|\,v\,| & K_{w|w|}\,|\,w\,| & K_{p|p|}\,|\,p\,| & K_{q|q|}\,|\,q\,| & K_{r|r|}\,|\,r\,| \\ M_{u|u|}\,|\,u\,| & M_{v|v|}\,|\,v\,| & M_{w|w|}\,|\,w\,| & M_{p|p|}\,|\,p\,| & M_{q|q|}\,|\,q\,| & M_{r|r|}\,|\,r\,| \\ N_{u|u|}\,|\,u\,| & N_{v|v|}\,|\,v\,| & N_{w|w|}\,|\,w\,| & N_{p|p|}\,|\,p\,| & N_{q|q|}\,|\,q\,| & N_{r|r|}\,|\,r\,| \end{bmatrix} \quad (1.16)$$

- τ_R - Represents the hydrostatic restoring force due to gravity and fluid density. According to [15], two forces are considered in the hydrostatics: the *buoyancy* force, f_B, which acts

upwards, on the CB, and the *gravitational* force, f_g, that acts downwards on the CG.

Archimedes' principle gives the buoyancy force, $B = \rho g \nabla$, where ρ is the density of the fluid, g the gravitational acceleration and ∇ the volume of fluid displaced by the vehicle [15]. In the $\{n\}$ frame:

$$f_B^n = \begin{bmatrix} 0 \\ 0 \\ -B \end{bmatrix} \quad (1.17)$$

The gravitational force is derived from the Newton's 2^{nd} law, $W = mg$, where m is the mass, and g the gravitational acceleration. In the $\{n\}$ frame [15]:

$$f_g^n = \begin{bmatrix} 0 \\ 0 \\ W \end{bmatrix} \quad (1.18)$$

For the $\{b\}$ frame:

$$f_B^b = R_b^n(\Theta_{nb})^{-1} f_B^n \quad (1.19)$$

$$f_g^b = R_b^n(\Theta_{nb})^{-1} f_g^n \quad (1.20)$$

The restoring force vector is equal to [15]:

$$\tau_R = -g(\eta) \quad (1.21)$$

And:

$$g(\eta) = -\begin{bmatrix} f_B^b + f_g^b \\ r_B^b f_B^b + r_g^b f_g^b \end{bmatrix} \quad (1.22)$$

Finally, expanding these equations will result in [15]:

$$\mathbf{g}(\eta) = \begin{bmatrix} (W-B)\sin(\theta) \\ -(W-B)\cos(\theta)\sin(\phi) \\ -(W-B)\cos(\theta)\cos(\phi) \\ -(y_g W - y_B B)\cos(\theta)\cos(\phi) + (z_g W - z_B B)\cos(\theta)\sin(\phi) \\ (z_g W - z_B B)\sin(\theta) + (x_g W - x_B B)\cos(\theta)\cos(\phi) \\ -(x_g W - x_B B)\cos(\theta)\sin(\phi) - (y_g W - y_B B)\sin(\theta) \end{bmatrix} \quad (1.23)$$

1.2.1.4 Complete Dynamic Model

By associating the kinematic and kinetic equations and expanding equation 1.8, the complete dynamic model is written as [15]:

$$M\dot{\nu} + C(\nu)\nu + D(\nu)\nu + g(\eta) = \tau \quad (1.24)$$

$$\dot{\eta} = J(\eta)\nu \quad (1.25)$$

Where $M = M_{rb} + M_A$ and $C = C_{rb} + C_A$.
The dynamic model can be conveniently arranged to the form $\dot{x} = f(x,t)$ as:

$$\dot{\nu} = M^{-1}[-(C(\nu)\nu + D(\nu)\nu - g(\eta) + \tau] \quad (1.26)$$

1.2.2 Motion Control

An autopilot for an AUV is a GNC, *Guidance*, *Navigation* and *Control*, system in its most basic form [15]. The communication sequence can be seen in the figure 1.9 [15].

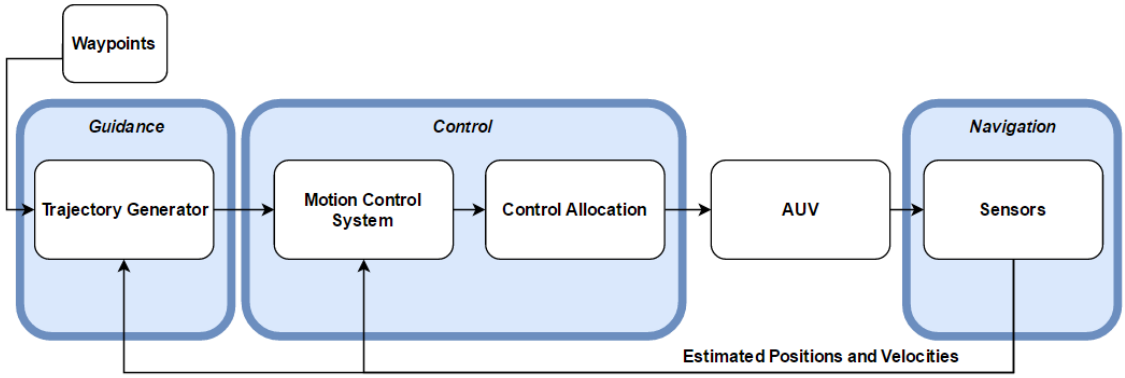

Figure 1.9: GNC signal flow diagram.

For proper operation, each block should work in accordance with the other. That means imperfections/errors in one will reduce the efficiency of the other [18]. Since the controller works on guidance data, developing a controller without addressing guidance may not be prudent. Therefore, both of these blocks are covered in this thesis, while navigation block is considered to provide all readings of the current state of the vehicle. A brief literature review was performed to assess the state-of-the-art in this matter.

1.2.2.1 Guidance

According to Fossen [15], guidance is the act of determining the course, attitude and speed of the vehicle, relative to some reference frame, to be followed by the vehicle.
It is the guidance system that decides the best trajectory to be followed by the vehicle, based on target location and vehicle's capabilities [18]. For a remotely operated vehicle, those references are sent from a human trained operator. However, for autonomous underwater vehicles, the guidance system plays a vital role in bringing autonomy to the system [18].

Among current solutions, waypoint guidance by Line Of Sight (LOS) is the most common approach for guidance in underwater vehicles [18]. In [19] an improved LOS law, which calculates an additional angle by taking into account AUV's current position and the next waypoint, is presented. Path following algorithms are also common solutions [15]. A three-dimensional path following algorithm is presented in [20] .

1.2.2.2 Control

This block is accountable for calculating the necessary forces and moments to achieve the *control objective* [15].
The AUV's dynamics is inherently nonlinear and time-variant. The uncertain external disturbances that the vehicle is subjected to make the AUV controller design task a very challenging one. Therefore, and with the growing need for advanced capabilities and features, a necessity for more capable control systems is mandatory [1].
Numerous control strategies have been developed, being possible to classify them into two main groups, *the linear methods* and *the nonlinear methods* [21].

- **Linear methods:** The linear theory has evolved over the years and powerful design tools, to meet control robustness and stability requirements, were developed. By linearizing the AUV dynamic equations, it is possible to make the control problem more tractable [22]. Despite the nonlinear environment, there are successfully implemented linear controllers in the nonlinear environment. Among the solutions, the most common two will be studied in this thesis.

    1. **PID (Proportional Integral Derivative) Controller:** As stated in [15], a state-of-the-art control system is designed using PID control methods. Jalving [23] proposed a simple PD, to the steering control system, and PI to the speed control system. In [24], to control each Degree Of Freedom (DOF) of the *DepthX* AUV, 4DOFs, four independent loops were implemented, each loop containing an experimentally tuned PI controller.
    2. **LQR (Linear Quadratic Regulator):** In [25], the dynamics were divided into three subsystems. The dynamic model was linearized around a set of operating conditions, namely, surge velocity $u = 1.5m/s$, and for the remaining states, to zero. In [26], an LQR controller was proposed to control depth; [27] the Linear Quadratic Gaussian (LQG) was the technique suggested to control the AUV *REMUS* in the horizontal plane. Finally, [18] proposed an LQG to the autopilot of *Hammerhead* AUV.

- **Nonlinear methods:** As stated before, linear techniques can be applied to the nonlinear environment. However, for high-speed motion, nonlinear effects are significant, and linear control may not deliver the required performance [28]. There is a rich collection of alternatives and complementary techniques, to answer the AUV nonlinear needs. Sliding Mode Control (SMC) [21, 29], gain-scheduled LQR approach [30], fuzzy logic [31, 32], NN (Neural Networks) [33], adaptive control [34], nonlinear model predictive control [22], among others; are examples of nonlinear controllers implemented in underwater vehicles [1].

1.3 Motion Control Fundamentals

Some fundamental concepts need to be addressed when developing a motion controller. Namely: operating spaces, actuation properties, and motion control scenarios [35].

1.3.1 Operating Spaces

When designing a controller it is useful to distinguish between two operating spaces: *workspace* and *configuration space* [15]. The workspace, also known as the operational space, represents

the physical space in which the vehicle moves. For a car, the workspace is bi-dimensional (planar position) [35].
The configuration space represents all the possible states of a given vehicle in the workspace [35].

1.3.2 Vehicle Actuation Properties

According to Fossen, Degree-Of-Freedom, DOF, is the set of independent displacements and rotations that completely specify the displaced position and orientation of the vehicle [15]. The type, amount, and distribution of the vehicle's actuators (thrusters and control surfaces) will determine the actuation of the vehicle. The vehicle can be *underactuated* or *fully actuated* [35].
A *fully actuated* vehicle can control all its DOFs simultaneously independently. In opposite, an *underactuated* vehicle can only independently control some DOFs simultaneously [15]. However, a vehicle that cannot satisfy a 6 DOF control objective can still achieve meaningful tasks in its workspace [35].
Let us consider an AUV in the horizontal plane. The vehicle needs to follow a path, and it is equipped with one thruster and one rudder, which are the surge and yaw actuators. Although the vehicle does not have active control in sway motion, it can still achieve the control objective with a combination of the action of both actuators. So, even though the AUV is underactuated in the configuration space (three-dimensional: surge, sway and yaw), the vehicle is fully actuated in the workspace (bi-dimensional) [15].
In conclusion, if the vehicle is underactuated in the configuration space but fully actuated in the workspace, it is possible to achieve the control objective [15].

1.3.3 Motion Control Scenarios

To design a motion control system is essential to properly define the *control scenarios/objectives*, to meet the safe operational requirements of the vehicle. According to [15], motion control objectives are divided into:

- *Setpoint regulation*: The control objective is to track a desired position, or a desired attitude [15];
- *Trajectory tracking*: Is a time dependent method, where the system output $y(t)$, is forced to track the desired one $y_d(t)$. For an AUV (6 DOF), this means that the signal represents the desired position/attitude, velocity and acceleration as function of time [15];
- *Path following*: The control objective is to track a predefined path independent of time [15].

Tracking scenario can also be designed as *target tracking* and *path tracking*. On target tracking, the control objective is to track the target's motion that is either stationary or that moves, which in that case, only the instantaneous motion is known. On the path tracking scenario, the control objective is to track a target that moves along a predefined path [35].
These scenarios are typically defined by control objectives given as configuration space tasks. However, for underactuated vehicles, these control objectives should be defined as workspace tasks [15].

1.3.4 Motion Control Hierarchy

Motion control systems can usually be conceptualized into a three-level hierarchical structure: high-level control, intermediate level control and low-level control, figure 1.10.
The high-level control, labeled as kinematic control is accountable for prescribing vehicle velocity commands to achieve the control objective in the workspace [35]. Therefore, this level deals with the geometrical aspects of motion.
Once calculated the reference speeds, the intermediate level deals with the calculation of the forces that the different actuators have to perform to achieve the input references. *Kinetic controllers* do the calculation of the forces, and the control allocation is responsible for the distribution of the kinetic control commands among the vehicle actuators. These controllers are often designed by model-based methods, and must handle both parametric uncertainties and environmental disturbances [35].
The last level, low-level control, will ensure that the individual actuators will behave as requested by the intermediate level control.

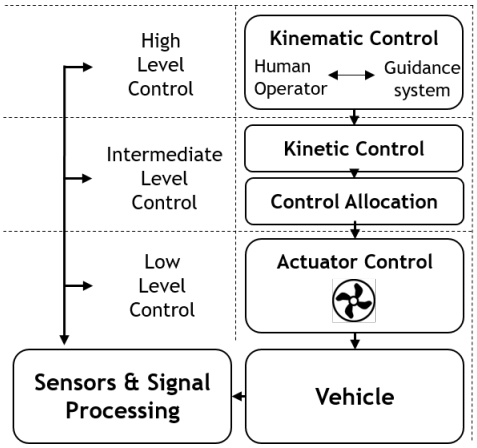

Figure 1.10: Motion control hierarchy (adapted from [35]).

For the purpose of this thesis only high and intermediate control levels are addressed.

1.4 Control Systems Fundamentals

1.4.1 *Open loop* and *Closed loop* systems

Designing a controller is about making dynamic systems perform certain tasks, to behave in a desired way [36]. Among the control systems configurations, two major will be discussed: *open loop* and *closed loop*, or *feedback*. Although both of the configurations start with the *input* or *reference*, and both achieve one *output*, the open-loop configuration, figure 1.11, cannot compensate for any added disturbance [37]. As an example, if the control system in figure 1.11, represents an electronic amplifier, and the *Disturbance 1* represents noise, both input signal and noise will be amplified.

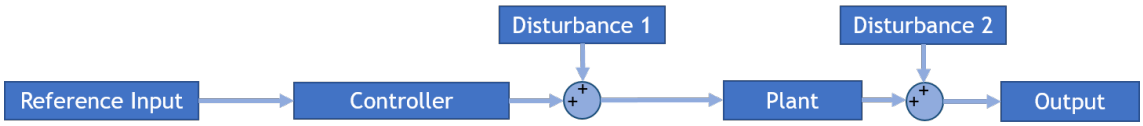

Figure 1.11: Block diagram of a generic architecture of a open-loop system.

The feedback configuration by taking into account the system's output, figure 1.12, will correct disturbances, creating a much more accurate and robust control [37].
From this point on, only feedback control systems will be discussed.

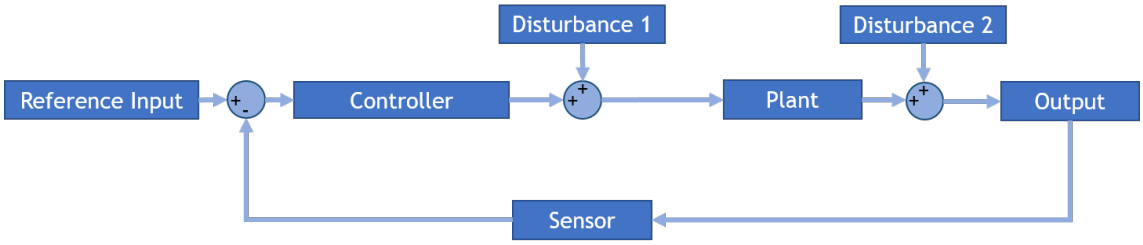

Figure 1.12: Block diagram of a generic architecture of a closed-loop system.

The design of control systems usually starts with modeling the system's plant[36]. To model a system, the designer uses physical laws, like *Kirchhoff's laws* for electrical networks, and *Newton's law* for mechanical systems. Such laws will lead to mathematical models that describe the relationship between input and output, I/O.
Therefore, two approaches are available for the analysis and design of feedback control systems, namely: *classical*, or *frequency-domain*, technique, and *modern*, or *time-domain*, technique [38].

1.4.2 Classical Control

The classical approach is based on converting the system's differential equation, into a *transfer function*. Thus generating a mathematical model that algebraically relates the output and the input. The main advantage is that information, like *stability* and *transient response*, is promptly provided. Therefore, the variation in the system parameters can instantly be seen and adapted to fulfill the requirements [37].

1.4.2.1 Transfer Function

The transfer function represents the relationship between the system's input $r(t)$ and system's output $y(t)$. A physical system that can be represented by an LTI, Linear Time-Invariant, differential equation can be modeled as a transfer function [37].
Considering the feedback system from figure 1.13:

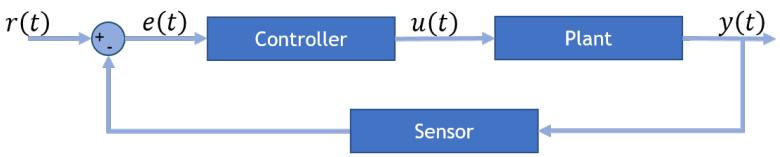

Figure 1.13: Feedback system block diagram.

The transfer function is given by:

$$G(s) = \frac{Y(s)}{R(s)} \quad (1.27)$$

where $R(s)$ and $Y(s)$ are the *Laplace transforms* from $r(t)$ and $y(t)$. Reminding that the Laplace transform is defined as:

$$\mathcal{L}[f(t)] = F(s) = \int_0^\infty f(t)e^{-st}dt \quad (1.28)$$

where s is a complex variable ($s = \sigma + j\omega$). Hence, knowing $f(t)$ and that the integral from equation1.28 exists, it is possible to find the Laplace transform, $F(s)$ from $f(t)$ [37].
This transformation (time-domain to frequency-domain) will result in a polynomial fraction:

$$G(s) = \frac{b(s)}{a(s)} \quad (1.29)$$

where the roots from $b(s)$ represent the **zeros** from the system, and the roots of $a(s)$ the **poles**. Therefore, in the complex plane, the magnitude of $G(s)$ will go to zero at each **zero**, and to infinity at the **poles** [39].

1.4.2.2 PID Control Theory

Proportional integral derivative control, figure 1.14, is by far the most common control technique, due to the general applicability to most control systems [40]. In particular, when the plant's mathematical model is unknown, PID control design methods can still provide satisfactory control. However, in some situations, these may not provide optimal control [38].

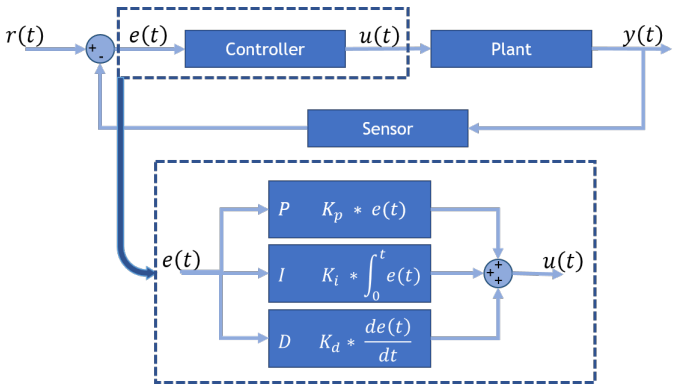

Figure 1.14: Feedback block diagram with PID controller.

This controller works on the principle of closed-loop feedback, where the proportional term is linear to the error, the integral term accumulates the error over time, and the derivative measures how fast the error is changing. So, the control law is given by:

$$\mathbf{u}(t) = K_p e(t) + K_i \cdot \int_0^t e(\tau)d\tau + K_d \cdot \frac{de(t)}{dt} \quad (1.30)$$

where, K_p, K_i and K_d represent the proportional, integral and derivative gains, respectively.

The controller also can be parametrized as:

$$\mathbf{u}(t) = K_p(e(t) + \frac{1}{T_i} \cdot \int_0^t e(\tau)d\tau + T_d \cdot \frac{de(t)}{dt}) \quad \textbf{(1.31)}$$

where T_i is called integral time and T_d derivative time [40]. The respective transfer function between the input, error, and the output, control law, is then:

$$\frac{U(s)}{E(s)} = K_p(1 + \frac{1}{T_i s} + T_d s) \quad \textbf{(1.32)}$$

The gains are tuned according to system's requirements. By increasing the proportional gain, the system responsiveness will increase, but for high values, instability can occur, and the steady-state error will remain. Adding the integral term (PI) the steady state can be eradicated. However, it can cause overshoot. Therefore, the addition of the derivative term (PID) increases damping and reduces overshoot [22].
From figure 1.15, it can be seen how the PID controller works. The integral term accounts for the error up to time t (*past*), (shaded portion); the proportional term accounts for the instantaneous value of the error (*present*); and the derivative estimates the growth, or decay, of the error over time (*future*) [40].

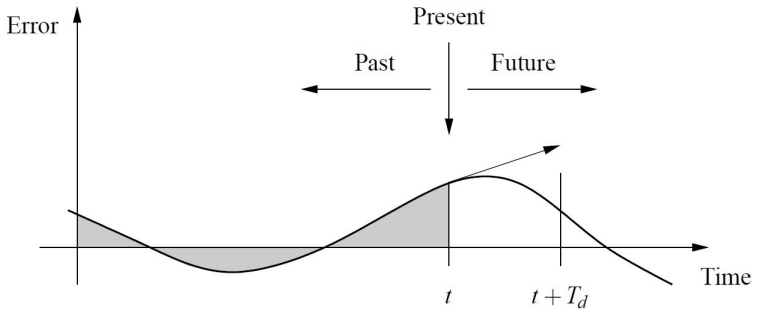

Figure 1.15: Action of a PID controller (adapted from [40]).

Integrator Wind-up

Linear models can provide an understanding of many aspects of control systems. However, some nonlinear effects should be accounted for when designing a controller, namely the physical limitations of the actuators. For example, a thruster has limited speed, and a valve cannot be more than fully opened or fully closed.
When this happens, the feedback loop is no longer doing its job since, at the moment that the system reaches the desired state, the value of the integrator output is still significant. To compensate that, the error needs to have opposite sign for an extended period, as shown in figure 1.16. This phenomenon is referred to as integrator wind-up [40].

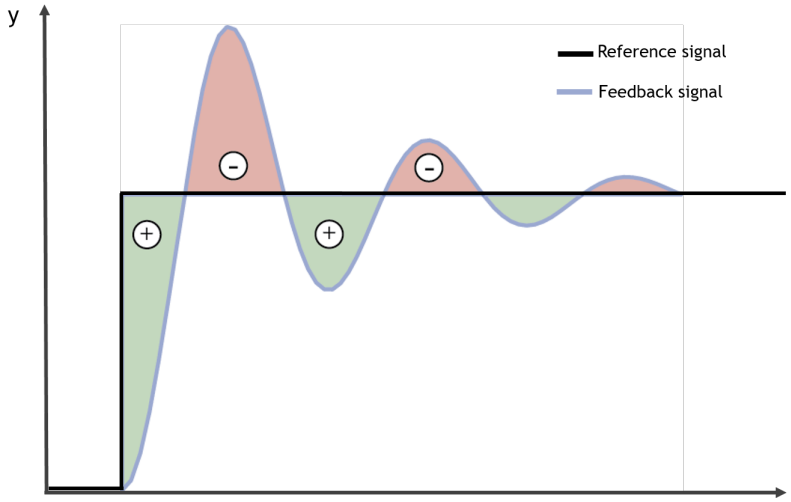

Figure 1.16: Wind-up effect.

Literature presents different solutions to this problem [40], two common ones are clamping, or conditional integration which prevents the output from accumulating when the controller output is saturated, and back-calculation (figure1.17). In this last method, when the extra feedback path becomes active (saturation in actuators) the integral term is recomputed, so that its new value helps to stabilize the integrator. It is advantageous to not instantaneously reset the integrator, but instead do it dynamically, with a constant T_t [40].

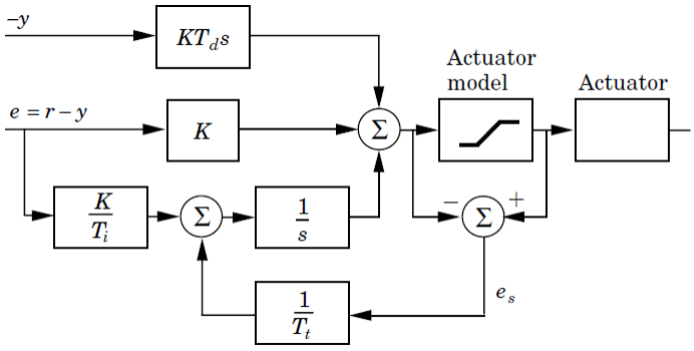

Figure 1.17: Controller with back-calculation loop (adapted from[40]).

1.4.3 Modern Control

During the 1950s, several authors, including Kalman, began working on the Ordinary Differential Equations (ODEs), as a model for control systems, known as the state-space approach. Allied to these works, the advances in the digital computers allowed the direct work with ODE in the state form. Even though this work's foundation took place in the 19^{th} century, this state-space approach, for control purposes, is often referred to as modern approach [41].
In the first stage, modern control allows the study of the system's *controllability* and *observability*. Considering an initial time as t_0, the terms are defined as:

- **Controllability**: *The system is controllable if and only if exists a control vector that can drive any arbitrary state $x(t_0)$ to any other, in a finite interval of time.*

- **Observability**: *The system is observable at a time t if, in the $x(t_0)$ state, it is possible to determine this state from the observation of the output, over a finite time interval.*

To prove controllability and observability lets consider the linear continuous-time system in the state-state space form, where n is the number of states, p the number of inputs and q the number of outputs [37].

$$\begin{cases} \dot{x} = Ax + B\mathbf{u} \\ y = Cx + D\mathbf{u} \end{cases} \quad (1.33)$$

where:

x = state vector, $x \in \Re^n$
$\mathbf{u}$ = input or control vector, $\mathbf{u} \in \Re^p$
y = output vector, $y \in \Re^q$
A = system matrix, $A \in \Re^{n \times n}$
B = input matrix, $B \in \Re^{n \times p}$
C = output matrix, $C \in \Re^{q \times n}$
D = feedforward matrix, $D \in \Re^{q \times p}$

For the system to be controllable, the controlability matrix C_o needs to have rank n.

$$Co = \begin{bmatrix} B & AB & A^2B & \dots & A^{n-1}B \end{bmatrix} \quad (1.34)$$

In the same way, the system is observable if, and only if, the observability matrix Q has rank n.

$$O = \begin{bmatrix} C^T & A^TC^T & (A^T)^2C^T & \dots & (A^T)^{n-1}C^T \end{bmatrix} \quad (1.35)$$

According with [42], the controlability condition is enough to prove the closed loop stability;

1.4.3.1 Linear Quadratic Regulator

Linear quadratic regulator (LQR) is an optimal feedback controller that in its original form, forces all the states to go to zero. With some modifications can be used to track a reference as seen in the figure 1.18 [39].

Figure 1.18: Linear quadratic regulator system.

To derive the LQR control, *controllability* and *observability* need to be ensured [38]. Assuming the state-space form:

$$\dot{x} = Ax + B\mathbf{u} \quad (1.36)$$

Considering that all states are available for the controller, the optimal control problem determines the feedback gain, K matrix, of the optimal control vector:

$$\mathbf{u}(t) = -Kx(t) \quad (1.37)$$

The feedback control law for the system is found by minimizing the quadratic cost function, or performance index:

$$J = \int_0^\infty (x^T Q x + \mathbf{u}^T R \mathbf{u}) dt \quad (1.38)$$

where Q is a positive-definite (or positive-semidefinite) Hermitian or real symmetric matrix, $Q \geq 0$, and R is a positive-definite Hermitian or real symmetric matrix, $R > 0$. They act like weights, i.e. the Q matrix, for being related with the system state x, will account for the errors' importance, and R, by being related to the control u, will account for the expenditure of the energy in control signal [38].
The solution to the minimization problem is the positive-definite Hermitian or real symmetric matrix P, which corresponds to the *Algebraic Riccati Equation* (ARE) [38]:

$$A^T P + PA - PBR^{-1}B^T P + Q = 0 \quad (1.39)$$

Resulting in the feedback law:

$$\mathbf{u} = -R^{-1}B^T P x \quad (1.40)$$

If working as set point tracker, the feedback law can be given by [39]:

$$\mathbf{u} = -R^{-1}B^T P(x - x_{desired}) \quad (1.41)$$

With the goal of making the weight selection step more intuitive, Bryson's method suggests that each element of the diagonal matrices Q and R is the inverse square of the maximum expected value for the variable [42], i.e.:

$$Q = diag(Q_i),\ Q_i = \frac{1}{x_{i,max}^2} \quad (1.42)$$

$$R = diag(R_i),\ R_i = \frac{1}{\mathbf{u}_{i,max}^2} \quad (1.43)$$

Where $x_{i,max}^2$ and $\mathbf{u}_{i,max}^2$ are the maximum expected values for the x_i and $\mathbf{u}_i$.
The design process can be summed up by the following steps [42]:

1. Dynamic system definition (A, B);
2. Weight selection (Q, R);
3. ARE solution (P);
4. Control matrix solution (K);
5. Feedback through equation 1.37.

Integral Action

As in the PID controller, it is also possible to add an integral term to the LQR controller. The basic approach in integral feedback is to create a state within the controller that computes the integral of the error signal, which is then used as feedback term. Lets consider the new variable

z defined by [15]:

$$\dot{z} = y = Cx \quad (1.44)$$

Where C matrix is used to extract potential integral states from the state vector x. The system is now defined as:

$$\dot{x}_a = A_a x_a + B_a \mathbf{u} \quad (1.45)$$

Where;

$$x_a = \begin{bmatrix} z \\ x \end{bmatrix}; A_a = \begin{bmatrix} 0 & C \\ 0 & A \end{bmatrix}, B_a = \begin{bmatrix} 0 \\ B \end{bmatrix} \quad (1.46)$$

The performance is now calculated by:

$$J = \int_0^\infty (x_a^T Q_a x_a + \mathbf{u}^T R \mathbf{u}) dt \quad (1.47)$$

Where $Q_a = Q_a^T \geq 0$ and $R = R^T > 0$ are the weighting matrices. Then the solution to the LQR setpoint regulation is given by:

$$\mathbf{u} = -R^{-1} B_a^T P_\infty x_a \quad (1.48)$$

Where P_∞ is the solution to the Riccati equation:

$$P_\infty A_a + A_a^T P_\infty - P_\infty B_a R^{-1} B_a^T P_\infty + Q_a = 0 \quad (1.49)$$

Now, the control objective is to regulate the x_a state to zero using **u** [15]. Reminding that:

$$z = \int_0^\infty e(\tau) d\tau \quad (1.50)$$

Remarks about LQR

There are some key characteristics of LQR worth mentioning [18]:

- Excellent stability margins: according to [18], the gain margin up to infinity and over 60 degrees of phase margin. That means robustness for all magnitude of disturbances [43];
- Optimality: Since the closed-loop eigenvalues are found according to the minimization of the cost function J, there is no need for pole placement and therefore the resulting value is optimal;
- Unique analytical solution.

1.4.4 Stability

The first and most important question about the various properties of a control system is whether it is stable or not. An unstable control system is useless and potentially dangerous [28]. Therefore, every control system whether linear or nonlinear involves a stability problem and must be addressed properly [28].

1.4.4.1 Linear Systems

Concerning linear time-invariant systems, there are two concepts that need to be addressed: *natural response* and *forced response*.
The natural response describes the way that the system dissipates or acquires energy. The nature of this response only depends on the system, not on the input. Contrarily, the forced response is dependent on the input [37]. For an LTI system, it is allowed to say [37]:

$$Output\,response = Natural\,response + Forced\,response \quad (1.51)$$

Using these concepts, a system is:

- **Stable** if the natural response approaches zero as time goes to infinity;
- **Unstable** if the natural response grows without bounds, as time goes to infinity;
- **Marginally stable** if the natural response neither decays nor grows but remains constant or oscillates as time goes to infinity.

Therefore, the definition of stability states that only forced response remains as the natural tends to zero [37].
Considering the natural response stability, many techniques, such as solving a differential equation or taking the inverse Laplace, enable the evaluation of this output response. However, many are time-consuming and painstaking [37]. A simple and faster method to determine whether the system is stable or not is to analyze the transfer function, namely the poles' location in the complex plane ($s = \sigma + j\omega$), as can be seen in figure 1.19. Therefore, according to [37] a system is:

- **Stable** if all the poles are located in the Left Half Plane (LHP);
- **Unstable** if one or more poles are located in the Right Half Plane (RHP);
- **Marginally stable** if at least one pole is located in the imaginary axis ($j\omega$).

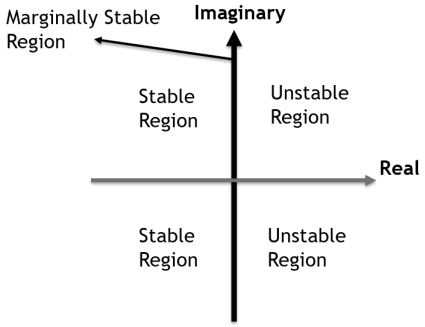

Figure 1.19: Stability in the complex plane.

Looking now at stability from the perspective of state-space. Considering the linear system:

$$\dot{x} = Ax \quad (1.52)$$

The solution is given by [44]:

$$x(t) = e^{(t-t_0)A}x_0 \quad (1.53)$$

where x_0 is the initial state. The exponential of a matrix is defined by the Taylor series [44]:

$$e^X = I + X + \frac{1}{2}X^2 + \frac{1}{3!}X^3 + ... \quad (1.54)$$

By assuming that the matrix X, with the dimension $n \times n$, has n distinct eigenvectors, i.e is non defective, the solution is given by [44]:

$$e^X = Pe^{\Lambda}P^{-1} \quad (1.55)$$

where Λ is the eigenvalues diagonal matrix and P the matrix of eigenvectors. Applying now to equation 1.53:

$$x(t) = Pe^{(t-t_0)\Lambda}P^{-1} \quad (1.56)$$

where the quantity $e^{(t-t_0)\Lambda}$, namely the values of Λ, will determine if the system converges to the origin. Therefore, the linear system is:

- Stable if all eigenvalues of A are strictly in the left-half complex plane;
- Unstable if at least one eigenvalue of A is strictly in the righ-half complex plane;
- Marginally stable if all eigenvalues of A are strictly in the left-half complex plane, but at least one is on the imaginary axis $j\omega$.

1.4.4.2 Nonlinear Systems

Physical systems are inherently nonlinear. However, no universal technique has been devised for the analysis of nonlinear control systems [28]. However serious efforts have been made to provide the right tools for this task [28]. Among those tools is the *Lyapunov theory*. The basic Lyapunov theory is comprised of two methods to address the nonlinear system stability, the indirect method, and the direct method [28]. For this thesis purpose, only the indirect method will be addressed.
According to Lyapunov, a system is stable if it starts near an equilibrium point and stays around it ever after [28]. Since nonlinear systems may exhibit much more complex behavior than the linear systems, some additional/refined stability concepts are required.

Asymptotic Stability and Exponential Stability

In some systems, knowing that the state will stay in the neighborhood of the equilibrium is not enough. Therefore it may be a necessity to understand if the state actually converges to the original value. Hence, [28]:

An equilibrium point is said to be asymptotic stable, in addition to the Lyapunov stability, if the states that start close to the equilibrium point actually converge to it.

In many application, there is a need to estimate how fast that convergence occurs. Therefore [28]:

An equilibrium point is said to be exponentially stable if there is two strictly positive numbers α and λ such that:

$$\forall t > 0, \quad \|x(t)\| \leq \alpha \|x(0)\| e^{-\lambda t} \quad \textbf{(1.57)}$$

where λ is a positive number and it is called as the rate of exponential convergence.

Linearization and Local Stability

The nonlinear system can be linearized around an operating point, or equilibrium point, through a Taylor expansion, and then linear control techniques can be used to control the system.
The Lyapunov indirect method, or Lyapunov's linearization method, is concerned with local stability of the nonlinear system. This method justifies the use of linear control techniques on nonlinear systems. Therefore, the Lyapunov indirect method states that [28]:

- *If the linearized system is strictly stable (i.e all eigenvalues of A are strictly in the left-half complex plane), then the equilibrium point is asymptotically stable for the actual nonlinear system.*
- *If the linearized system is unstable (i.e at least one eigenvalues of A is strictly in the righ-half complex plane), then the equilibrium point is unstable for the actual nonlinear system.*
- *If the linearized system is marginally stable (i.e all eigenvalues of A are strictly in the left-half complex plane, but at least one of them is on the imaginary axis $j\omega$), then one cannot conclude about the linear approximation.*

1.4.4.3 Stability Margins

Knowing that the system is stable, in practice, is not enough [40]. Control design is usually done based on mathematical models or through experimental tests in a controlled environment. Both of these methods may not consider all the process variations that can affect the control system. Since the designer cannot have perfect knowledge of the process variations margins must be accounted [43].
First the concepts of *phase* and *gain* need to be addressed.

Considering a LTI system $G(s)$. Assuming that the system is subjected to a sinusoidal input [40]:

$$u(t) = sin(\omega t) \quad \textbf{(1.58)}$$

the output is distorted based on the properties of $G(s)$. For an LTI system, the distortion is presented in two ways: in the magnitude of the signal and in the phase of the signal. The response will be in the form [40]:

$$y(t) = A(\omega) sin(\omega t + \phi(\omega)) \quad \textbf{(1.59)}$$

where $A(\omega)$ is the amplitude, and $\phi(\omega)$ the phase shift [40]. The gain is the proportion of the magnitude of the output, to the magnitude of the input at steady state, and phase is the shift of the signal, measured as an angle [43].

Considering a closed loop system $G(s)$, the transfer function is given by [43]:

$$\frac{G(s)}{1+G(s)} \quad (1.60)$$

Reminding that the instability happens if at least one pole is on the Right Half Plane (RHP), it is concluded that this system is unstable if $1+G(s)=0$, which corresponds to the case where $G(s)=-1$. Therefore, $G(s)$ must be kept away from -1 for the closed loop system to be stable. This condition corresponds to the case where the gain of the system is 1, or 0dB, and the phase is $-180°$ because it flips the input upside down [43]. Margin corresponds to how far away from this point the system is.
Gain and phase margins are the amount of gain and phase that can be added to the system before it goes unstable. These margins can be inferred from a *Bode* plot [43]. However, since the system is subjected to external disturbances, some results may mislead the designer to assume that the system is robust. Therefore, *sensitivity* is as important to analyze, like gain and phase margin.

Considering the simplified system in figure 1.20.

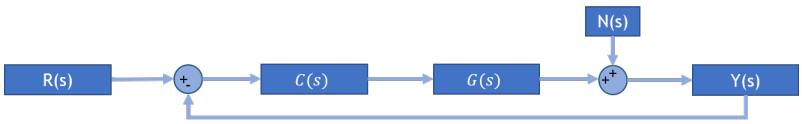

Figure 1.20: Closed loop system subjected to external disturbances.

The transfer function of the system is [43]:

$$Y(s)=\frac{C(s)G(s)}{1+C(s)G(s)}R(s)+\frac{1}{1+C(s)G(s)}N(s) \quad (1.61)$$

where $N(s)$ represents the disturbances. The sensitivity function is given by the second term of this equation. Using this result, it is possible to determine the process sensitivity across the spectrum of frequencies. According to [43], the typical values of maximum sensitivity are in the range of 1 to 2. Closest to 1 represent a more conservative controller and closest to 2 a more aggressive controller.

1.5 Purpose and Contribution

Control systems are an integral part of the modern society [37]. Being able to develop a control system is being capable of understanding the system at its most basic level.
For autonomous vehicles, there is a continuous demand for advanced features. Therefore, the control system design must be able to provide the right performance, ensuring both task accomplishment and the integrity of the system.
Developing a control system for an underwater vehicle is not straightforward. The highly nonlinear underwater environment [45] makes the mathematical modeling of the vehicle a complex task and the outcome may not be an accurate representation of the AUV's dynamics, affecting the controller performance. It is therefore paramount to devote the necessary effort to develop a control that can be robust to disturbances.

In this context, the purpose of this thesis is to, among the fields of study that the AUV development entails (figure 1.21), design and analyze two control solutions for the AUV being developed at CEiiA. This work is aimed at increasing CEiiA's capabilities in the field of control for underwater vehicles.

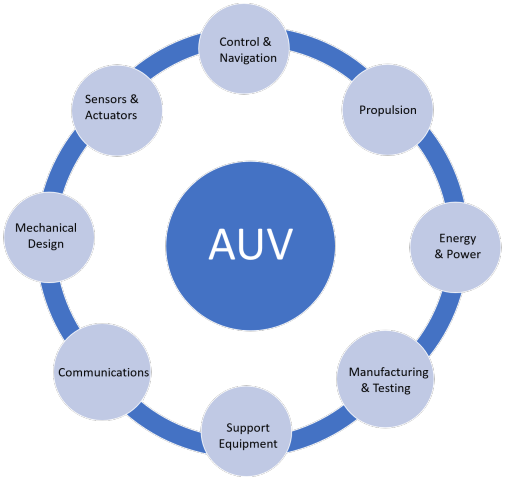

Figure 1.21: AUV's fields of study.

An overview of the controllers shows that state-of-art motion control systems are usually designed using PID control methods [15]. However, more advanced control systems have been devised. Example of that is the LQR controller. Therefore, two control designs are proposed based on both of these methods. Since the controller can only be as good as its guidance inputs, it will be proposed two guidance solutions, one based on waypoint following and other on path following. For the simulation/validation purpose, the nonlinear model devised in [17] will be used.

1.6 Thesis Outline

This thesis is organized as follows.

- In **chapter 1** the research developed in this thesis is contextualized, by providing an overview of the AUV in study and the required bibliographic review.
- **Chapter 2** addresses the nonlinear model devised in [17].
- **Chapter 3** highlights two guidance solutions, one based on waypoint following and the other on path following.
- **Chapter 4** presents the linearization of the complete nonlinear model, the control design of PID and LQR and the control allocation law.
- In **chapter 5** are simulated both guidance methods for PID and LQR controllers.
- **Chapter 6** concludes the thesis, reporting the remarks about this work and guidance for further works.

Chapter 2

AUV Dynamic Model

The dynamic model allows for controller design and respective simulation and validation. In this chapter, the nonlinear dynamic model of the AUV being developed at CEiiA is briefly described, as well as an overview of the modeling process used to estimate vehicle's parameters. For a detailed description of the modeling process of this AUV, please refer to [17]. Some modifications in the damping term, later to [17], are also presented.

2.1 General Dimensions of the AUV

The dimensions of interest for the AUV are presented in table 2.1, which corresponds to figure 2.1.

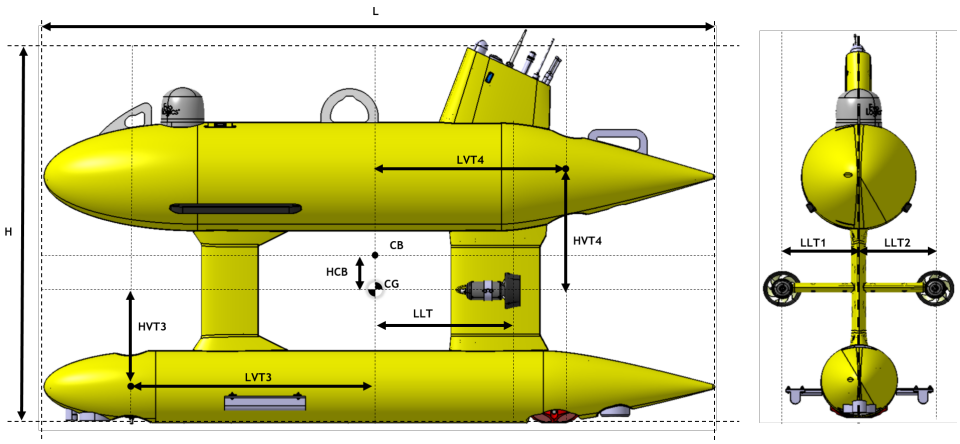

Figure 2.1: General dimensions of the AUV (not to scale).

Table 2.1: Dimensions for figure 2.1 in meters obtained from 3D model.

L	2.800
H	1.563
HCB	0.093
LLT	0.689
HVT3	0.326
HVT4	0.549
LLT1	0.300
LLT2	0.300

As stated in section 1.2.1, the origin of the body fixed frame is chosen to coincide with the CG, i.e. $r_g^b = [0 \quad 0 \quad 0]^T$. The inertial frame is the local NED (figure 1.8). According to figure 2.1, the CB, defined with respect to the body fixed frame, is given by $r_B^b = [0 \quad 0 \quad -HCB]^T$.

2.2 Dynamic Model of the AUV

In literature, there are several methods to estimate the dynamic parameters, such as experimental, analytical, and computational methods [46]. In [17], the parameters were obtained resorting to analytical and computational methods. Computer Aided Design (CAD) software was used to determine the inertial parameters of the vehicle, analytical methods to the estimation of added mass, and Computational Fluid Dynamics (CFD), which involves solving the Navier-Stokes flow equations numerically using a computer [46], to the hydrodynamic coefficients. These methods allow for fast estimation of the parameters and, because there is no need for experimental methods, at a reduced cost [17].

As mentioned in section 1.1, the AUV during the mission has three different stages. For this thesis purpose, only the data acquisition stage will be considered.

2.2.1 Rigid Body Term

The rigid-body matrices parameter of the AUV, namely the mass and the inertia, were obtained from the CAD software according to [17], are:

$$\begin{aligned} M &= 440.48\ kg \\ I_x &= 58.35\ kg \cdot m^2 \\ I_y &= 148.71\ kg \cdot m^2 \\ I_z &= 94.04\ kg \cdot m^2 \\ I_{xz} &= -2.44\ kg \cdot m^2 \end{aligned}$$

Therefore, the rigid body matrix, M_{rb}, as seen in the equation 1.6, results in:

$$M_{rb} = \begin{bmatrix} 440.48 & 0 & 0 & 0 & 0 & 0 \\ 0 & 440.48 & 0 & 0 & 0 & 0 \\ 0 & 0 & 440.48 & 0 & 0 & 0 \\ 0 & 0 & 0 & 58.35 & 0 & 2.44 \\ 0 & 0 & 0 & 0 & 148.71 & 0 \\ 0 & 0 & 0 & 2.44 & 0 & 94.04 \end{bmatrix} \quad (2.1)$$

With respect to the rigid body Coriolis and centripetal matrix, $C_{rb}(\nu)$, as stated in 1.7, is given by:

$$C_{rb}(\nu) = \begin{bmatrix} 0 & 0 & 0 & 0 & 440.48w & -440.48v \\ 0 & 0 & 0 & -440.48w & 0 & 440.48u \\ 0 & 0 & 0 & 440.48v & -440.48u & 0 \\ 0 & 440.48w & -440.48v & 0 & 2.44p + 94.04r & -148.71q \\ -440.48w & 0 & 440.48u & -2.44p - 94.04r & 0 & 2.44r + 58.35p \\ 440.48v & -440.48u & 0 & 148.71q & -2.44r - 58.35p & 0 \end{bmatrix} \quad (2.2)$$

2.2.2 Added Mass Term

As presented in equation 1.10, the added mass term is divided into two terms: the added mass matrix (equation 1.11) and the hydrodynamic Coriolis and centripetal matrix (equation 1.12). In [17], the added mass was estimated using ellipsoid approximation for both hulls and flat plate approximation for fairings. The resulting values, from the sum of all components, are:

$$
\begin{aligned}
X_{\dot{u}} &= -11.64kg \\
X_{\dot{q}} &= 1.74kgm \\
Y_{\dot{v}} &= -450.58kg \\
Y_{\dot{p}} &= -23.33kgm \\
Y_{\dot{r}} &= -82.23kgm \\
Z_{\dot{w}} &= -419.13kg \\
Z_{\dot{q}} &= -76.78kgm \\
K_{\dot{p}} &= -60.82kgm^2 \\
K_{\dot{r}} &= -2.92kgm^2 \\
M_{\dot{q}} &= -155.56kgm^2 \\
N_{\dot{r}} &= -181.84kgm^2
\end{aligned}
$$

The added mass matrix, for this AUV, is:

$$
\boldsymbol{M}_A = \begin{bmatrix}
11.64 & 0 & 0 & 0 & -1.74 & 0 \\
0 & 450.58 & 0 & 23.33 & 0 & 82.23 \\
0 & 0 & 419.13 & 0 & 76.78 & 0 \\
0 & 23.33 & 0 & 60.82 & 0 & 2.92 \\
-1.74 & 0 & 76.78 & 0 & 155.56 & 0 \\
0 & 82.23 & 0 & 2.92 & 0 & 181.84
\end{bmatrix} \tag{2.3}
$$

For the Coriolis and centripetal term due to added mass, the values from equation 1.12 can be devised [17]:

$$
\begin{aligned}
a_1 &= -11.64u + 1.74q \\
a_2 &= -450.58v - 23.33p - 82.23r \\
a_3 &= -419.13w - 76.78q \\
b_1 &= -23.33v - 60.82p - 2.92r \\
b_2 &= 1.74u - 76.78w - 155.56q \\
b_3 &= -82.23v - 2.92p - 181.84r
\end{aligned}
$$

2.2.3 Hydrodynamic Term

In [17] only CFD analysis on damping due to linear velocities were available. The coefficients that will be presented were updated due to small changes in geometry. Also, a quartic approximation of damping term was developed in CEiiA. This accounts for different dynamics in reverse motion, which is actually true because there is no symmetry in the yz plane.
The damping coefficients provided are:

- Damping due to motion in surge:

Table 2.2: Linear damping coefficients due to motion in surge.

$$
\begin{aligned}
X_u &= -24.6 \\
Y_u &= 0 \\
Z_u &= 1.8 \\
K_u &= 0 \\
M_u &= 0 \\
N_u &= 0
\end{aligned}
$$

Table 2.3: Quadratic damping coefficients due to motion in surge.

$$
\begin{aligned}
X_{u|u|} &= -5.2 \\
Y_{u|u|} &= 0 \\
Z_{u|u|} &= 3.1 \\
K_{u|u|} &= 0 \\
M_{u|u|} &= 0 \\
N_{u|u|} &= 0
\end{aligned}
$$

Table 2.4: Cubic damping coefficients due to motion in surge.

$$
\begin{aligned}
X_{uu|u|} &= -21.1 \\
Y_{uu|u|} &= 0 \\
Z_{uu|u|} &= 1.4 \\
K_{uu|u|} &= 0 \\
M_{uu|u|} &= 0 \\
N_{uu|u|} &= 0
\end{aligned}
$$

Table 2.5: Quartic damping coefficients due to motion in surge.

$$
\begin{aligned}
X_{uuu|u|} &= 3.79 \\
Y_{uuu|u|} &= 0 \\
Z_{uuu|u|} &= 0 \\
K_{uuu|u|} &= 0 \\
M_{uuu|u|} &= 0 \\
N_{uuu|u|} &= 0
\end{aligned}
$$

- Damping due to motion in sway:

Table 2.6: Linear damping coefficients due to motion in sway.

$$
\begin{aligned}
X_v &= 0.0 \\
Y_v &= -219.5 \\
Z_v &= 0.0 \\
K_v &= 79.7 \\
M_v &= 171.8 \\
N_v &= -246.1
\end{aligned}
$$

Table 2.7: Quadratic damping coefficients due to motion in sway.

$$
\begin{aligned}
X_{v|v|} &= 0.0 \\
Y_{v|v|} &= -1844.4 \\
Z_{v|v|} &= 0.0 \\
K_{v|v|} &= -170.7 \\
M_{v|v|} &= -52.6 \\
N_{v|v|} &= -215.3
\end{aligned}
$$

- Damping due to motion in heave:

Table 2.8: Linear damping coefficients due to motion in heave.

$$
\begin{aligned}
X_w &= 0.0 \\
Y_w &= 0.0 \\
Z_w &= -284.8 \\
K_w &= 0.0 \\
M_w &= 100.3 \\
N_w &= 0.0
\end{aligned}
$$

Table 2.9: Quadratic damping coefficients due to motion in heave.

$$
\begin{aligned}
X_{w|w|} &= 0.0 \\
Y_{w|w|} &= 0.0 \\
Z_{w|w|} &= -43.8 \\
K_{w|w|} &= 0.0 \\
M_{w|w|} &= 56.1 \\
N_{w|w|} &= 0.0
\end{aligned}
$$

Table 2.10: Cubic damping coefficients due to motion in heave.

$$
\begin{aligned}
X_{ww|w|} &= 0.0 \\
Y_{ww|w|} &= 0.0 \\
Z_{ww|w|} &= -255.5 \\
K_{ww|w|} &= 0.0 \\
M_{ww|w|} &= 206.9 \\
N_{ww|w|} &= 0.0
\end{aligned}
$$

Table 2.11: Quartic damping coefficients due to motion in heave.

$$
\begin{aligned}
X_{www|w|} &= 0.0 \\
Y_{www|w|} &= 0.0 \\
Z_{www|w|} &= 10.8 \\
K_{www|w|} &= 0.0 \\
M_{www|w|} &= -55.1 \\
N_{www|w|} &= 0.0
\end{aligned}
$$

- Damping due to rotation:

Table 2.12: Linear damping coefficients due to rotation.

$$
\begin{aligned}
K_p &= -34.0 \\
M_q &= -59.0 \\
N_r &= -45.0
\end{aligned}
$$

Table 2.13: Quadratic damping coefficients due to rotation.

$$
\begin{aligned}
K_{p|p|} &= -84.0 \\
M_{q|q|} &= -148.0 \\
N_{r|r|} &= -100.0
\end{aligned}
$$

Replacing the coefficients into equations 1.15 and 1.16, plus the cubic and quartic damping matrix yields:

$$
D_l = \begin{bmatrix}
24.6 & 0 & 0 & 0 & 0 & 0 \\
0 & 219.5 & 0 & 0 & 0 & 0 \\
-1.8 & 0 & 284.8 & 0 & 0 & 0 \\
0 & -79.7 & 0 & 34.0 & 0 & 0 \\
0 & -171.8 & -100.3 & 0 & 59.0 & 0 \\
0 & 246.1 & 0 & 0 & 0 & 45.0
\end{bmatrix} \tag{2.4}
$$

$$
D_q(\nu) = \begin{bmatrix}
5.2 \mid u \mid & 0 & 0 & 0 & 0 & 0 \\
0 & 1844.4 \mid v \mid & 0 & 0 & 0 & 0 \\
-3.1 \mid u \mid & 0 & 43.8 \mid w \mid & 0 & 0 & 0 \\
0 & -170.7 \mid v \mid & 0 & 84.0 & 0 & 0 \\
0 & 52.6 \mid v \mid & -56.1 \mid w \mid & 0 & 148.0 \mid q \mid & 0 \\
0 & 215.3 \mid v \mid & 0 & 0 & 0 & 100 \mid r \mid
\end{bmatrix} \tag{2.5}
$$

$$
D_{cub} = \begin{bmatrix}
21.1uu & 0 & 0 & 0 & 0 & 0 \\
0 & 0 & 0 & 0 & 0 & 0 \\
-1.4uu & 0 & 255.5ww & 0 & 0 & 0 \\
0 & 0 & 0 & 0 & 0 & 0 \\
0 & 0 & -206.9ww & 0 & 0 & 0 \\
0 & 0 & 0 & 0 & 0 & 0
\end{bmatrix} \tag{2.6}
$$

$$D_{qt}(\nu) = \begin{bmatrix} -3.79 \mid u \mid uu & 0 & 0 & 0 & 0 & 0 \\ 0 & 0 & 0 & 0 & 0 & 0 \\ 0 & 0 & -10.8 \mid w \mid ww & 0 & 0 & 0 \\ 0 & 0 & 0 & 0 & 0 & 0 \\ 0 & 0 & 55.1 \mid w \mid ww & 0 & 0 & 0 \\ 0 & 0 & 0 & 0 & 0 & 0 \end{bmatrix} \quad (2.7)$$

2.2.4 Hydrostatic Term

Reminding that the CG is denoted as $r_g^b = [0 \quad 0 \quad 0]^T$ and CB as $r_B^b = [0 \quad 0 \quad -0.093]^T$. It can be concluded that CG is aligned with CB in x and y axis, but misaligned in the z axis. The distance of 0.093 meters between the two centers, according to [47], provides sufficient height for inducing a righting moment that passively controls vehicle's roll and pitch angles.
The weight is found to be 3482.6 N and the buoyancy as 3486.5 N. Therefore the residual buoyancy has the value of 3.9240 N.
According to equation 1.23, the resulting hydrostatic term yields:

$$\mathbf{g}(\eta) = \begin{bmatrix} -3.9240 \sin(\theta) \\ 3.9240 \cos(\theta) \sin(\phi) \\ 3.9240 \cos(\theta) \cos(\phi) \\ -324.24 \cos(\theta) \sin(\phi) \\ -324.24 \sin(\theta) \\ 0 \end{bmatrix} \quad (2.8)$$

2.2.5 Thrust Term

The AUV has four thrusters, as mentioned in section 1.1. Each of the thrusters, according to [48], is capable of 120 N of forward thrust, and 85 N of backward thrust. The vector location, with respect to CG, of each thruster is [17]:

- Right longitudinal thruster (Thruster 1):

$$r_{T1}^g = \begin{bmatrix} -0.689 & 0.300 & 0 \end{bmatrix}$$

- Left longitudinal thruster (Thruster 2):

$$r_{T2}^g = \begin{bmatrix} -0.689 & -0.300 & 0 \end{bmatrix}$$

- Forward vertical thruster (Thruster 3):

$$r_{T3}^g = \begin{bmatrix} 0.910 & 0 & 0.326 \end{bmatrix}$$

- Aft vertical thruster (Thruster 4):

$$r_{T4}^{g} = \begin{bmatrix} -0.910 & 0 & -0.549 \end{bmatrix}$$

Therefore, the mapping matrix L, from the equation 1.9, is devised as:

$$L = \begin{bmatrix} 1 & 1 & 0 & 0 & 0 & 0 \\ 0 & 0 & 0 & 0 & 0 & 0 \\ 0 & 0 & 1 & 1 & 0 & 0 \\ 0 & 0 & 0 & 0 & 0 & 0 \\ 0 & 0 & -|r_{T3}^{g}(1)| & |r_{T4}^{g}(1)| & 0 & 0 \\ -|r_{T1}^{g}(2)| & |r_{T2}^{g}(2)| & 0 & 0 & 0 & 0 \end{bmatrix} = \begin{bmatrix} 1 & 1 & 0 & 0 & 0 & 0 \\ 0 & 0 & 0 & 0 & 0 & 0 \\ 0 & 0 & 1 & 1 & 0 & 0 \\ 0 & 0 & 0 & 0 & 0 & 0 \\ 0 & 0 & 0.910 & -0.910 & 0 & 0 \\ 0.300 & -0.300 & 0 & 0 & 0 & 0 \end{bmatrix} \tag{2.9}$$

The force/control vector, U, is expressed as:

$$U = \begin{bmatrix} U_1 & U_2 & U_3 & U_4 & 0 & 0 \end{bmatrix}^T$$

where U_1, U_2, U_3 and U_4 are the thrust force of thruster 1, 2, 3, 4, respectively.
The vector of forces and torques created by the thrusters, is then expressed as:

$$\tau = \begin{bmatrix} 1 & 1 & 0 & 0 & 0 & 0 \\ 0 & 0 & 0 & 0 & 0 & 0 \\ 0 & 0 & 1 & 1 & 0 & 0 \\ 0 & 0 & 0 & 0 & 0 & 0 \\ 0 & 0 & -0.910 & 0.910 & 0 & 0 \\ -0.300 & 0.300 & 0 & 0 & 0 & 0 \end{bmatrix} \begin{bmatrix} U_1 \\ U_2 \\ U_3 \\ U_4 \\ 0 \\ 0 \end{bmatrix} \tag{2.10}$$

From the mapping matrix analysis, it is possible to understand that the AUV can only independently control 4 DOF. Despite the vehicle's underactuation, the metacentric height suggests that roll DOF is passively controlled. With respect to sway DOF, even though it is not passively nor actively controlled, the ability to control yaw allows for complete freedom of movement.

From this point on, the term common mode will be used to describe the external force in surge (τ_1) and external force in heave (τ_3); and the differential mode to describe the external torque about the z axis (τ_6) and external torque about the y axis (τ_5).

2.3 Dynamic Model Considerations

The methods used to estimate the vehicle's parameters induce two limitations [17]:

- Hydrodynamic coefficients estimation is only valid for angles of attack (α) and side-slip (β) within $-25°$ and $25°$;
- Added mass and inertia parameters are underestimated.

The underestimation is considered a common practice when modeling underwater vehicles [49]. Despite the fact that the result may load the model-based control, it does not necessarily compromise the performance significantly. On the other hand, for the overestimation scenario, the controller might compensate for forces that are not there, leading to abnormal control [49].

Furthermore, to improve the controller performance, it is possible to tune the controller gains resorting to experimental tests.

Chapter 3

Guidance

Guidance systems play a vital role in bringing autonomy to an AUV. Its purpose is to determine the reference values to be used in the control block. Thus, this chapter highlights two guidance laws: a waypoint and station-keeping guidance algorithm, characterized by steering by Line Of Sight (LOS) law and a path following algorithm characterized by the lookahead-based steering.

3.1 Waypoint and Station-keeping Guidance

3.1.1 Steering Guidance by Line Of Sight

The LOS guidance algorithm provides a reference angle (ψ_r) that will guide the AUV from its current position ($P(x, y)$) towards the waypoint ($W(x_k, y_k)$), figure 3.1. The solution for this problem is [19]:

$$\psi_r = \arctan\left(\frac{y_k - y}{x_k - x}\right) \quad \in [-\pi/2, \pi/2] \quad (3.1)$$

where ψ_r can be calculated by the four-quadrant version of $\arctan(y/x) \in [-\pi, \pi]$, usually defined as $\text{atan2}(y, x)$ in mathematically oriented programming languages [19]. The waypoint is reached if the vehicle lies inside a Circle Of Acceptance (COA) of radius ρ_k, around the waypoint. That is [19]:

$$d_k = \sqrt{(x_k - x)^2 + (y_k - y)^2} \leq \rho_k \quad (3.2)$$

According to [45], a good initial value for the size of ρ_k is $2 \times L$, where L stands for vehicle's length.

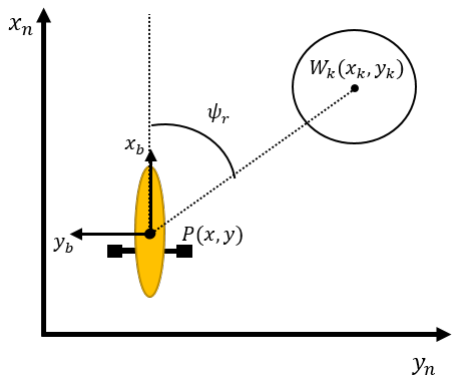

Figure 3.1: Line Of Sight guidance in the steering plane.

3.1.2 Reference Speed Law and Station-keeping

As in [14], the speed reference (u_{ref}) is calculated as function of the distance to the waypoint by:

$$u_d = k_u \sin^{-1}\left(\frac{d_u}{|d_u| + k_s}\right)\frac{2}{\pi} \quad (3.3)$$

where k_u is the upper limit of the reference speed, $k_s > 0$ a parameter for tuning, that adjust the reference speed value according to the distance error (figure 3.2), and d_u is defined as:

$$d_u = d_k - \rho_u \quad (3.4)$$

where ρ_u is a secondary COA. This is defined to avoid unnecessary usage of batteries with the thrusters once close to the waypoint. Soon as the vehicle exits this COA, due to external perturbations, the thrusters will bring the AUV back. Since $\rho_k > \rho_u$, the reference speed never reaches zero, unless the current waypoint is the last one.

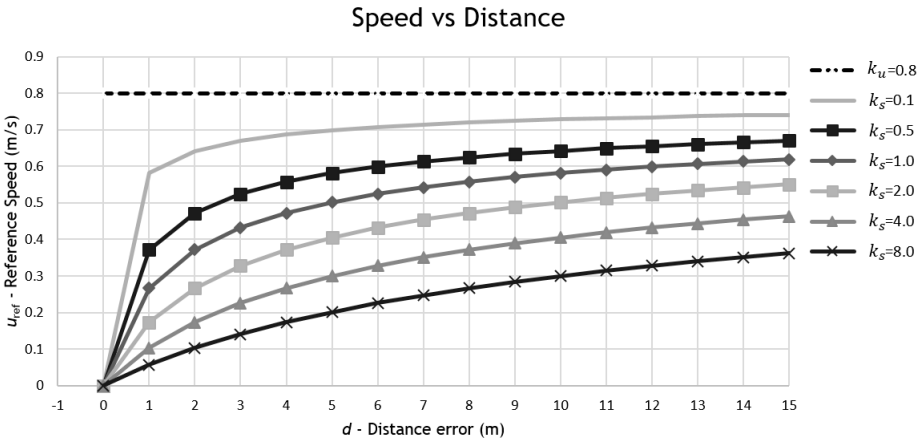

Figure 3.2: Influence of the parameter k_s in the reference speed.

3.1.3 Diving Guidance

Underwater vehicles often control depth by adjusting the pitch angle. In this case, the vertical common mode can be added to the equation. Therefore, there are two alternatives to dive, one via controlling pitch angle (differential mode), and the other via controlling heave speed (common mode).

For the differential mode, as in steering, the desired depth can be achieved through a combination of velocity and pitch angle. The reference pitch angle (θ_r) is given by:

$$\theta_r = \text{atan2}(z_k - z, x_k - x) \quad (3.5)$$

For the common mode, it is possible to calculate the vertical velocity as function of the vertical distance, as in the reference speed law. The new commanded vertical velocity (w_d) is given by:

$$w_d = k_w \sin^{-1}\left(\frac{e_z}{|e_z| + k_s}\right)\frac{2}{\pi} \quad (3.6)$$

where k_w is the upper limit of the vertical velocity, k_s a tuning parameter, and e_z the difference between the depth of the waypoint and the current depth of the AUV expressed as:

$$e_z = (z_k - z); \quad (3.7)$$

To devise a guidance law, there is a need to understand the advantages and disadvantages of both approaches for the diving scenario.
Concerning common mode, this strategy cannot be used effectively at high speeds since the power consumption increases due to reduction of thruster effectiveness with forward motion [50], and the increased cross-sectional area when diving generates higher hydrodynamic forces that counter the ones produced by the thrusters.
On the other hand, the pitching approach can take advantage of forward motion which is hydrodynamically more efficient. However, the effectiveness of pitch is as greater as the forward velocity.
Therefore, a unified control strategy that enables the operation of the AUV for an entire range of operating speeds is proposed. As in [51, 52], a weight factor for both θ_r and w_d that manages the contribution of each mode is added a function of the forward velocity. The resulting weights are:

$$\begin{aligned} W_{cm} &= 1 - \frac{1}{2}\left(\tanh\left(\frac{u - \frac{(u_{cmS}+u_{cmI})}{2}}{\sigma^*_{cm}}\right) + 1\right) \\ W_{dm} &= \frac{1}{2}\left(\tanh\left(\frac{u - \frac{(u_{dmS}+u_{dmI})}{2}}{\sigma^*_{dm}}\right) + 1\right) \end{aligned} \quad (3.8)$$

where u_{cmS}, u_{cmI}, u_{dmS} and u_{dmI} correspond to the upper limit and lower limit of the transitional speed zone for common mode and differential mode respectively, σ^*_{cm} and σ^*_{dm} shape the steepness of the transitional speed for both modes, i.e. for lower values the transition will be faster and vice-versa. The resulting action can be seen on figure 3.3.

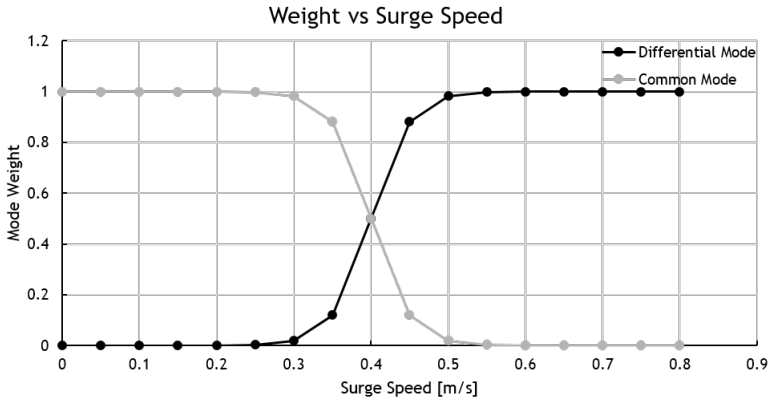

Figure 3.3: Mode weight funtion: u_{cmS}=u_{dmS}=0.5 m/s; u_{cmI}=u_{dmI}=0.3 m/s and σ^*_{cm}=σ^*_{dm}=0.05.

As velocity increases the common mode weight decreases and, at a predefined speed, only differential mode is nonzero, and vice-versa. Since the same thrusters provide both modes, it is important not to exceed the thruster capacity. For the real scenario, some experimental trials should be conducted to access the critical velocity values and power consumption, to adapt the above-presented law. However, two extra laws are suggested to tackle two problems in

different scenarios.
Let us consider the vehicle performing a two-dimensional path (xy plane). Once in the desired depth, it is useful to maintain the pitch angle at zero and avoid pitching up and down to correct depth deviations. Therefore, common mode weight (W_{cm}) should be 1 and the differential (W_{dm}) 0 if already at the reference depth.
The other scenario is that, when the vehicle starts the mission, the common mode will be on just for a few seconds, until it reaches the operational velocity. The initial effort to accelerate the vehicle to reference vertical speed will be worthless since right after the reference will be zero.

Therefore, in addition to 3.8, it is proposed:

$$\begin{aligned} \textsf{if} \quad & |e_z| < 1 \\ & W_{cm} = 1; \\ & W_{dm} = 0; \\ \textsf{elseif} \ & d > 2 \\ & W_{cm} = 0; \end{aligned} \tag{3.9}$$

The waypoint acceptances is now done for both horizontal and vertical coordinates. Therefore, the condition for acceptance becomes:

$$| \, z - z_r \, | \, | < \varepsilon_z \quad \wedge \quad d_k = \sqrt{(x_k - x)^2 + (y_k - y)^2} \leq \rho_k \tag{3.10}$$

where ε_z is the acceptance depth error.

3.1.4 Waypoint Following and Station Keeping Algorithm

Considering the aforementioned laws, figure 3.4 represents the implementation details of the waypoint following and station keeping algorithm.
Firstly, the n waypoint are defined as matrix in the form:

$$W = \begin{bmatrix} x_1 & y_1 & z_1 \\ x_2 & y_2 & z_2 \\ \vdots & \vdots & \vdots \\ x_n & y_n & z_n \end{bmatrix} \quad (3.11)$$

Then two variables are defined: K as the number of lines of waypoint matrix, i.e., the number of waypoints; and i as 1, which will be used to access the waypoint coordinates.
Secondly, the distance to the waypoint is calculated (d_k and e_z). If the vehicle is directed towards the last waypoint ($i = K$), the reference values are calculated. If not, the guidance will assess if the vehicle lies inside of the waypoint's COA. If the condition is true, guidance block will switch for the next waypoint, which corresponds to incrementing i.

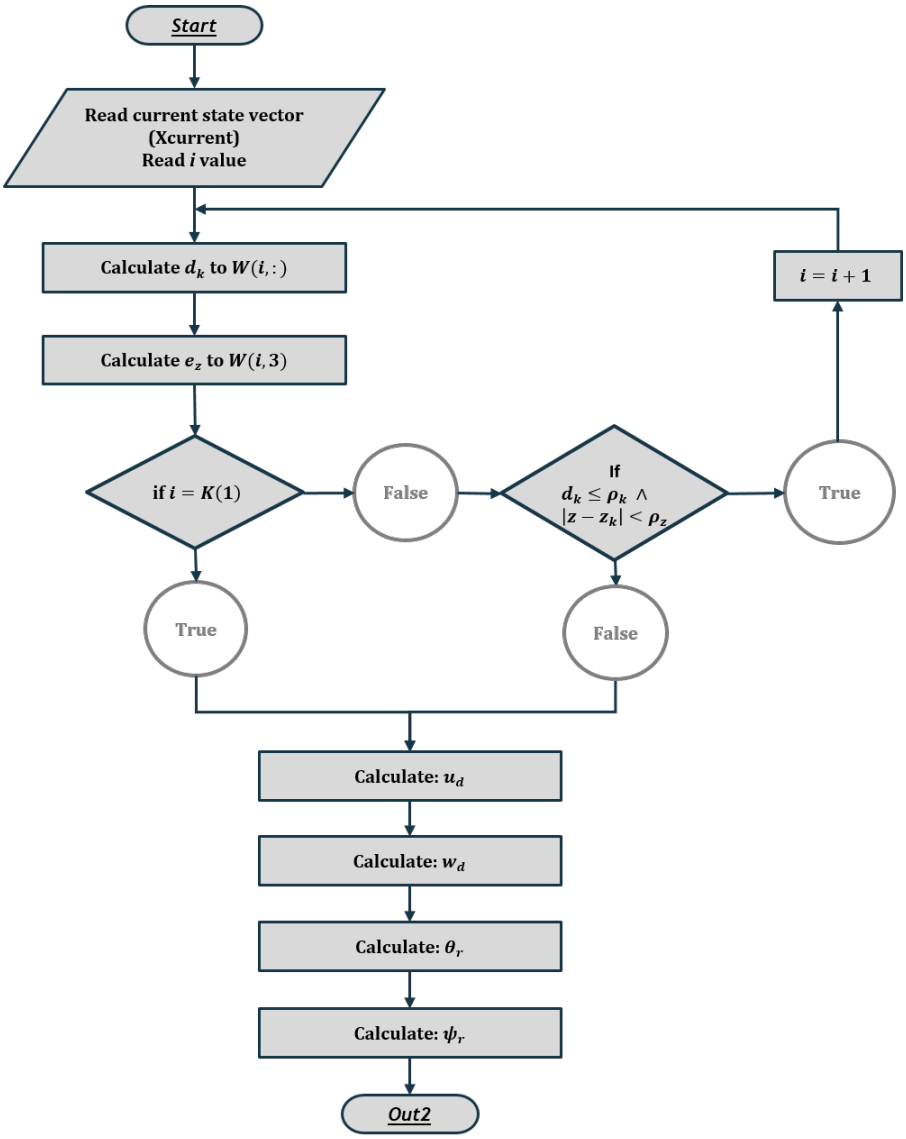

Figure 3.4: Waypoint follower and position holder fluxogram.

3.2 Path Following Guidance

For path following, the guidance laws are composed of speed and steering laws that can be rearranged for the specific control objectives [35]. Assuming positive speed, only assigning steering laws becomes necessary to accomplish the path following objective. The LOS method is frequently used for path following [15]. For simplicity, it will be considered that the path is two-dimensional. For the case where the path is defined at a different depth, the vehicle will reach it according to the above-derived depth law. The reference speed is calculated as in the previous section.

3.2.1 Lookahead-based Steering

The speed of the AUV is given by:

$$U(t) = \sqrt{\dot{x}(t)^2 + \dot{y}(t)^2 + \dot{z}(t)^2} = \sqrt{u(t)^2 + v(t)^2 + w(t)^2} \quad (3.12)$$

while steering is:

$$\psi(t) = \text{atan2}(\dot{y}, \dot{x}) \quad (3.13)$$

Considering a straight-line between two waypoint $W_k(x_k, y_k)$ and $W_{k+1}(x_{k+1}, y_{k+1})$, figure 3.5. The angle between the x_n axis and the straight line is obtained by:

$$\alpha_k = \text{atan2}(y_{k+1} - y_k, x_{k+1} - x_k) \quad (3.14)$$

Therefore, it is possible to calculate both along-track distance (tangential to path), s, and the cross-track error (normal to path), e, by [15]:

$$s(t) = [x(t) - x_k]\cos(\alpha_k) + [y(t) - y_k]\sin(\alpha_k) \quad (3.15)$$

$$e(t) = -[x(t) - x_k]\sin(\alpha_k) + [y(t) - y_k]\cos(\alpha_k) \quad (3.16)$$

where $(x(t), y(t))$ is the current position of the AUV in the horizontal plane.
For the lookahead-based steering, the steering assignment is divided into two terms:

$$\psi_{ref} = \alpha_k + \psi_{LA}(e) \quad (3.17)$$

where α_k is the path tangential angle [15], while the lookahead angle (ψ_{LA}) yields:

$$\psi_{LA}(e) = \arctan\left(\frac{-e}{\Delta}\right) \quad (3.18)$$

which corresponds to a velocity-path angle, which assures that the velocity is directed toward a point on the path. This point is located a distance $\Delta > 0$ ahead of the projection point, of the AUV, in the path [35].
According to the Pythagoras theorem, the expression for the lookahead distance is:

$$\Delta(t) = \sqrt{R^2 - e(t)^2} \quad (3.19)$$

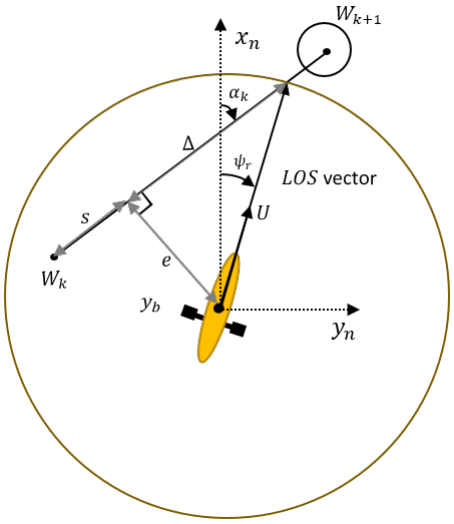

Figure 3.5: Path following scheme.

The steering law in equation 3.18 can also be interpreted as a saturating control law [15]:

$$\psi_{LA} = \arctan(-K_p e) \quad (3.20)$$

where $K_p(t) = 1/\Delta(t)$. Therefore, the steering behavior is aggressive for high values of K_p, which means small lookahead distances.
The along the track distance s should be used as switching criteria. Therefore, the condition is given by:

$$s_{k+1} - s(t) \leq \rho_k \quad (3.21)$$

where ρ_k represents the radius of the COA. As in section 3.1.4, in the end of the mission the vehicle will maintain within the COA of the last waypoint.

3.2.2 Path Following Algorithm

Figure 3.6 represents the implementation details about the path following algorithm. Following the same considerations as in section 3.1.4, where the waypoint matrix is defined as W, the variable i as 1 and K as the number of waypoints.
Firstly, α_k, $s(t)$, s_{k+1}, $e(t)$ and e_z are calculated. Then, it is verified if the vehicle is on the last straight line, which corresponds to $i+1 = K(1)$. In this case, the reference values are calculated. On the contrary, if the vehicle is not on the last straight line, guidance will assess if the switching condition is verified, which in this case i will be incremented to generate the next straight line.

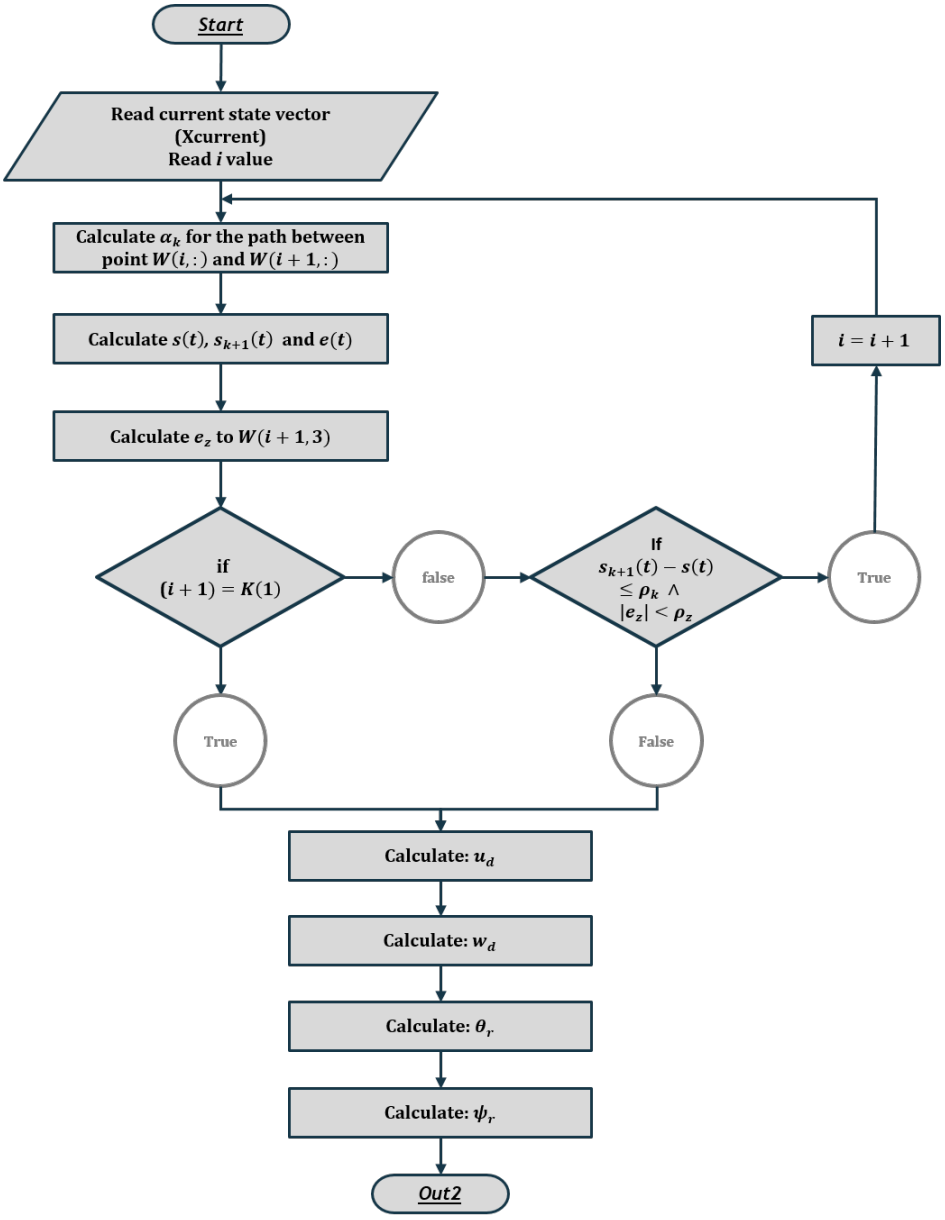

Figure 3.6: Path following fluxogram.

3.3 Block Representation

Simulink® is a block diagram environment integrated with *Matlab R2017a*[1]. The general structure for the guidance block is then represented in the block diagram of figure 3.7.

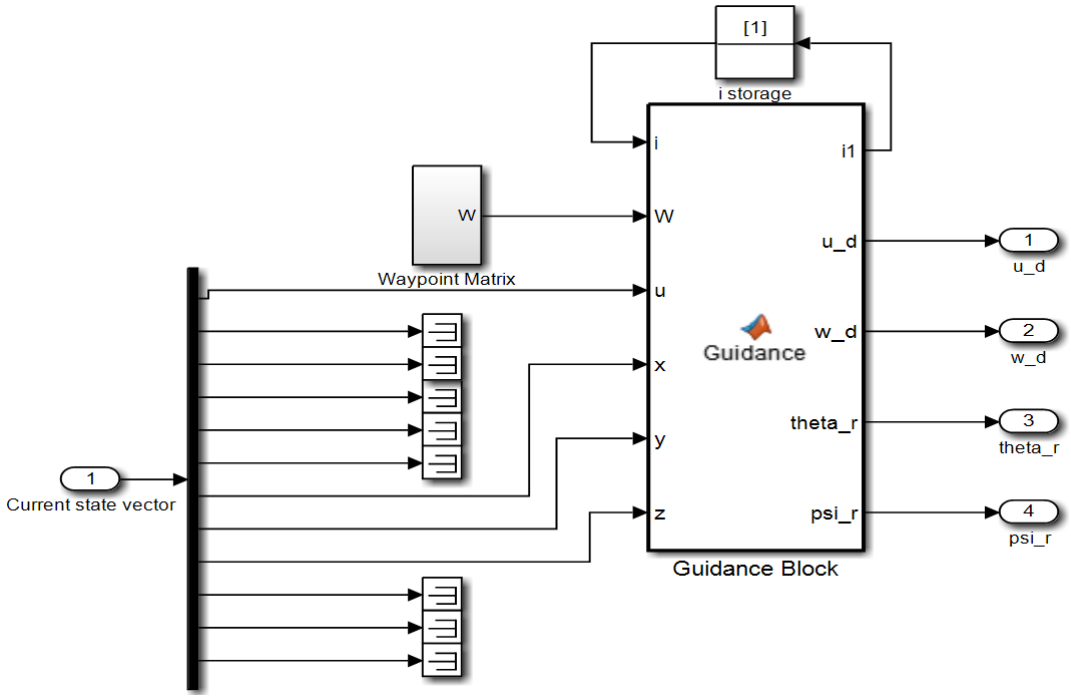

Figure 3.7: Waypoint follower and position holder diagram.

3.4 Guidance Considerations

The AUV can independently control 4 DOFs, namely surge, heave, pitch, and yaw (see section 2.9). This chapter highlights the laws which determine the reference values to manipulate these DOFs according to the control objective.
Two guidance solutions are hereby presented: following waypoints or a predefined path. However, if the AUV's mission is to map a predefined area, the waypoint solutions may not provide the expected mapping results. Since there is no spacial constraint, the vehicle may exit the predefined area in the presence of ocean currents, maintaining only the heading to the next waypoint (see figure 3.8). On the other hand, the path following solution would correct for the predefined path in case of external disturbances.

[1] ©1994-2017 The MathWorks, Inc.

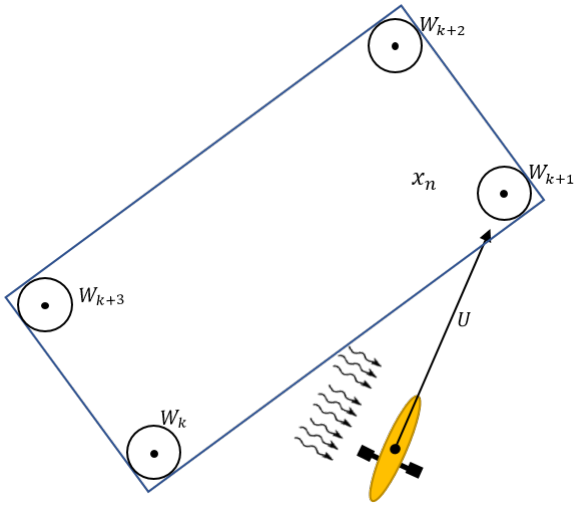

Figure 3.8: Illustration of the waypoint following scenario in the presence of ocean currents.

Concerning the diving maneuver, to switch between diving modes, two velocity dependent weights are defined. The speed values presented in the graph from figure 3.3 were assumed based on the longitudinal speed envelope of the AUV, considering the midpoint (0.4 m/s) as the transitional velocity. For a proper choice of these values, some trials should be conducted to understand the loss of effectiveness of the vertical thrusters, as well the hydrodynamic efficiency for different velocities. However, two situations arise regarding the considerations of the dynamic model when diving (see section 2.3).
Since hydrodynamic coefficients are valid for angles-of-attack within $-25°$ and $25°$, for differential mode, the value of the reference pitch angle is limited to $-25° \leq \theta_r \leq 25°$. However, for common mode, the angle-of-attack will reach $\pm 90°$. For the purpose of this thesis, it will be assumed that the hydrodynamic estimation is valid for this situation. The implications of this assumption are addressed in section 4.2.

Chapter 4

Controller Design

Having presented the mathematical equations that rule the dynamics of the AUV (chapter 2), it is now possible to formulate the controller. To develop linear controllers, the dynamic model should be adapted. On this chapter, the linearization procedure will be presented. Then, two linear control designs, namely PID and LQR. Respective performance and stability are addressed. To map the desired control forces generated by PID and LQR into commands of different actuators a control allocation law is devised.

4.1 Linearization of the AUV model

To design a linear control system firstly is necessary to obtain a linear model. The non-linear model for the AUV, equations 1.24 and 1.25, following a state-space formulation yields [53]:

$$\begin{bmatrix} \dot{\nu} \\ \dot{\eta} \end{bmatrix} = \begin{bmatrix} -M^{-1}(C(\nu)\nu + D(\nu)\nu + g(\eta)) \\ J(\eta)\nu \end{bmatrix} + \begin{bmatrix} M^{-1} \\ 0 \end{bmatrix} \tau \quad (4.1)$$

where the state vector dimension is 12, 6 components expressed in body-fixed frame and 6 on the inertial frame. The objective is to transform into the form:

$$\dot{x} = Ax + B\mathbf{u} \quad (4.2)$$

where A and B are the associated matrices with the linearized equation of motion, and $\mathbf{u}$ the control input.

4.1.1 Linearized Model

The linear equations can be formulated by linearizing about an equilibrium point [54, 29]. Let the perturbations be described as:

$$\Delta\nu = \nu - \nu_0 \quad (4.3)$$

$$\Delta\eta = \eta - \eta_0 \quad (4.4)$$

where ν_0 and η_o are the equilibrium points. Introducing the following vector notation [55]:

$$f_c(\nu) = C(\nu)\nu \quad (4.5)$$

$$f_d(\nu) = D(\nu)\nu \quad (4.6)$$

The linearization procedure is based on the expansion of the nonlinear function into a Taylor series [38]. Therefore, neglecting the high order terms [38], equations 1.24 and 1.25 can be

linearized as follows:

$$M\Delta\dot{\nu} + \left.\frac{\partial f_c(\nu)}{\partial \nu}\right|_{\nu_0} \Delta\nu + \left.\frac{\partial f_d(\nu)}{\partial \nu}\right|_{\nu_0} \Delta\nu + \left.\frac{\partial g(\eta)}{\partial \eta}\right|_{\eta_0} \Delta\eta = \Delta\tau \quad (4.7)$$

$$\dot{\eta} \approx J(\eta_0)\nu_0 + \left.\frac{\partial J(\eta)\nu}{\partial \nu}\right|_{\nu_0\eta_0} \Delta\nu + \left.\frac{\partial J(\eta)\nu}{\partial \eta}\right|_{\nu_0\eta_0} \Delta\eta \quad (4.8)$$

Replacing $\dot{\eta} = \dot{\eta}_0 + \Delta\dot{\eta}_0$, and because $\dot{\eta}_0 = J(\eta_0)\nu_0$ the equation 4.8 reduces to:

$$\Delta\dot{\eta} \approx J(\eta_0)\Delta\nu + \left.\frac{\partial J(\eta)}{\partial \eta}\right|_{\eta_0} \nu_0\Delta\eta \quad (4.9)$$

Defining the state-space as $x = (x_1, x_2)^T$, where $x_1 = \Delta\nu$ and $x_2 = \Delta\eta$, the linear equations of motion are given by:

$$M\dot{x}_1 + Cx_1 + Dx_1 + Gx_2 = \tau \quad (4.10)$$

$$\dot{x}_2 = Jx_1 + J^* \quad (4.11)$$

where:

$$C = \left.\frac{\partial f_c(\nu)}{\partial \nu}\right|_{\nu_0}; \qquad D = \left.\frac{\partial f_d(\nu)}{\partial \nu}\right|_{\nu_0}; \qquad G = \left.\frac{\partial g(\eta)}{\partial \eta}\right|_{\eta_0};$$

$$J = J(\eta_0); \qquad J^* = \left.\frac{\partial J(\eta)}{\partial \eta}\right|_{\eta_0} \nu_0;$$

Finally, assuming $\tau = \mathbf{u}$, the equations 4.10 and 4.11 lead to the following state-space model [55]:

$$\begin{bmatrix}\dot{x}_1 \\ \dot{x}_2\end{bmatrix} = \begin{bmatrix}-M^{-1}[C+D] & -M^{-1}G \\ J & J^*\end{bmatrix}\begin{bmatrix}x_1 \\ x_2\end{bmatrix} + \begin{bmatrix}M^{-1} \\ 0\end{bmatrix}\mathbf{u} \quad (4.12)$$

In many AUV applications, it is reasonable to assume that the AUV is moving with nonzero surge, u_0, and heave, w_0 speed [54]. Therefore the matrices from equations 4.10 and 4.11 are given by:

- The mass term [55]: The term of mass is the sum of the rigid body term, equation 1.6, with the added mass term, 1.11.
- The Coriolis term [55]:

$$C = \begin{bmatrix}0 & C_{12} \\ -C_{12}^T & C_{22}\end{bmatrix} \quad (4.13)$$

$$C_{12} = \begin{bmatrix}0 & -X_{\dot{w}}u_0 + (m - Z_{\dot{w}})w_0 & X_{\dot{v}}u_0 + Y_{\dot{w}}w_0 \\ X_{\dot{w}}u_0 - (m - Z_{\dot{w}})w_0 & 0 & (m - X_{\dot{u}})u_0 - X_{\dot{w}}w_0 \\ -X_{\dot{v}}u_0 - Y_{\dot{w}}w_0 & -(m - X_{\dot{u}})u_0 + X_{\dot{w}}w_0 & 0\end{bmatrix} \quad (4.14)$$

$$C_{22} = \begin{bmatrix}0 & -(X_{\dot{r}}u_0 + Z_{\dot{r}}w_0) & X_{\dot{q}}u_0 + Z_{\dot{q}}w_0 \\ X_{\dot{r}}u_0 + Z_{\dot{r}}w_0 & 0 & -(X_{\dot{p}}u_0 + Z_{\dot{p}}w_0) \\ -(X_{\dot{q}}u_0 + Z_{\dot{q}}w_0) & X_{\dot{p}}u_0 + Z_{\dot{p}}w_0 & 0\end{bmatrix} \quad (4.15)$$

- Hydrodynamic damping term [55]:
  Since the high order terms are neglected [38, 29], the damping matrix is simply equal to the linear damping term (D_l) from equation 1.15.

- Hydrostatic term [55]: Since the vehicle is not neutrally buoyant i.e. $B \neq W$, the hydrostatic term is given by:

$$G = \begin{bmatrix} 0 & 0 & 0 & 0 & (W-B) & 0 \\ 0 & 0 & 0 & -(W-B) & 0 & 0 \\ 0 & 0 & 0 & 0 & 0 & 0 \\ 0 & 0 & 0 & (z_g W - z_B B) & 0 & 0 \\ 0 & 0 & 0 & 0 & (z_g W - z_B B) & 0 \\ 0 & 0 & 0 & -(x_g W - x_B B) & -(y_g W - y_B B) & 0 \end{bmatrix} \quad (4.16)$$

4.2 Linear Model Considerations

The above derived linear system has two nonzero linearization points, namely u_0 and w_0. Since no flight envelope is available, some assumptions are mandatory to obtain the controllers.

As mentioned before, for this thesis purpose, it is being considered the data acquisition operational scenario (see section 1.1). According to CFD analysis performed by engineers at CEiiA, the AUV is intended to perform missions at a cruise speed of 0.8 m/s. Therefore, a good linearization value for surge in cruise is $u_0 = 0.8$ m/s.
For w_0, the AUV has two distinct ways to perform diving: through differential thrust, controlling pitch angle; or through common mode, controlling heave speed.
Diving with differential mode leads to heave speeds up to 0.05 m/s, suggesting that it could be neglected [23].
For common mode, in addition to higher velocities (up to 0.4 m/s), it leads to angles-of-attack of $\pm 90^\circ$, which means that the hydrodynamic coefficients are not valid [17]. However, this will not be considered for this thesis. This assumption should be further addressed once the coefficients are updated. Three scenarios can occur: there is no need for altering the controller parameters; a simple change in the common mode controller gains, or the inclusion of another linearization point, and with this adopting a gain-scheduled approach.
Therefore, since the nominal mission is planar (xy), the heave speed linearization value to be considered is $w_0 = 0$ m/s, resulting in the linearization point $\nu_0 = [0.8 \quad 0 \quad 0 \quad 0 \quad 0 \quad 0]^T$.

A standard approach in controller design is to reduce the order of the dynamic model [55]. Healey and Marco [45] suggest that, for reduced velocities, the 6DOF linear differential equations can be divided into three non-interactive (or lightly interacting) subsystems for speed, steering, and diving. The work presented in [17] also suggests that decoupling the lateral and longitudinal subsystems is valid for this AUV.

4.3 PID control

As mention before, PID control has successfully been implemented in many nonlinear systems [22]. As in [23] the 6DOF dynamic model is divided into three subsystems. The subsystems and their state variables are [55]:

1. Speed system state: $u(t)$;
2. Steering system states: $v(t)$, $r(t)$ and $\psi(t)$;
3. Diving system states: $w(t)$, $q(t)$ and $\theta(t)$.

The roll dynamic ($p(t)$ and $\phi(t)$) is neglected [23]. That is motivated by the fact that the roll is passively controlled (see section 2.2.4).
The Matlab PID tuning tool [56] allowed for the first estimation of the gain values through the generation of Bode and step plots. Then, by applying the controller to the nonlinear dynamic model, the gains were manually tuned to fit the desired performance. The process can be seen in the figure 4.1.

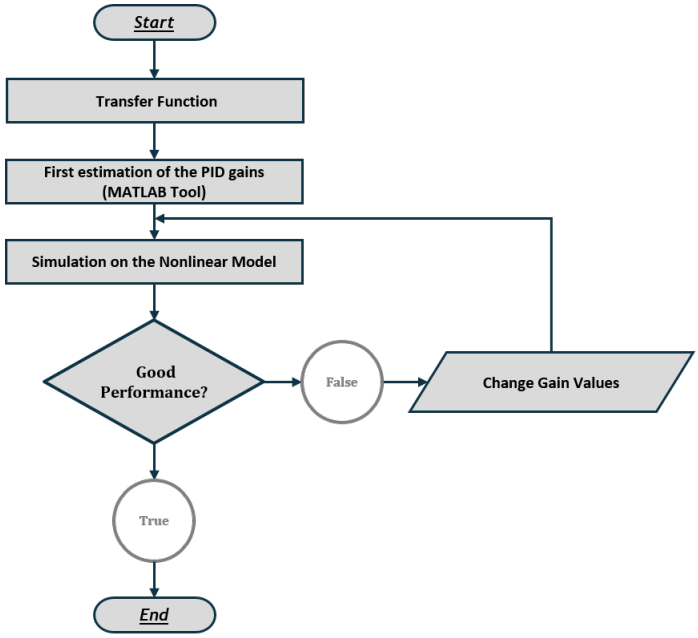

Figure 4.1: PID design process.

4.3.1 Speed Controller

The common mode (τ_1) allows for the vehicle to control motion in surge. Surge differential equation is:

$$(m - X_{\dot{u}})\dot{u} - X_u u = \tau_1 \quad (4.17)$$

Replacing values and applying the Laplace transform, the transfer function is given by:

$$\frac{u(s)}{\tau_1(s)} = \frac{0.0022}{s + 0.0544} \quad (4.18)$$

A PID control was applied, taking the form [23]:

$$\tau_1 = K_p\tilde{u} + K_i \int_0^t \tilde{u}(\tau)d\tau + K_d\frac{d\tilde{u}}{dt} \quad (4.19)$$

where $\tilde{u} = u_d - u$. To confine the output of the controller to the operational bounds of the thrusters, saturation blocks are used. The back-calculation method is used to avoid integral windup. Since the poles are located in the LHP, the system is stable [40]. From the analysis of Bode plot from figure 4.2, stability margins can be inferred. The infinity gain margin and 84.7 degrees of phase margin, in addition to maximum sensitivity of 1, suggests that the system is robust to external disturbances [18, 43].

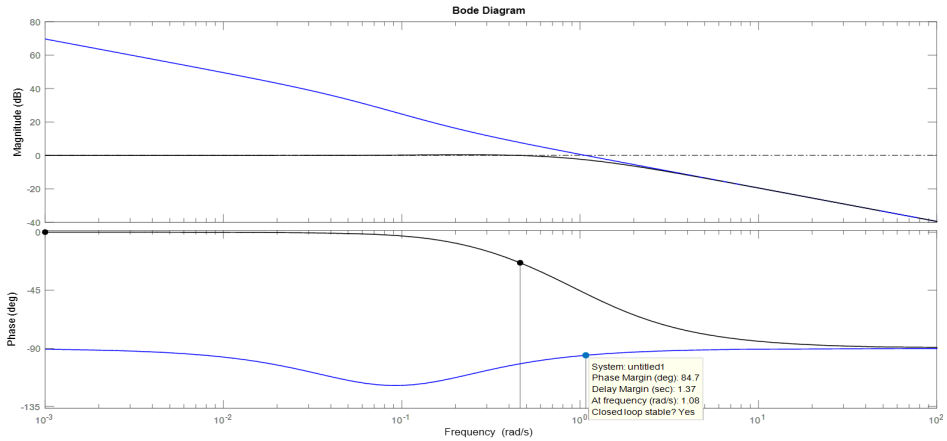

Figure 4.2: Open- and closed-loop Bode plot of PID speed controller.

To assess the performance the controller, it is defined a time-varying reference surge speed, and the resulting tracking of the controller using the nonlinear model can be seen in the figure 4.3.

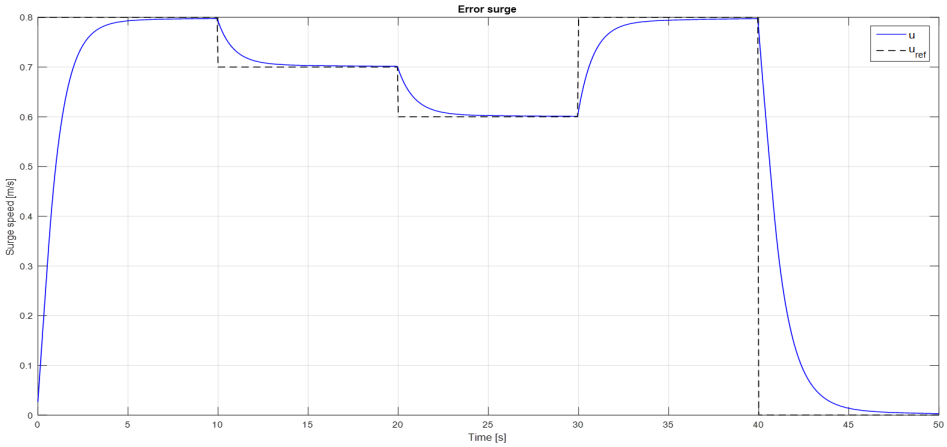

Figure 4.3: PID speed controller simulation.

4.3.2 Heading Controller

Heading control is accomplished through the differential mode (τ_6), i.e., the longitudinal thrusters with different thrust output. For this subsystem, the state variables to account for are: $v(t), r(t)$

and $\psi(t)$. The equations are [23]:

$$(m - Y_{\dot{v}})\dot{v} - Y_{\dot{r}}\dot{r} - Y_v v(-Y_r + mu_0)r = \tau_2 \quad (4.20)$$

$$-N_{\dot{v}}\dot{v} + (I_z - N_{\dot{r}})\dot{r} - N_v v - N_r r = \tau_6 \quad (4.21)$$

$$\dot{\psi} \approx r \quad (4.22)$$

where τ_2 is 0 since sway is not actively controlled. Expressing in state-space form yields:

$$\begin{bmatrix} m - Y_{\dot{v}} & -Y_{\dot{r}} & 0 \\ -N_{\dot{v}} & (I_z - N_{\dot{r}}) & 0 \\ 0 & 0 & 1 \end{bmatrix} \begin{bmatrix} \dot{v} \\ \dot{r} \\ \dot{\psi} \end{bmatrix} + \begin{bmatrix} -Y_v v & -Y_r + mu_0 & 0 \\ -N_v & -N_r & 0 \\ 0 & -1 & 0 \end{bmatrix} \begin{bmatrix} v \\ r \\ \psi \end{bmatrix} = \begin{bmatrix} 0 \\ \tau_6 \\ 0 \end{bmatrix} \quad (4.23)$$

Rearranging to $\dot{x} = Ax + B\mathbf{u}$ form, where $x = [v \quad r \quad \psi]^T$, for the above mentioned linearization point yields:

$$\begin{bmatrix} \dot{v} \\ \dot{r} \\ \dot{\psi} \end{bmatrix} = \begin{bmatrix} -0.1653 & -0.4167 & 0 \\ 0.5672 & -0.0503 & 0 \\ 0 & 1.0000 & 0 \end{bmatrix} \begin{bmatrix} v \\ r \\ \psi \end{bmatrix} + \begin{bmatrix} -0.0003 \\ 0.0037 \\ 0 \end{bmatrix} \tau_6 \quad (4.24)$$

The transfer function for this subsystem is:

$$\frac{\psi(s)}{\tau_6(s)} = \frac{0.003729s + 0.0009888}{s^3 + 0.3549s^2 + 0.2147s} \quad (4.25)$$

The heading measurement (ψ) is given by a compass reading and the yaw rate (r) by a gyroscope. As in [23] a PD controller is implemented. Moreover, the derivative term provides additional phase margin, which increases robustness [23]. The result is:

$$\tau_6 = K_p\tilde{\psi} - K_d r \quad (4.26)$$

where $\tilde{\psi} = \psi_{ref} - \psi$. Special attention to the yaw error. It must be redefined, as [14]:

$$\begin{aligned} &\text{if} \quad \tilde{\psi} > \pi \\ &\tilde{\psi} = \tilde{\psi} - 2\pi \\ &\text{if} \quad \tilde{\psi} < -\pi \\ &\tilde{\psi} = \tilde{\psi} + 2\pi \end{aligned} \quad (4.27)$$

Once more, the closed-loop poles are located in the left half plane; therefore the system is stable. The analysis of the Bode plot in figure 4.4, shows that the open-loop system has infinity gain margin and 84.9 degrees of phase margin, ensuring robustness to external disturbances.

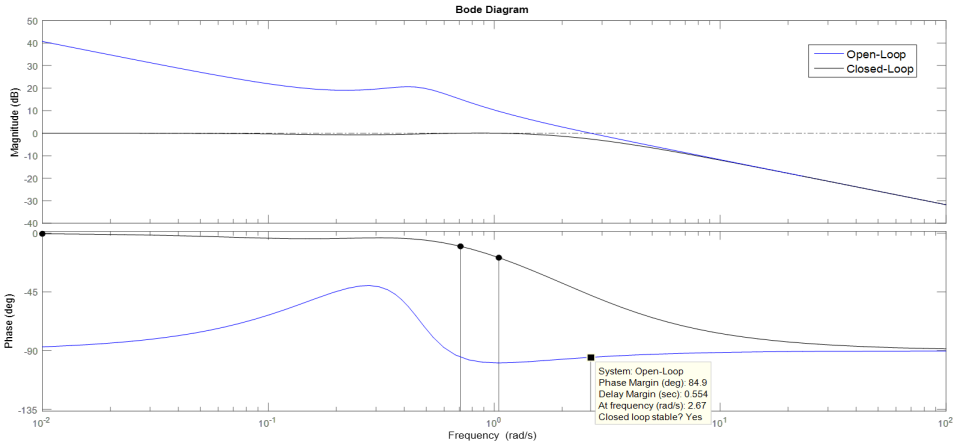

Figure 4.4: Open- and closed-loop Bode plot of PD heading controller.

To assess the performance, it is defined a time varying yaw reference, and the tracking result can be seen in the figure 4.5. The common mode (τ_1) was fixed at zero.

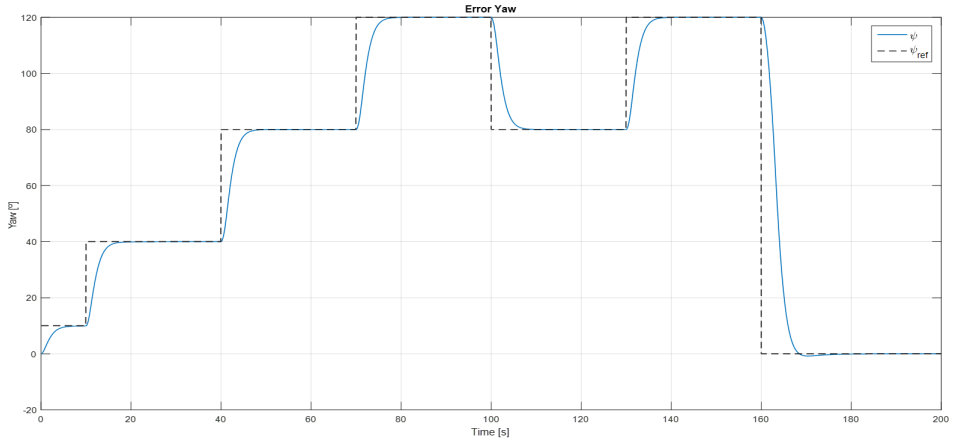

Figure 4.5: PD heading controller simulation.

4.3.3 Depth Controller

For the depth control, as stated in section 3.1.3, there is a common mode (τ_3) and a differential mode (τ_5). The associated state variables are: $w(t), q(t)$ and $\theta(t)$. Since $z(t)$ is controlled by the heave speed (equation 3.6), it will not be included. The resulting equations are:

$$(m - Z_{\dot{w}})\dot{w} - Z_{\dot{q}}\dot{q} - Z_w w + ((m - X_{\dot{u}})u_0 - Z_q)q = \tau_3 \quad (4.28)$$

$$-M_{\dot{w}}\dot{w} + (I_y - M_{\dot{q}})\dot{q} + ((m - X_{\dot{u}})u_0 - M_w)w - M_q q + (z_g W + z_B B)\theta = \tau_5 \quad (4.29)$$

$$\dot{\theta} \approx q \quad (4.30)$$

Expressing in the compact form yields:

$$\begin{bmatrix} m - Z_{\dot{W}} & -Z_{\dot{q}} & 0 & \\ -M_{\dot{w}} & (I_y - M_{\dot{q}}) & 0 & \\ 0 & 0 & 1 & 0 \end{bmatrix} \begin{bmatrix} \dot{w} \\ \dot{q} \\ \dot{\theta} \end{bmatrix} + \begin{bmatrix} -Z_w & (m - X_{\dot{u}})u_0 - Z_q & 0 \\ (m - X_{\dot{u}})u_0 - M_w & -M_q & (z_g W + z_B B) \\ 0 & -1 & 0 \end{bmatrix} \begin{bmatrix} w \\ q \\ \theta \end{bmatrix} = \begin{bmatrix} \tau_3 \\ \tau_5 \\ 0 \end{bmatrix} \tag{4.31}$$

Once more rearranging to $\dot{x} = Ax + B\mathbf{u}$ form, where $x = [w \quad q \quad \theta]^T$, yields:

$$\begin{bmatrix} \dot{w} \\ \dot{q} \\ \dot{\theta} \end{bmatrix} = \begin{bmatrix} -0.2604 & 0.4482 & 0.0974 \\ -0.7934 & -0.3070 & -1.0902 \\ 0 & 1.0000 & 0 \end{bmatrix} \begin{bmatrix} w \\ q \\ \theta \end{bmatrix} + \begin{bmatrix} 0.0012 & -0.0003 \\ -0.0003 & 0.0034 \\ 0 & 0 \end{bmatrix} \begin{bmatrix} \tau_3 \\ \tau_5 \end{bmatrix} \tag{4.32}$$

Through the differential mode (τ_5), the controller will approach θ_r angle.
The transfer function of heave speed is:

$$\frac{w(s)}{\tau_3(s)} = \frac{0.00119s^2 + 0.0002308s + 0.001268}{s^3 + 0.5675s^2 + 1.526s + 0.3612} \tag{4.33}$$

After several tests combining P, I and D, it is designed a PI controller according to [23]:

$$\tau_3 = K_p\tilde{w} + K_i \int_0^t \tilde{w}(\tau)d\tau \tag{4.34}$$

where $\tilde{w} = w_d - w$, where the measurement of depth is done by a pressure sensor. To avoid integral windup the back-calculation method is used. The closed-loop poles are located in the left half plane; therefore the system is stable. The Bode plot from figure 4.6 shows infinity gain margin and 78.2 degrees of phase margin, therefore the system it is considered robust to external disturbances [43].

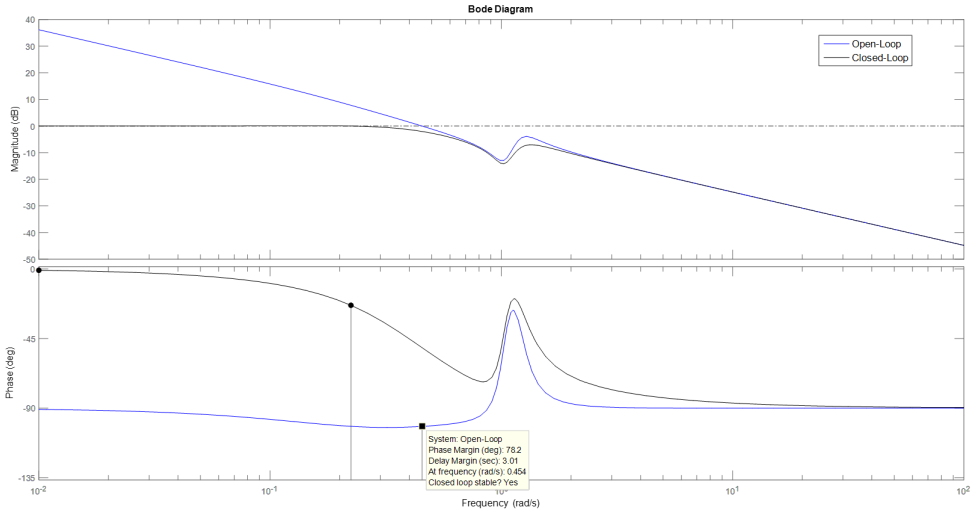

Figure 4.6: Open- and closed-loop Bode plot of PID heave controller.

To assess the performance, the controller is applied to the nonlinear dynamic model, where τ_1 and τ_6 are maintained at zero. The resulting tracking is presented in figure 4.7.

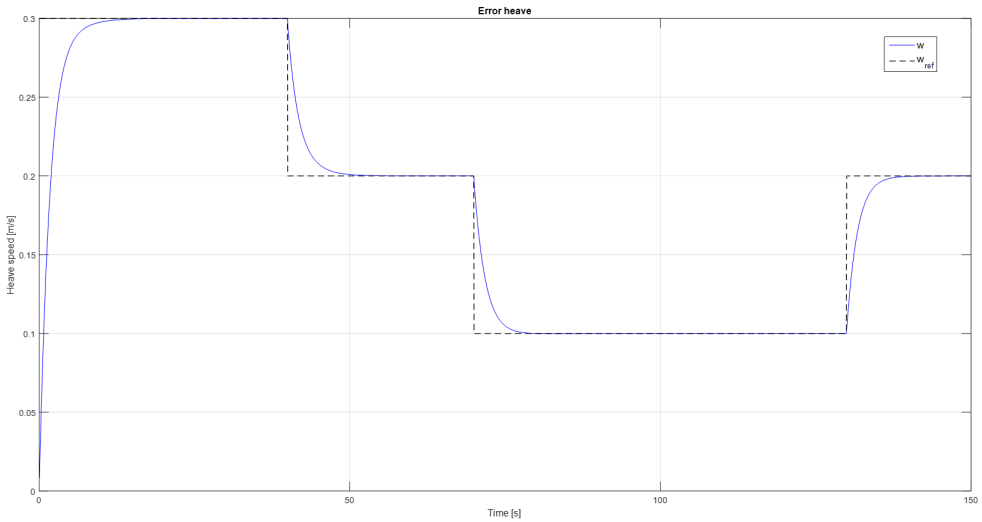

Figure 4.7: PID heave controller simulation.

The transfer function for the pitch controller is:

$$\frac{\theta(s)}{\tau_5(s)} = \frac{0.003362s + 0.001114}{s^3 + 0.5675s^2 + 1.526s + 0.3612} \quad (4.35)$$

Implementing a PID controller:

$$\tau_5 = K_p\tilde{\theta} + K_i \int_0^t \tilde{\theta}(\tau)d\tau + K_d\frac{d\tilde{\theta}}{dt} \quad (4.36)$$

where $\tilde{\theta} = \theta_{ref} - \theta$. The negative closed loop poles assure the stability of the system. The stability margins seen in figure 4.8, i.e., infinity gain margin and the 85.6 degrees of phase margin, allows for the conclusion that the control system is robust to external disturbances.

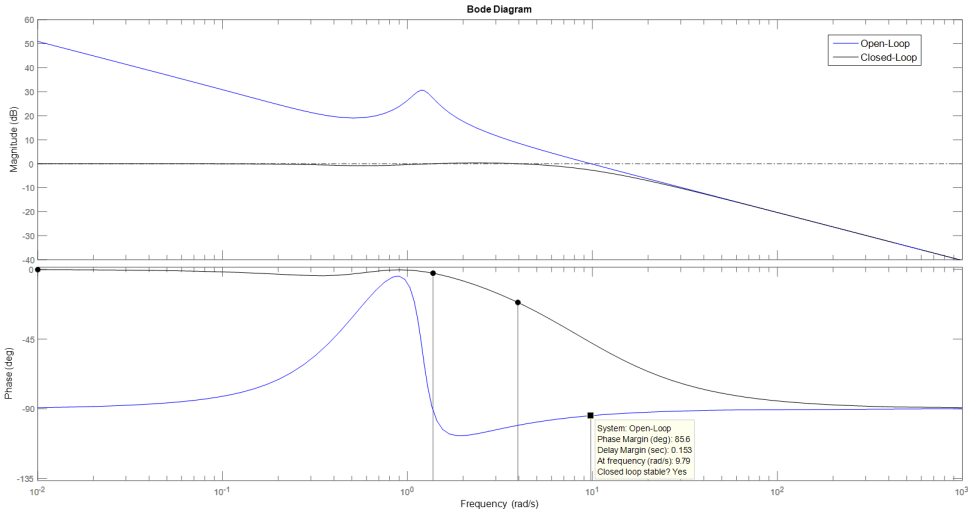

Figure 4.8: Open- and closed-loop Bode plot for the PID pitch controller.

To assess the performance, the controller is once more applied to the nonlinear dynamic model and τ_1,τ_3 and τ_6 are maintained at zero. The resulting tracking is presented in figure 4.9.

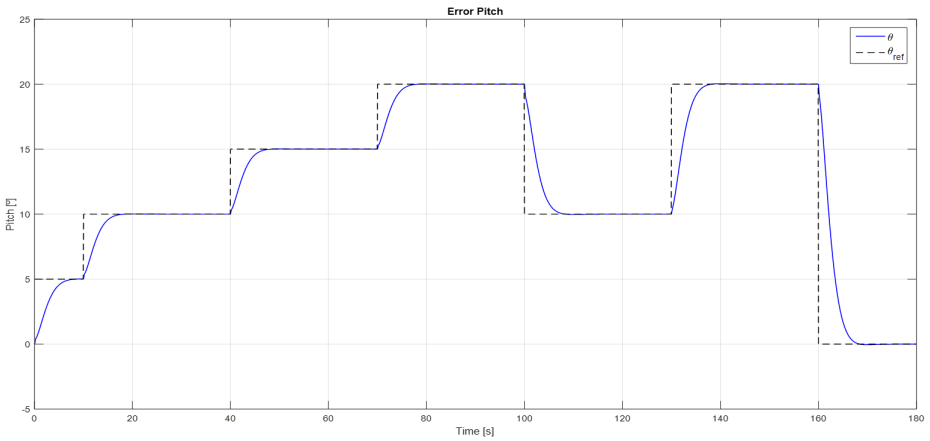

Figure 4.9: PID pitch controller simulation.

4.3.4 Simulink Representation

As in chapter 3.3, the block diagram of the PID can be represented by figure 4.10.

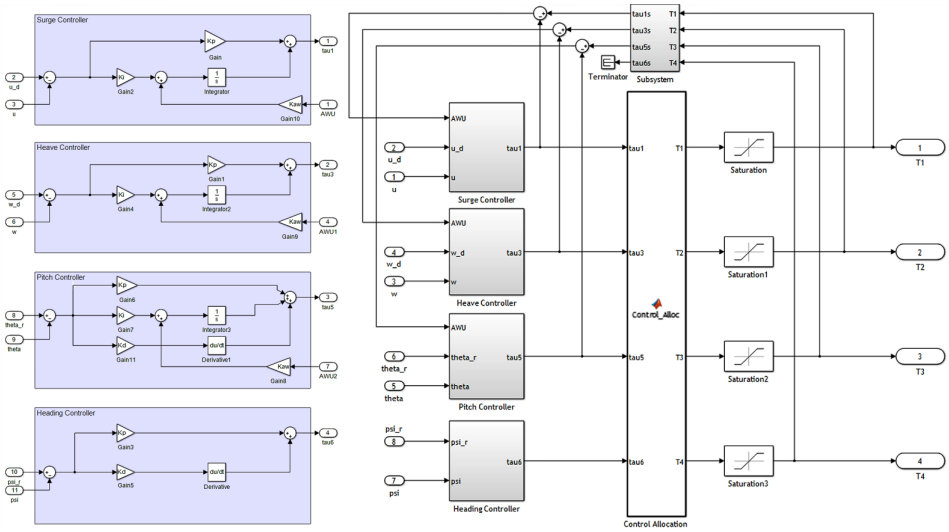

Figure 4.10: Simulink implementation of PID control.

4.4 LQR control

The linear dynamic system is divided into [17, 29]: longitudinal subsystem and lateral subsystem. For the initial choice of the weights Q and R, it was used the method described in [43], where Q is initiated as the identity matrix ($Q = I$) and R as the identity matrix multiplied by a constant ρ ($R = \rho I$). Then by changing ρ, it is possible to tune the response, usually decreasing it. If the response still far from the desired, the respective diagonal term from Q is altered. The process used to design the controllers is presented in figure 4.11.

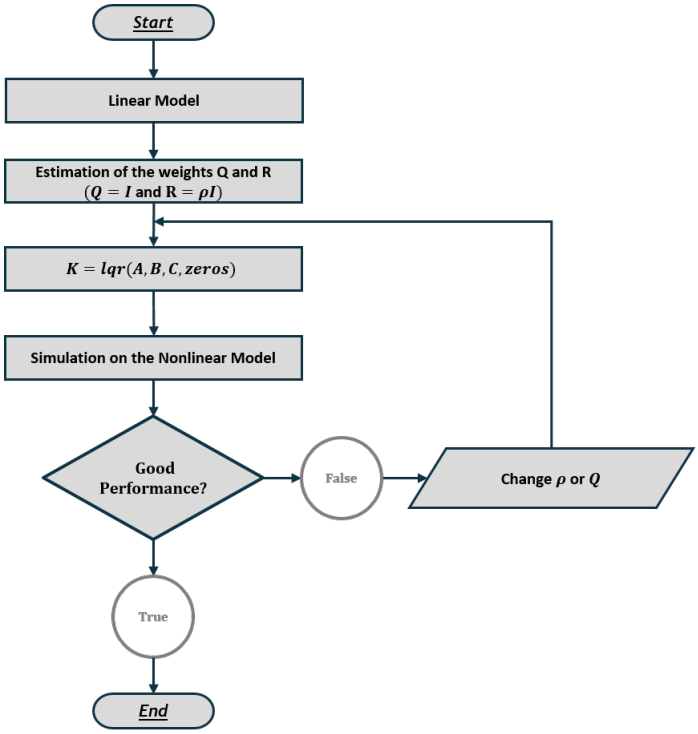

Figure 4.11: LQR design process.

4.4.1 Longitudinal Controller

The longitudinal controller is dedicated to control the speed (τ_1) and depth (τ_3 for the common mode and τ_5 for the differential mode). The sate vector is constituted by the states: u, w and θ. Since z is controlled through w and θ (see section 3.1.3) it is not included into the state vector. For the longitudinal state vector x_L, the state and input matrices from the linearized model for the longitudinal controller are:

$$\begin{bmatrix} \Delta\dot{u} \\ \Delta\dot{w} \\ \Delta\dot{q} \\ \Delta\dot{\theta} \end{bmatrix} = A_L x_L + B_L \mathbf{u}_L \quad (4.37)$$

To the matrix of equation 4.31, is added the surge state, resulting in:

$$A_L = \begin{bmatrix} -0.0544 & -0.0031 & -0.0012 & 0.0045 \\ 0.0022 & -0.2604 & 0.4482 & 0.0974 \\ -0.0009 & -0.7934 & -0.3070 & -1.0902 \\ 0 & 0 & 1.0000 & 0 \end{bmatrix}; \quad x_L = \begin{bmatrix} u - u_0 \\ w - w_0 \\ q - q_0 \\ \theta - \theta_0 \end{bmatrix}; \quad (4.38)$$

$$B_L = \begin{bmatrix} 0.0022 & -0.0000 & 0.0000 \\ -0.0000 & 0.0012 & -0.0003 \\ 0.0000 & -0.0003 & 0.0034 \\ 0 & 0 & 0 \end{bmatrix}$$

Reminding that the state for the linear system is defined by $[x_1, x_2]^T = [\Delta\nu, \Delta\eta]^T$ and that the input vector is inserted as a perturbation to the equilibrium point, the desired state is:

$$x_{dL} = \begin{bmatrix} u_r - u_o \\ w_r - w_0 \\ 0 \\ \theta_r - \theta_0 \end{bmatrix} \quad (4.39)$$

Therefore, the control input $\mathbf{u}_L$, according to equation 1.41, yields:

$$\mathbf{u}_L = -K_L(x_L - x_{dL}) = -K_H \begin{bmatrix} u - u_0 - (u_d - u_0) \\ w - w_0 - (w_d - w_0) \\ q - q_0 \\ \theta - \theta_0 - (\theta_r - \theta_0) \end{bmatrix} \quad (4.40)$$

Since steady state errors were detected, three integrative states were added, namely the surge error ($u - u_d$), heave error ($w - w_d$) and pitch error ($\theta - \theta_r$), resulting in:

$$x_{\int u} = \int_0^t (u - u_d) d\tau \quad (4.41)$$

$$x_{\int w} = \int_0^t (w - w_d) d\tau \quad (4.42)$$

$$x_{\int \theta} = \int_0^t (\theta - \theta_r) d\tau \quad (4.43)$$

Therefore, the new state-space equation is:

$$\begin{bmatrix} \dot{x}_L \\ \dot{x}_{\int u} \\ \dot{x}_{\int \theta} \end{bmatrix} = \begin{bmatrix} & A_L & & & & 0_{5\times3} \\ \begin{bmatrix} 1 & 0 & 0 & 0 & 0 \\ 0 & 1 & 0 & 0 & 0 \\ 0 & 0 & 0 & 1 & 0 \end{bmatrix} & & & & 0_{3\times3} \end{bmatrix} \begin{bmatrix} x_L \\ x_{\int u} \\ x_{\int \theta} \end{bmatrix} + \begin{bmatrix} B_L \\ 0_{1\times3} \\ 0_{1\times3} \\ 0_{1\times3} \end{bmatrix} \mathbf{u_L} \quad (4.44)$$

Replacing the values, the new state matrix is given by:

$$A_{La} = \begin{bmatrix} -0.0544 & -0.0031 & -0.0012 & 0.0045 & 0 & 0 & 0 \\ 0.0022 & -0.2604 & 0.4482 & 0.0974 & 0 & 0 & 0 \\ -0.0009 & -0.7934 & -0.3070 & -1.0902 & 0 & 0 & 0 \\ 0 & 0 & 1.0000 & 0 & 0 & 0 & 0 \\ 1.0000 & 0 & 0 & 0 & 0 & 0 & 0 \\ 0 & 1.0000 & 0 & 0 & 0 & 0 & 0 \\ 0 & 0 & 0 & 1.0000 & 0 & 0 & 0 \end{bmatrix} \quad (4.45)$$

The input matrix is:

$$B_{La} = \begin{bmatrix} 0.0022 & -0.0000 & 0.0000 \\ -0.0000 & 0.0012 & -0.0003 \\ 0.0000 & -0.0003 & 0.0034 \\ 0 & 0 & 0 \\ 0 & 0 & 0 \\ 0 & 0 & 0 \\ 0 & 0 & 0 \end{bmatrix} \quad (4.46)$$

Because there is an output limitation, the actuators will most likely saturate, inducing once again integral windup. Therefore, an anti-windup method is used. Let us consider the case of surge speed:

$$x_{\int u} = \int_0^t \phi_u e_u \tau \quad (4.47)$$

where $e_u = (u - u_d)$ and ϕ_u represents a gain which sets the area of activity of the integrative portion, and it is obtained through [57]:

$$\phi_u = \begin{cases} 0, & \text{for} \quad e_u \leq -K_{trg} \\ \frac{e_u + K_{trg}}{K_{trg}}, & \text{for} \quad -K_{trg} < e_u \leq 0 \\ \frac{K_{trg} - e_u}{K_{trg}}, & \text{for} \quad 0 < e_u \leq K_{trg} \\ 0, & \text{for} \quad e_u > K_{trg} \end{cases} \quad (4.48)$$

where K_{trg} is a tuning parameter which defines the range of the integral action. The effect can be seen in figure 4.12 . For example, if $K_{trg} = 0.5$, the integral will only be active ($\phi_u \neq 0$) when the error is within $[-0.5, 0.5]$. Same is defined for heave (ϕ_w) and pitch (ϕ_θ).

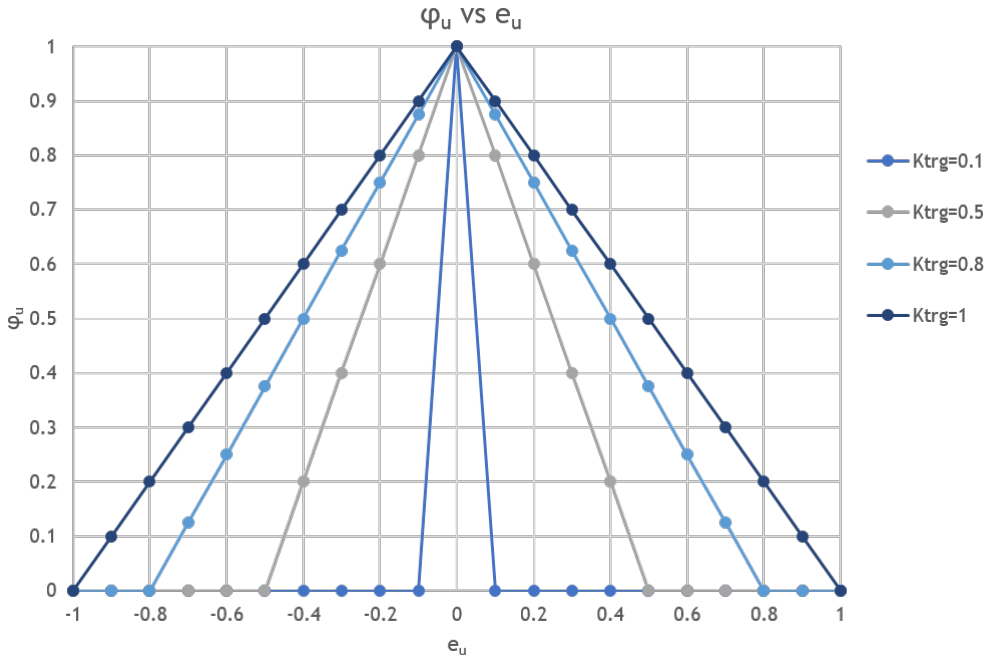

Figure 4.12: Influence of K_{trg} in gain ϕ_z.

Due to the magnitude of the longitudinal controllability matrix (W_{La}), this will not be presented here. However, $rank(Co_{La}) = 7$, therefore the system is controllable. Regarding the weights, Q_{La} and R_{La} matrix are:

$$Q_{La} = \begin{bmatrix} 25 & 0 & 0 & 0 & 0 & 0 & 0 \\ 0 & 60 & 0 & 0 & 0 & 0 & 0 \\ 0 & 0 & 60 & 0 & 0 & 0 & 0 \\ 0 & 0 & 0 & 40 & 0 & 0 & 0 \\ 0 & 0 & 0 & 0 & 5 & 0 & 0 \\ 0 & 0 & 0 & 0 & 0 & 15 & 0 \\ 0 & 0 & 0 & 0 & 0 & 0 & 10 \end{bmatrix} \quad R_{La} = \begin{bmatrix} 0.00004 & 0 & 0 \\ 0 & 0.00004 & 0 \\ 0 & 0 & 0.00004 \end{bmatrix} \tag{4.49}$$

As expected, the closed-loop eigenvalues $(eig(A_{La} - B_{La}K_{La}))$ are negative, which proves that the system is stable [28]. These weight values correspond to the situation of cheap control ($R << Q$) [39]. Therefore, the cost function is dominated by the output errors, and there is no penalty in using large $\mathbf{u}$. However, since there is an output limitation two alternatives exist: increasing R and confine the output to thrusters' limitations, which results in a sluggish response, or as in PID, limit the output by adding a saturation block. Then the second approach is chosen.

As in PID, the controllers are applied to the nonlinear model and it is set a time-varying reference. The tracking simulations with the final gains are presented in figures 4.13, 4.14 and 4.15. These were made separately, maintaining the remaining control signals to zero.

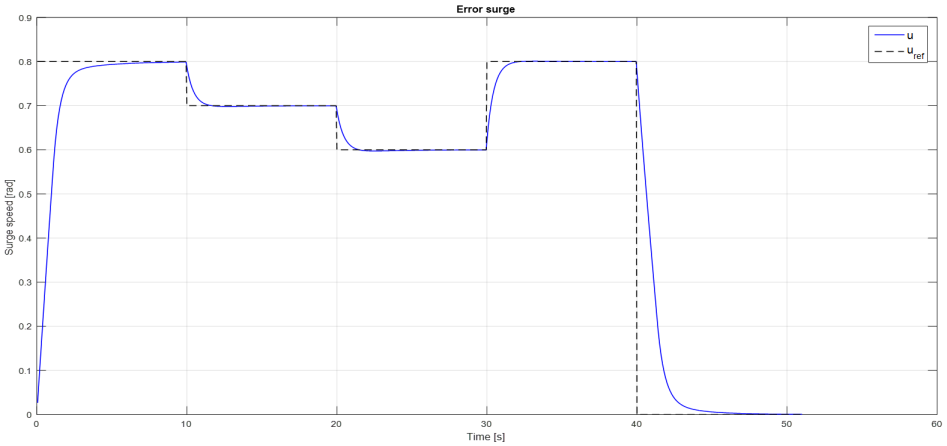

Figure 4.13: LQR speed controller tracking a reference over time.

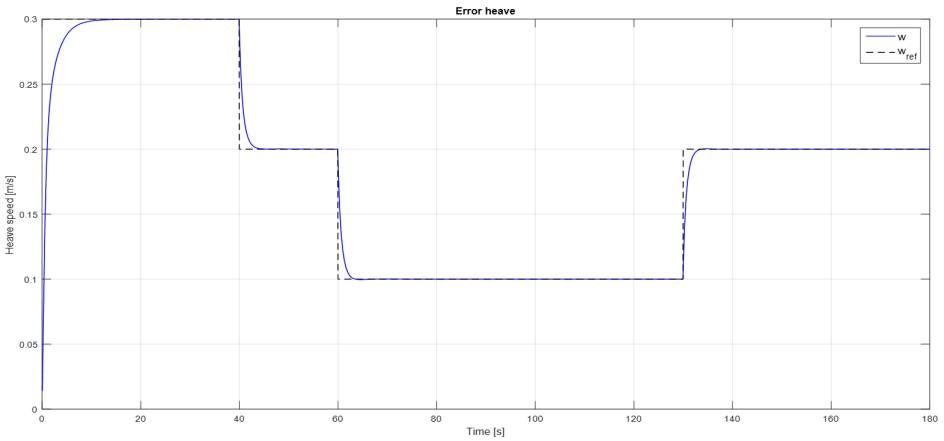

Figure 4.14: LQR heave controller tracking a reference over time.

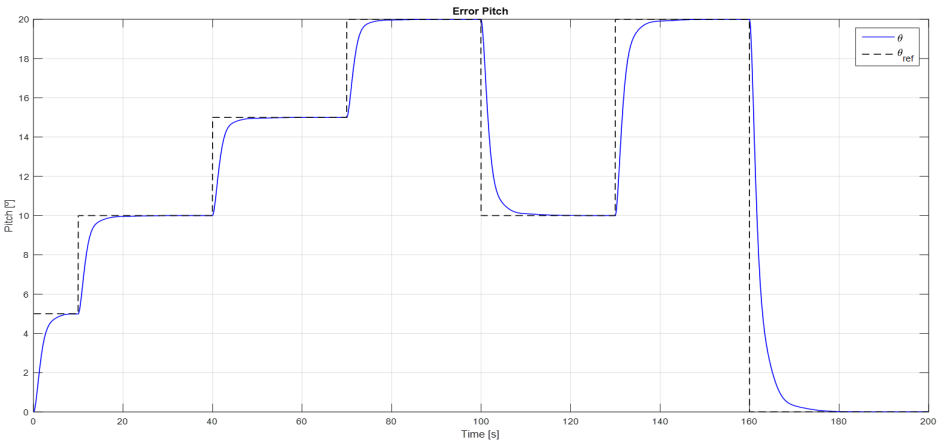

Figure 4.15: LQR pitch controller tracking a reference over time.

4.4.2 Lateral Controller

The purpose of the lateral system is to control the yaw angle ψ. As in the PID heading control, the state vector is constituted by the states: v,r and ψ. Assuming the state-space vector of the lateral subsystem as x_H, the state and input matrices from the linearized model are:

$$\begin{bmatrix} \Delta\dot{v} \\ \Delta\dot{r} \\ \Delta\dot{\psi} \end{bmatrix} = A_H x_H + B_H \mathbf{u}_H \quad (4.50)$$

From equation 4.24, the state-space yields:

$$A_H = \begin{bmatrix} -0.1653 & -0.4167 & 0 \\ 0.5672 & -0.0503 & 0 \\ 0 & 1.0000 & 0 \end{bmatrix}; \quad x_H = \begin{bmatrix} v - v_0 \\ r - r_0 \\ \psi - \psi_0 \end{bmatrix}; \quad B_H = \begin{bmatrix} -0.0003 \\ 0.0037 \\ 0 \end{bmatrix} \quad (4.51)$$

The desired state is:

$$x_{dH} = \begin{bmatrix} 0 \\ 0 \\ \psi_r - \psi_0 \end{bmatrix} \quad (4.52)$$

Therefore, the control input $\mathbf{u}_H$, according to equation 1.41, yields:

$$\mathbf{u}_H = -K_H(x_H - x_{dH}) = -K_H \begin{bmatrix} v - v_0 \\ r - r_0 \\ \psi - \psi_0 - (\psi_r - \psi_0) \end{bmatrix} \quad (4.53)$$

As metioned in section 1.4.3.1, a definite requirement of the LQR controller is that the plant must be controllable. Therefore, the controllability matrix is given by (see equation 1.34):

$$Co_H = \begin{bmatrix} -0.0003 & -0.0014 & 0.0006 \\ 0.0037 & -0.0003 & -0.0007 \\ 0 & 0.0037 & -0.0003 \end{bmatrix} \quad (4.54)$$

The matrix W_H has full rank, therefore the system is controllable. After tuning, results show that only accounting for the weight referent to the state $\psi - \psi_{ref}$ ($q_{3,3}$) leads to overshoot. To reduce it, the weight corresponding to the yaw rate ($q_{2,2}$), was chosen to be nonzero. The resulting weight matrices are:

$$Q_H = \begin{bmatrix} 0 & 0 & 0 \\ 0 & 90 & 0 \\ 0 & 0 & 45 \end{bmatrix} \quad ; \quad R_H = 0.00004 \quad (4.55)$$

Again the situation of cheap control ($R << Q$) is verified [39]. The closed-loop eigenvalues ($eig(A_H - B_H K_H)$) are negative, which proves that the system is stable [28]. Finally, the resulting controller performance can be seen in the figure 4.16.

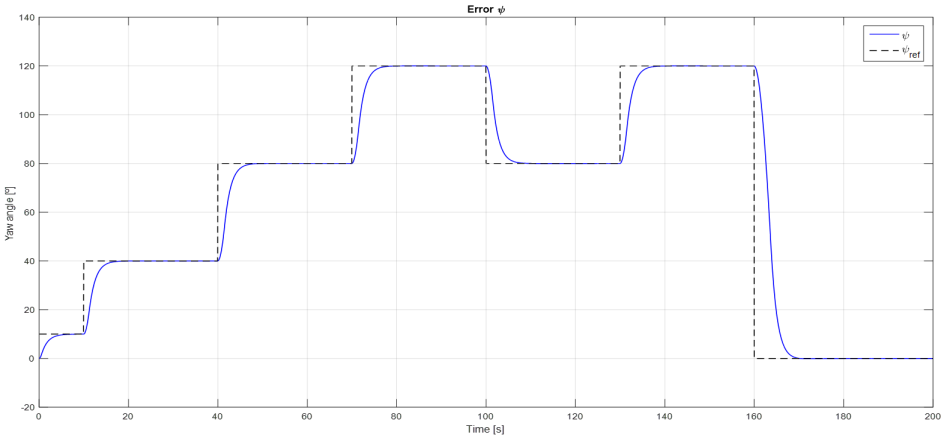

Figure 4.16: LQR lateral controller simulation.

4.4.3 Simulink Representation

The LQR block diagram can be seen in figure 4.17.

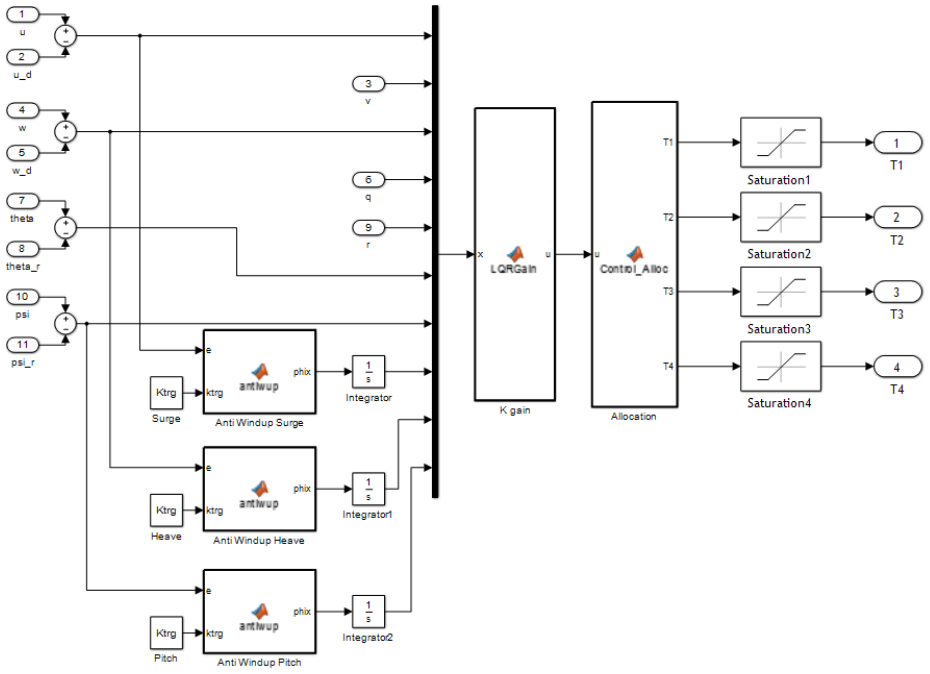

Figure 4.17: Simulink implementation of LQR control.

4.5 Control Allocation

The above-derived control methods calculate differential mode, τ_6, and the common mode, τ_1, through separate laws. This means that the two laws will compete for control authority. Without accounting any thrust constrains, this solution will lead to actuator saturation, resulting in poor performance and instability [58]. The control allocation law from [58] is adapted to solve this problem. Considering now the new common mode law, τ_1':

$$\tau_1' = \tau_1 e^{-\beta|\tau_6|} \quad (4.56)$$

where τ_1 is the control signal determined by the speed controller, β is user-set and dependent on the desired fraction of commanded surge, and τ_6 the control signal determined by the heading controller. This function gives precedence of to maintain a proper heading, over speed. The result allows for the increase in the maneuverability of the AUV at the expense of forward motion.
The thrust from the thruster 1, T_1, thruster 2, T_2, thruster 3, T_3s and thruster 4, T_4 is given by the relation:

$$\begin{bmatrix} T_1 \\ T_2 \\ T_3 \\ T_4 \\ 0 \\ 0 \end{bmatrix} = L^{-1} \begin{bmatrix} \tau_1' \\ 0 \\ \tau_3 \\ 0 \\ \tau_5 \\ \tau_6 \end{bmatrix} \quad (4.57)$$

where L is the mapping matrix from equation 2.9.

4.6 Control Considerations

In this chapter are devised two controllers for the AUV. Firstly, the nonlinear dynamic model is linearized around an operational point. Since the vehicle is not neutrally buoyant, the term $W - B$ is not depreciated.

For PID, the linearized model was decoupled into three lightly interactive subsystems. For each DOF of the AUV, it was designed a Single Input Single Output (SISO) controller, tuned from the respective transfer function. Since the PID method does not guarantee robustness to external disturbances, during the tuning process, the Bode plot was used to assess if the stability margins are within the values reported in [43].
For LQR, the linear model was divided into two subsystems, as suggested in [17, 29]. Two controllers were devised: one Multi Input Multi Output (MIMO) controller to control surge, heave and pitch; and one SISO controller to control yaw. Because LQR achieves infinity gain margin and ≥ 60 degrees of phase margins [39], it is considered to be robust to external disturbances.

Although the considerations about the dynamic model (see section 2.3) may have an impact on the derived controllers once corrected, this chapter provides the general recipe for deriving new controllers by changing the gains or the linearization point.

Chapter 5

Computational Simulation and Validation

This chapter addresses the simulation of both guidance and control laws. *Matlab R2017a*[1] was used. As simulation model, it will be used the 6DOF nonlinear model above presented. The simulations were divided according to the guidance algorithm used:

- Waypoint following for both 2D and 3D scenario;
- Path following scenario;

For the simulations, it was considered that the vehicle should stay on the last waypoint for a predefined time (W_t).
The structure of the code used to simulate can be represented through the following algorithm:

Begin

Introduce initial position and states;
Introduce the waypoint matrix;
Define time around last waypoint (W_T);
Define variable counting ($counter$);
Define the time step(dt);
While: $counter < W_T$
References from guidance block (Waypoint or Path Following);
if: last waypoint is reached?
$counter = counter + dt$;
end
Thrust vector the control block (PID or LQR);
Calculate $\dot{\nu}$ and $\dot{\eta}$;
Run numeric integration;
Store the state values;
End while
Plot data
End

[1] ©1994-2017 The MathWorks, Inc.

5.1 Considerations about the Simulations

5.1.1 State Feedback

A serious drawback of the LQR controller is that it assumes full state availability. That is often not the case whether no sensors are installed on the plant to measure that particular state, or the sensors output is corrupted with noise and the required information cannot be extracted without proper treatment. However, for the purpose of these simulations, none of these shortcomings will be considered.

5.1.2 Thrust Output

The thrust output was limited at 120 N, in forward thrust, and 85 N in reverse thrust. Thruster dynamics were not considered. However, this should have an overall minor effect on the simulation results, apart from an increase in the response time.

5.1.3 Simulation Parameters

The value of speed COA (ρ_u) was defined as 1 meter, the radius of the planar waypoint COA (ρ_k) as 1.5 meters of radius, and the depth COA (ρ_z) was defined as 0.5 m. For the reference speed velocity, the upper bound (k_u) was set at 0.8 m/s, and for the reference heave speed (k_w) 0.4 m/s.
The coordinates of the vehicle's initial position, in the inertial frame, are: $\eta_1 = (x_0, y_0, z_0) = (0, 0, 0)$.
To improve visualization, the Down coordinate was inverted and the simulation step to be considered is 0.01 seconds.

5.1.4 Ocean Currents

For the purpose of this thesis, the effect of ocean currents are not to be considered.

5.2 Waypoint following simulation

5.2.1 Two-dimensional simulation

The waypoints were chosen to simulate an zigzag trajectory, and the coordinates are presented in the table 5.1.

Table 5.1: Selected Waypoints coordinates.

	North[m]	East[m]	Up[m]
W_1	10	20	0
W_2	20	-20	0
W_3	30	20	0
W_4	40	-20	0
W_5	50	0	0

- PID Results:

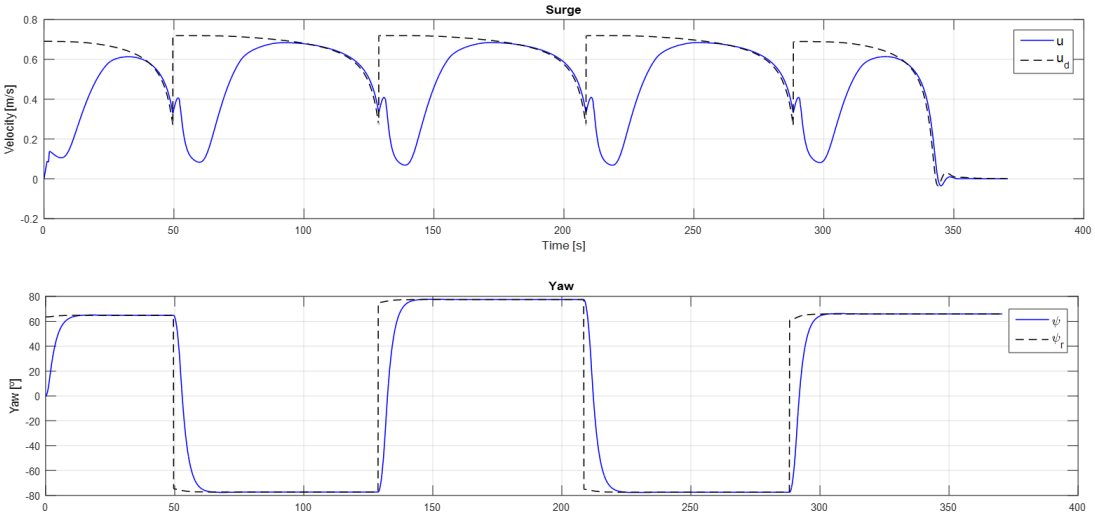

Figure 5.1: PID tracking results for two-dimensional simulation.

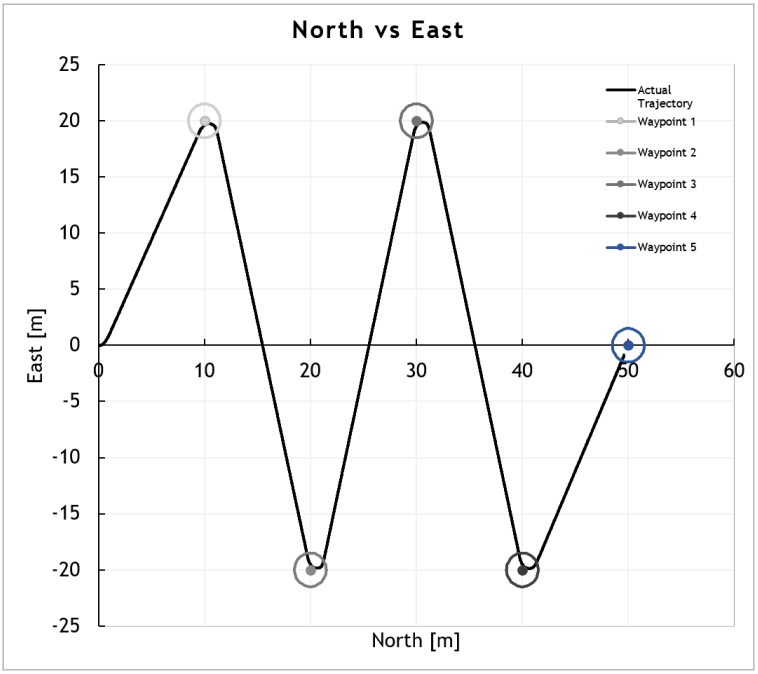

Figure 5.2: PID evolution of the vehicle's position in North vs East plot for the two-dimensional simulation.

- LQR Results:

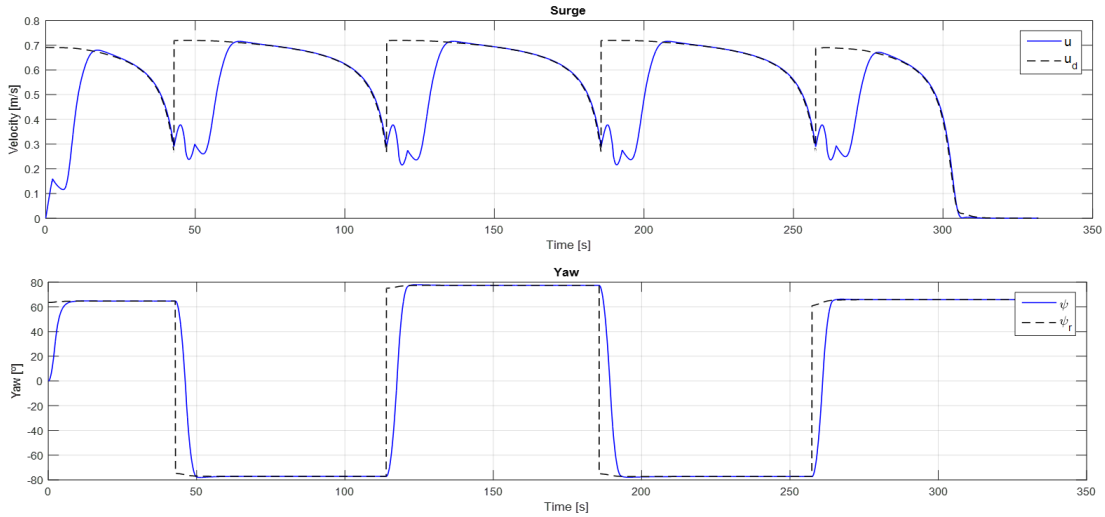

Figure 5.3: LQR tracking results for two-dimensional simulation.

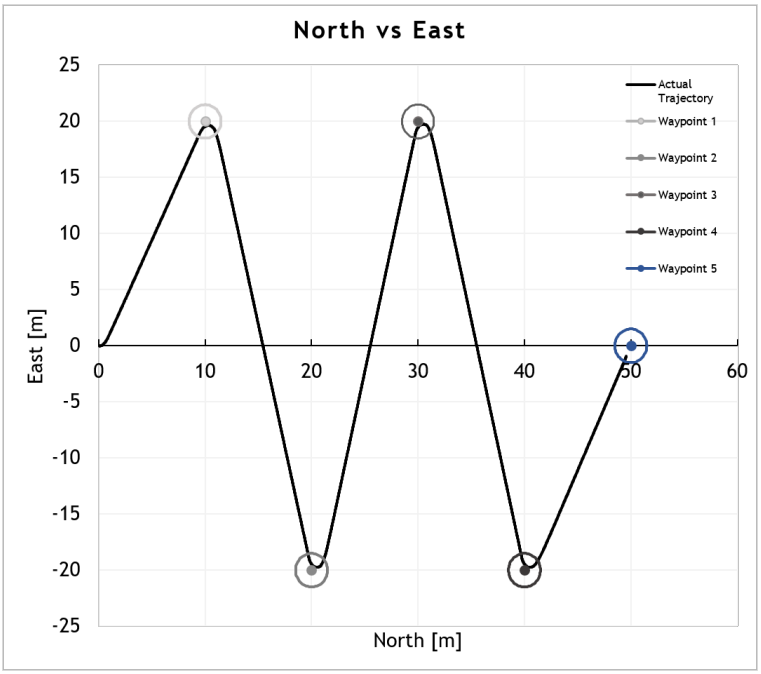

Figure 5.4: LQR evolution of the vehicle's position in North vs East plot for the two-dimensional simulation.

On the speed controller, it is possible to notice a peak in the velocity followed by a sudden reduction, after the waypoint switch. Such attitude is justified by the control allocation law, which values heading accuracy over speed.

The resulting motion is plotted in figure 5.2, for PID, and in figure 5.4, for LQR. The circles are representative of waypoints' COA. According to [19], the radius of COA should be twice the size of the vehicle, which corresponds to $2 \times 2.8 = 5.6$ m. However, since the control allocation law provides extra maneuverability, the vehicle will miss the waypoint if considered this radius. Therefore, after several simulations, the radius was decreased to 1.5 meters to allow for the AUV to reach the waypoint.
For the last waypoint, the vehicle will stay within 1 meter from it, because the complementary

planar distance used to calculate the surge desired speed is $d_u = d_k - 1$.
It is possible to notice a difference in the speed convergence from PID to LQR. The Time To Target (TTT) for LQR was 5 minutes and 32 seconds and for PID 6 minutes and 10 seconds.
With respect to roll angle (ϕ), as it can be seen figure 5.5, is passively controlled, as suggested in the section 2.2.4.

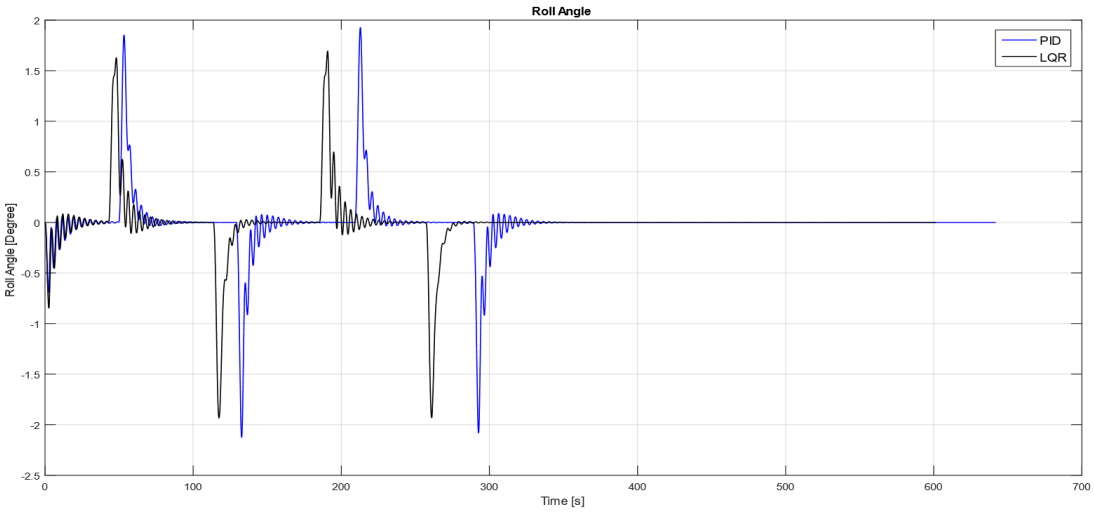

Figure 5.5: Roll angle for two-dimensional simulation.

5.2.2 Three-dimensional simulation

The waypoints used for this simulation are presented in table 5.2.

Table 5.2: Selected Waypoints coordinates.

	North[m]	East[m]	Up[m]
W_1	10	20	-20
W_2	30	20	-20
W_3	50	40	-20
W_4	60	40	0

The tracking results for both controllers are presented in figures 5.6 for PID and 5.7 for LQR.

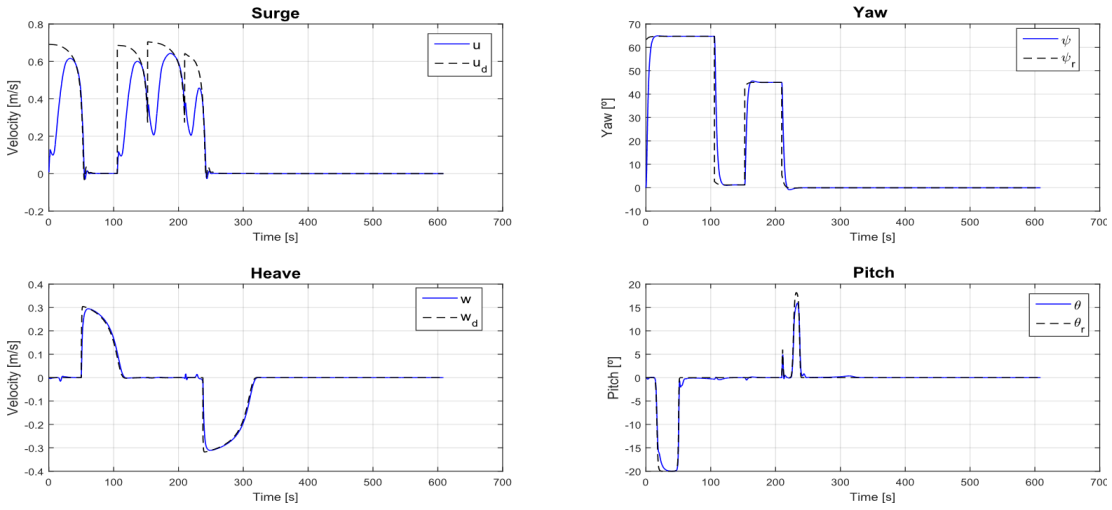

Figure 5.6: PID tracking results for three-dimensional simulation.

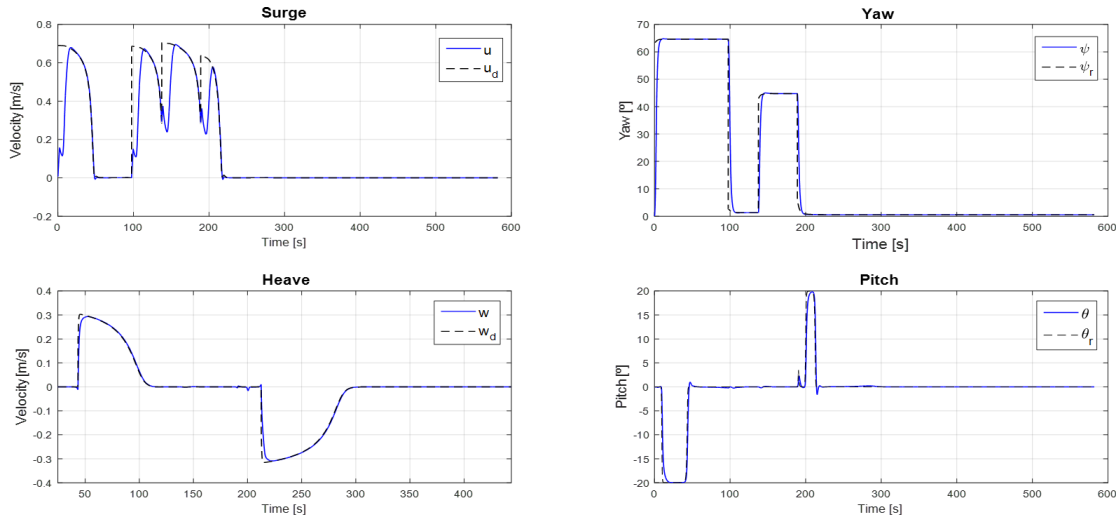

Figure 5.7: LQR tracking results for three-dimensional simulation.

To assess the differences, PID and LQR results were plotted together. The resulting three-dimensional graphical simulations are presented in appendix B.

In general, both controllers present a satisfactory performance. However, as it can be seen in figure 5.8, LQR is slightly faster, which leads to a higher rate of ascend in pitch mode (bottom plot of figure 5.8). The resulting TTT for LQR is 5 minutes and 13 seconds, and for the PID 5 minutes and 38 seconds.

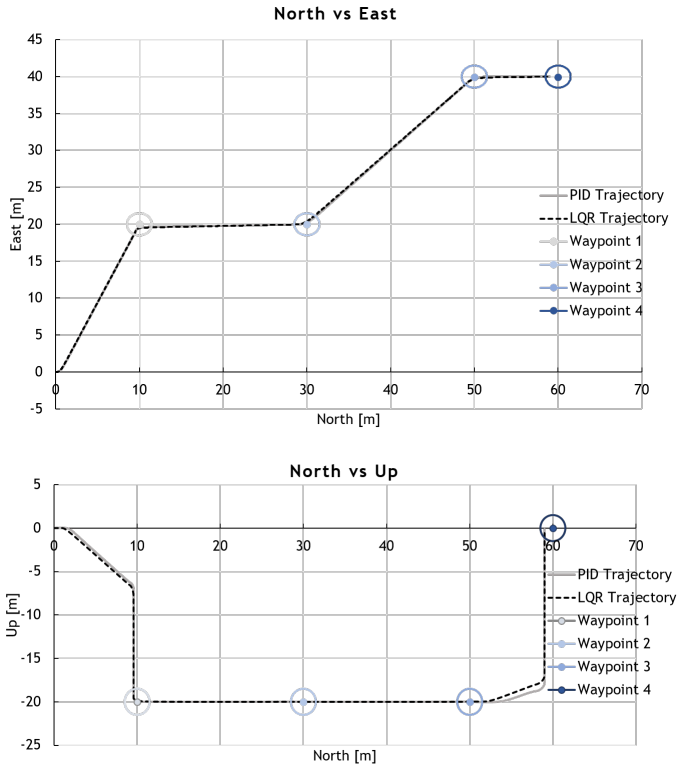

Figure 5.8: LQR and PID results of three dimensional waypoint following scenario.

5.3 Path following simulation

It is pretended to simulate the vehicle performing a lawn mow path, as in data acquisition stage (figure 1.7). The path generation is done through the waypoints present in table 5.3.

There are two ways to engage the path. The first scenario is without the requirement to reach the first point, i.e. the vehicle will converge to a point Δ meters ahead from its current projected position on the path (see figure 3.5). The second approach, the vehicle has to pass on first waypoint and then start the path. Both simulations are performed. The lookahead distance (Δ) was defined as 5 meters, to allow a soft steering behavior.

Table 5.3: Selected Waypoints for the path generation.

	North[m]	East[m]	Up[m]
W_1	0	10	-10
W_2	50	10	-10
W_3	50	20	-10
W_4	0	20	-10
W_5	0	30	-10
W_6	50	30	-10
W_7	50	40	-10
W_8	0	40	-10
W_7	0	50	-10
W_8	50	50	-10

For the first scenario, the North-East graphical result, for both PID and LQR can be seen in figure 5.9. The three-dimensional results are presented in figure 5.10. The resulting TTT for LQR is 13 minutes and 57 seconds, and for PID 14 minutes and 37 seconds.

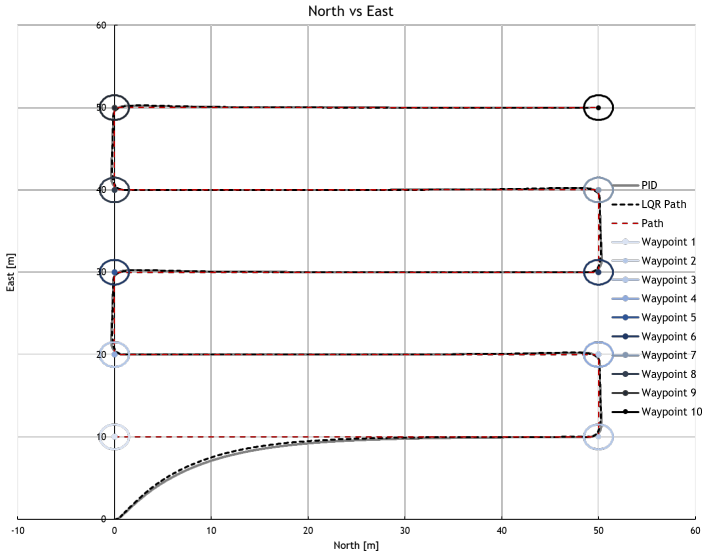

Figure 5.9: LQR and PID simulation of the vehicle's position in North vs East plot for the path following scenario without beginning constrain.

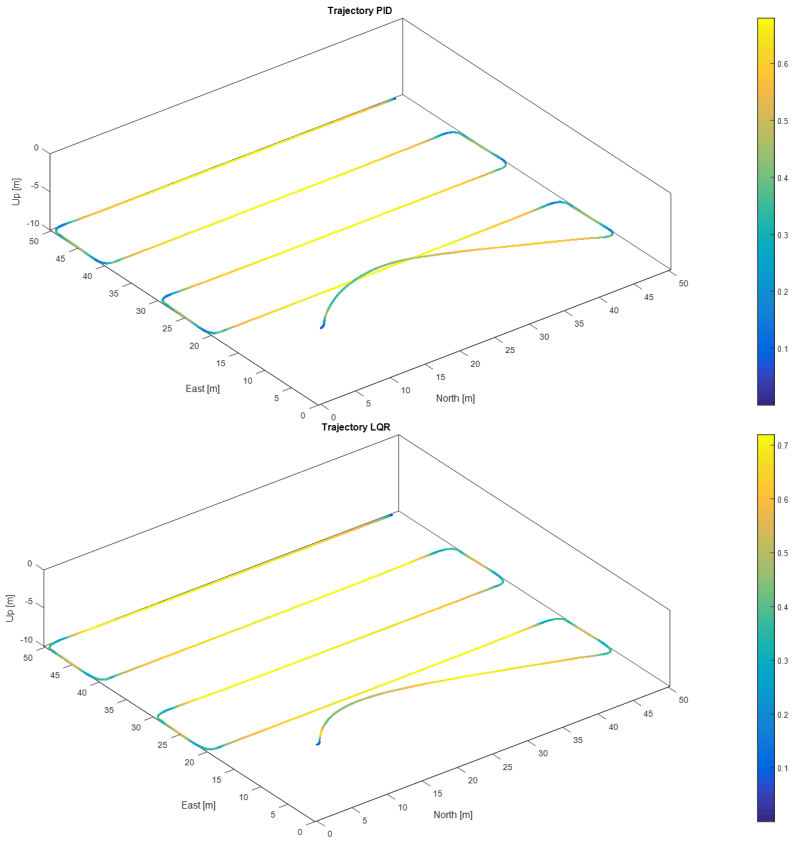

Figure 5.10: LQR and PID three-dimensional results for path following scenario, without beginning constrain (color bar indicates total velocity).

For the second scenario, the North-East graphical result can be seen in figure 5.11, and the three-dimensional plot in figure 5.12. The resulting TTT for LQR is 14 minutes and 26 seconds, and for PID 15 minutes and 19 seconds.

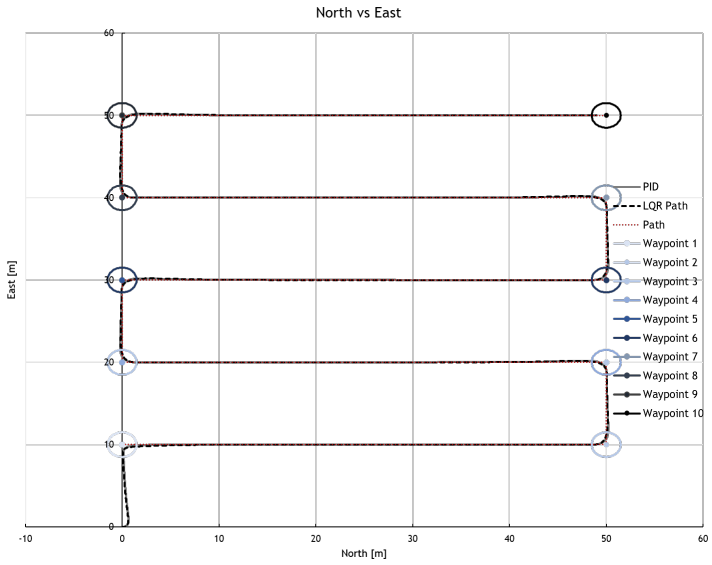

Figure 5.11: LQR and PID simulation of the vehicle's position in North vs East plot for the path following scenario, with beginning constrain.

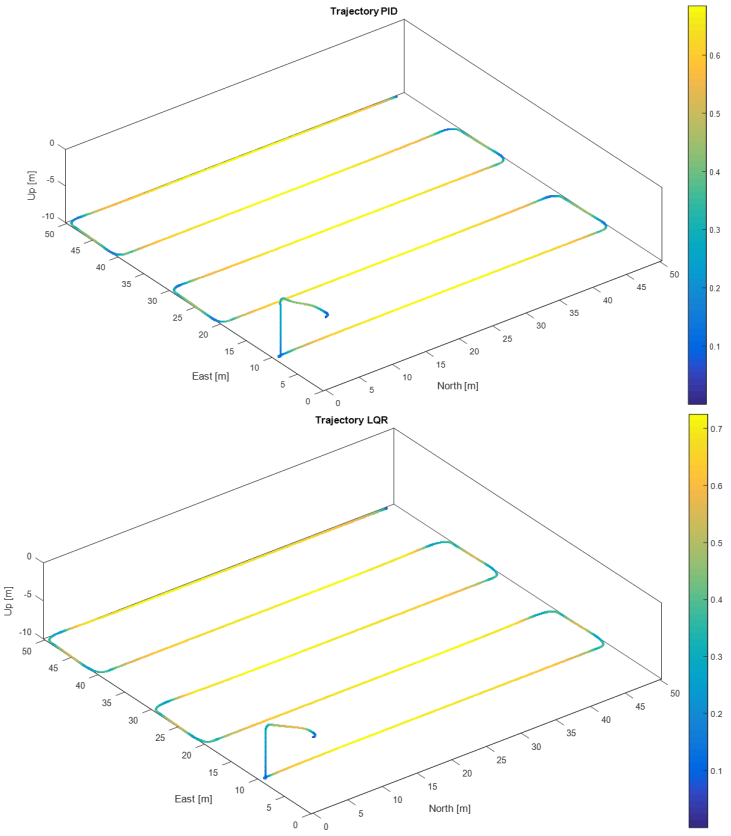

Figure 5.12: LQR and PID three-dimensiona results for path following scenario, with beginning constrain (color bar indicates total velocity).

Chapter 6

Conclusions and Future Work

The primary goal of this thesis is to devise a controller that could be implemented on the AUV being developed at CEiiA. With no access to the vehicle, the dynamic model presented in [17] is essential for validity of this work.
The addition of a fourth order approximation of damping allowed a more realistic representation of the vehicle. Since there is no symmetry on the yz- plane, this approximation allows for different dynamics in backward motions, which will be essential when considering the ascent phase (see section 1.1).
However, since this model is used to design the controller, the limitations/considerations in [17] were object of study in this work.

Since the controller works on the guidance data, devising suitable laws is crucial. For this purpose, a waypoint following and station keeping algorithm, as well a path-following based on lookahead steering, were presented. However, due to its spacial constraints, the path following solution should be the preferable, because it directs the vehicle to the desired path, even in the presence of ocean currents.
To allow for the AUV to dive, two laws were devised: manipulating the pitch angle through the differential mode, or heave speed through common mode. Due to the limitations of the dynamic model (see section 2.3), it is considered that reference pitch angle follows the same constraints that the angle-of-attack.

To devise the linear controllers, a linear version of the work developed in [17] was presented. Despite the fact that the linearization point only accounts for surge speed, the results suggests that, for the considered conditions, the remaining state variables are not critical for the dynamics.
As mentioned in section 1.4.3.1, LQR is a robust control method [18, 39]. However, for PID design, the stability margins were analyzed and taken into account when tuning. The results are within the values pointed in [43], which suggest robustness to external disturbances.
The resulting stability analysis serves as fundamental justification of using linear control techniques in the nonlinear systems, i.e., stable design by linear control guarantees the stability of the original system locally [28].
With respect to the dynamic model limitations (see section 2.3), the underestimation can be corrected by manipulating the gains for both the controllers. However, the situation of diving with common mode may require an extra linearization point, leading to the necessity of adopting a gain-scheduled approach.
Since heading and surge control is accomplished through manipulation of thrust output from longitudinal thrusters, and because the control signals are calculated through separate laws, an allocation law is proposed. The result law allowed for an increase in the manoeuvrability at the expense of forward motion.

Even though the simulation results proved solid performance for both controllers, LQR proved to be slightly faster than the PID, for the design conditions mentioned in section 4.

6.1 Concluding Remarks

In general, this work provides two linear control solutions for the AUV being developed at CEiiA. Even though only a single operational point was considered, this work provides the general approach to extend this design to multiple operational points.
To decide between the presented controllers, not only for this AUV but for future control problems, it is important to understand the factors that might have an impact on the final choice.
PID is a simpler approach and can be tuned without the system model, using methods like Ziegler and Nichols to find the gains [39]. However, as the order of the system increases, controlling the system becomes harder using only PID methods.
On the other hand, LQR, as stated in section 1.4.3.1, provides the optimal state-feedback law, which minimizes a certain quadratic cost function. The optimal pole location and the unique analytical solution [18], is what makes LQR the preferable choice. However, this controller has a drawback that it assumes full state feedback. If that is not the case, there is a need to build an observer to estimate the missing states. Also, it is required the model of the system.
Therefore, due to the nature of the operational environment of the AUV, and considering the advantages and disadvantages of each, LQR appears to be the best choice.

6.2 Future Work

This work presents two controllers which were built according to the theory of robust control. However, to prove robustness, it is essential to test control through several operational conditions, and in the presence of uncertainties in the nonlinear model. Despite the results, the work hereby presented should be extended towards nonlinear control.
Linear controllers rely on the key assumption of small operational range. However, the AUV must be controlled under all possible operational conditions. This can be accomplished by using a nonlinear control. The nonlinear gain-scheduling controller acts as a switch between several linear controllers, each one designed for a specific operational point. Through the analysis of the vehicle's flight envelope, the controller design methodology presented in this work can be applied to those multiple operational points, ensuring robust stability for each and one of them.
Regarding the dynamic model, some concerns should also be addressed:

- Hydrodynamic estimation for full envelope of angles of attack and side slip;
- The inclusion of ocean currents in the dynamic of the vehicle;
- The thruster dynamics should also be included.

Finally, the inclusion of a navigation block is of utmost importance.

Bibliography

[1] S. Zhao, “Advanced control of autonomous underwater vehicles,” Ph.D. dissertation, The University of Hawai, 2004. 1, 12

[2] Gemini, “We know more about the moon than the ocean floor.” [Online]. Available: https://geminiresearchnews.com/2015/06/we-know-more-about-the-moon-than-the-ocean-floor/ [Accessed: 22-Sep-2017]. 1

[3] S. Moore, H. Bohm, V. Jensen, and N. Johnston, Underwater Robotics: Science, Design & Fabrication. Marine Advanced Technology Education (MATE) Center, 2010. 1

[4] C. McClain, “Manned or unmanned?” [Online]. Available: http://www.deepseanews.com/2010/02/manned-or-unmanned/ [Accessed: 13-Mar-2017]. 1

[5] J. G. Bellingham, “Autonomous underwater vehicles.” [Online]. Available: https://auvlab.mit.edu/research/AUVoverview.html [Accessed: 10-Mar-2017]. 2

[6] D. R. Blidberg, “The development of autonomous underwater vehicles (auv); a brief summary,” in Ieee Icra, 2001. 2

[7] J. Yuh and H.-T. Choi, “Unmanned underwater vehicles,” Wiley Encyclopedia of Electrical and Electronics Engineering, 2015. 2

[8] T. B. Curtin, J. G. Bellingham, J. Catipovic, and D. Webb, “Autonomous oceanographic sampling networks,” Oceanography, vol. 6, no. 3, pp. 86–94, 1993. 2

[9] A. U. V. A. C. (AUVAC), “Auv database.” [Online]. Available: http://auvac.org/ [Accessed: 19-Jun-2017]. 2

[10] EMEPC, “The continental shelf extension.” [Online]. Available: https://www.emepc.pt/en/the-project [Accessed: 10-Mar-2017]. 2

[11] “Medusa deep sea.” [Online]. Available: http://www.medusadeepsea.com/ [Accessed: 10-Mar-2017]. 3, 4

[12] D. G. SE, Rules for Classification and Construction, I - Ship Technology, Part 5 - Underwater Technology. Germanischer Lloyd., 2009. 3

[13] D. Rudolph and T. A. Wilson, “Doppler velocity log theory and preliminary considerations for design and construction,” in Southeastcon, 2012 Proceedings of IEEE. IEEE, 2012, pp. 1–7. 3

[14] J. Ribeiro, “Motion control of single and multiple autonomous marine vehicles,” Master’s thesis, Instituto Superior Técnico, 2011. 5, 6, 8, 38, 52

[15] T. I. Fossen, Handbook of Marine Craft Hydrodynamics and Motion Control. John Wiley & Sons, 2011. 5, 6, 7, 8, 9, 10, 11, 12, 13, 21, 26, 42, 43

[16] SNAME, “Nomenclature for treating the motion of a submerged body through a fluid,” The Society of Naval Architects and Marine Engineers, Technical and Research Bulletin No., pp. 1–5, 1950. 5, 8

[17] C. A. Bentes, “Modeling of an autonomous underwater vehicle,” Master’s thesis, University Of Beira Interior, 2016. 7, 9, 26, 27, 29, 30, 31, 34, 35, 49, 57, 64, 75

[18] W. Naeem, “Guidance and control of an autonomous underwater vehicle,” phd, Univeristy of Plymouth, 2004. 11, 12, 21, 51, 75, 76

[19] V. Bakaric, Z. Vukic, and R. Antonic, “Improved line-of-sight guidance for cruising underwater vehicles,” IFAC Proceeding Volumes, vol. 37, pp. 447–452, 2004. 11, 37, 68

[20] M. Breivik and T. I. Fossen, “Guidance-based path following for autonomous underwater vehicles,” in Proceedings of OCEANS 2005 MTS/IEEE, 2005, pp. 2807–2814 Vol. 3. 11

[21] T. Salgado-Jimenez and B. Jouvencel, “Using a high order sliding modes for diving control a torpedo autonomous underwater vehicle,” in OCEANS 2003. Proceedings, vol. 2. IEEE, 2003, pp. 934–939. 12

[22] L. A. Cooney, “Dynamic response and maneuvering strategies of a hybrid autonomous underwater vehicle in hovering,” Master’s thesis, Massachusetts Institute of Technology, 2009. 12, 17, 50

[23] B. Jalving, “The ndre-auv flight control system,” IEEE Journal of Oceanic Engineering, vol. 19, no. 4, pp. 497–501, Oct 1994. 12, 49, 50, 51, 52, 54

[24] N. Fairfield, D. Jonak, G. Kantor, and D. Wettergreen, “Field results of the control, navigation, and mapping systems of a hovering auv,” in Proceedings of the Unmanned Untethered Submersible Technology Conference (UUST), 2007, pp. 20–22. 12

[25] C. Yang, “Modular modeling and control for autonomous underwater vehicle (auv),” Master’s thesis, National University of Singapore, 2007. 12

[26] N. Syahroni and J. W. Choi, “An autonomous underwater vehicle simulation using linear quadratic servo based on open control platform,” Model. Simul. Eng., vol. 2012, pp. 19:19–19:19, Jan. 2012. 12

[27] A. Okamoto, J. Feeley, D. Edwards, and R. Wall, “Robust control of a platoon of underwater autonomous vehicles,” in OCEANS’04. MTTS/IEEE TECHNO-OCEAN’04, vol. 1. IEEE, 2004, pp. 505–510. 12

[28] J. Slotine and W. Li, Applied Nonlinear Control, ser. Prentice-Hall International Editions. Prentice-Hall, 1991. 12, 21, 23, 24, 60, 62, 75

[29] T. I. Fossen, “Nonlinear modelling and control of underwater vehicles,” Ph.D. dissertation, Norwegian Institute of Technology, 1991. 12, 47, 49, 57, 64

[30] I. Masar and E. Stöhr, “Gain-scheduled lqr-control for an autonomous airship,” in 18th International Conference on Process Control, 2011. 12

[31] N. Kato, Y. Ito, J. Kojima, S. Takagi, K. Asakawa, and Y. Shirasaki, “Control performance of autonomous underwater vehicle” aqua explorer 1000” for inspection of underwater cables,” in OCEANS’94.’Oceans Engineering for Today’s Technology and Tomorrow’s Preservation.’Proceedings, vol. 1. IEEE, 1994, pp. I–135. 12

[32] A. Nag, S. S. Patel, and S. Akbar, “Fuzzy logic based depth control of an autonomous underwater vehicle,” in Automation, Computing, Communication, Control and Compressed Sensing (iMac4s), 2013 International Multi-Conference on. IEEE, 2013, pp. 117–123. 12

[33] P. W. van de Ven, C. Flanagan, and D. Toal, "Neural network control of underwater vehicles," Engineering Applications of Artificial Intelligence, vol. 18, no. 5, pp. 533–547, 2005. 12

[34] C. McGann, F. Py, K. Rajan, J. P. Ryan, and R. Henthorn, "Adaptive control for autonomous underwater vehicles." in AAAI, 2008, pp. 1319–1324. 12

[35] M. Breivik and T. I. Fossen, "Guidance laws for autonomous underwater vehicles," in Underwater vehicles. InTech, 2009. 12, 13, 14, 42

[36] M. S. Triantafyllou and F. S. Hover, Maneuvering and Control Of Marine Vehicles. Department of Ocean Engineering, Massachusetts Institute of Technology, 2003. 14, 15

[37] N. S. Nice, Control System Engineering. California State Polytechnic University, Pomona: John Wiley & Sons, Inc., 2011. 14, 15, 16, 19, 22, 26

[38] K. Ogata, Modern Control Engineering, ser. Instrumentation and controls series. Prentice Hall, 2010. 15, 16, 19, 20, 47, 49

[39] M. S. Triantafyllou and F. S. Hover, Maneuvering and Control of Marine Vehicles. Massachusetts Institute of Technology, 2003. 16, 19, 20, 60, 62, 64, 75, 76

[40] K. Aström and R. Murray, Feedback Systems: An Introduction for Scientists and Engineers. Princeton University Press, 2012. 16, 17, 18, 24, 51

[41] G. F. Franklin, J. D. Powell, and A. Emami-Naeini, Feedback Control of Dynamic Systems, 7th ed. Pearson, 2014. 18

[42] J. Azinheira, Controlo de Voo. Instituto Superior Técnico, 2009. 19, 20

[43] K. J. Åström and T. Hägglund, PID controllers: theory, design, and tuning. Isa Research Triangle Park, NC, 1995, vol. 2. 21, 24, 25, 51, 54, 57, 64, 75

[44] V. Kumar, Stability Theory. University of Pennsylvania, 2017. 22, 23

[45] A. J. Healey and D. Lienard, "Multivariable sliding mode control for autonomous diving and steering of unmanned underwater vehicles," IEEE journal of Oceanic Engineering, vol. 18, no. 3, pp. 327–339, 1993. 26, 37, 49

[46] J. S. Geisbert, "Hydrodynamic modeling for autonomous underwater vehicles using computational and semi-empirical methods," Master's thesis, Faculty of the Virginia Polytechnic Institute and State University, 2007. 30

[47] "Pressure hull and structures - Stability and buoyancy," DNV GL, Norm III-7, 2015. 34

[48] "Mini thruster datasheet." [Online]. Available: https://d37oegmkfg78j3.cloudfront.net/1499775771/ars-thr-800-minithruster-datasheet-reva.pdf [Accessed: 24-Aug-2017]. 34, 81

[49] J. E. G. Refsnes, "Nonlinear model-based control of slender body auvs," Ph.D. dissertation, Norwegian University of Science and Technology, 2007. 35

[50] A. Palmer, G. E. Hearn, and P. Stevenson, "Modelling tunnel thrusters for autonomous underwater vehicles," IFAC Proceedings Volumes, vol. 41, no. 1, pp. 91 – 96, 2008, 2nd IFAC Workshop on Navigation, Guidance and Control of Underwater Vehicles. 39

[51] M. Breivik and T. I. Fossen, “A unified control concept for autonomous underwater vehicles,” in 2006 American Control Conference, June 2006, pp. 7 pp.–. 39

[52] K. Tanakitkorn, P. A. Wilson, S. R. Turnock, and A. B. Phillips, “Depth control for an over-actuated, hover-capable autonomous underwater vehicle with experimental verification,” Mechatronics, vol. 41, no. Supplement C, pp. 67 – 81, 2017. [Online]. Available: http://www.sciencedirect.com/science/article/pii/S0957415816301477 39

[53] I. Schjølberg and O. Egeland, “Motion control of underwater vehicle-manipulator systems using feedback linearization,” IFAC Proceedings Volumes, vol. 28, no. 2, pp. 54 – 59, 1995, 3rd IFAC Workshop on Control Applications in Marine Systems, Trondheim, Norway, 10-12 May. [Online]. Available: http://www.sciencedirect.com/science/article/pii/S1474667017516511 47

[54] L. Moreira and C. G. Soares, “H_2 and H_∞ designs for diving and course control of an autonomous underwater vehicle in presence of waves,” IEEE Journal of Oceanic Engineering, 2008. 47, 48

[55] T. I. Fossen, Guidance and Control of Ocean Vehicles. John Wiley & Sons Inc, 1994. 47, 48, 49, 50

[56] T. MathWorks, “pidtuner.” [Online]. Available: https://www.mathworks.com/help/control/ref/pidtuner.html [Accessed: 3-Jul-2017]. 50

[57] C. M. R. Oliveira, M. L. Aguiar, W. C. A. Pereira, A. G. Castro, T. E. P. Almeida, and J. R. B. A. Monteiro, “Integral sliding mode controller with anti-windup method analysis in the vector control of induction motor,” in 2016 12th IEEE International Conference on Industry Applications (INDUSCON), 2016. 59

[58] I. R. Bertaska and K. D. von Ellenrieder, “Supervisory switching control of an unmanned surface vehicle,” in OCEANS 2015 - MTS/IEEE Washington, 2015, pp. 1–10. 64

Appendix A

Datasheet

Weight in air [kg]	2,2
Weight in water [kg]	1,4
Size, L x d x D [mm]	248 x 78 x 152
Power consumption, max [W]	800
Operating voltage	120 V DC
Supply current	7 A
Control signal	RS232
Rotational speed [rpm]	2000
Thrust, fwd [N]	120
Thrust, rev [N]	85
Depth rating [m]	6000

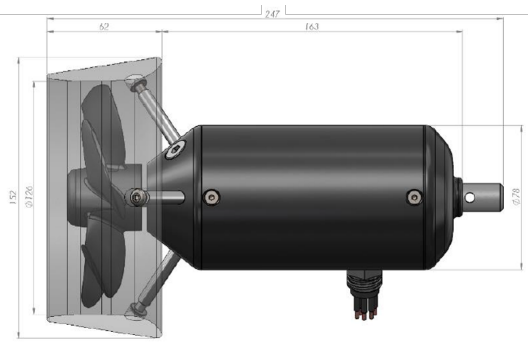

Figure A.1: Datasheet of the Argus Ars 800 mini thruster [48].

Appendix B

Simulations Graphics

B.1 Three-dimensional Waypoint Following

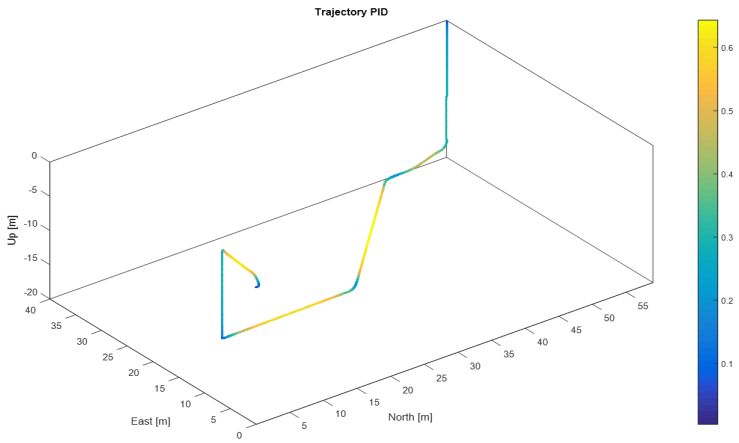

Figure B.1: Three-dimensional waypoint following simulation of the PID controller (color bar indicates velocity).

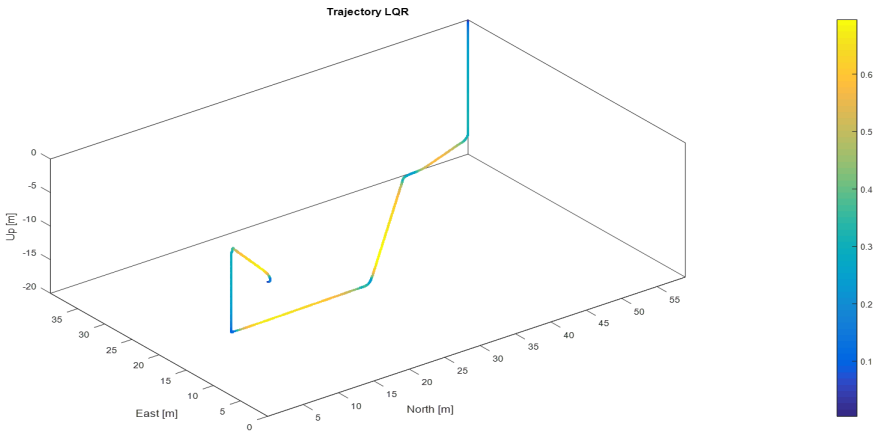

Figure B.2: Three-dimensional waypoint following simulation of the LQR controller (color bar indicates total velocity).

Appendix C

Publications

The research work conducted in this thesis produced the following paper:

- C. Mendes, C. Bentes, T. Rebelo, and K. Bousson (2017),"Guidance and robust control of a doublehull autonomous underwater vehicle," ICEUBI2017 - International Congress on Engineering - A Vision for the Future, 5-7 November, Covilhã (Portugal) (Submitted for approval).

Guidance and Robust Control of a double-hull Autonomous Underwater Vehicle

Introduction

Autonomous underwater vehicles are unmanned robotic systems whose main goal is to explore the ocean environment. In recent years, the interest in autonomous underwater vehicles has grown, as the technology provides more feasible solutions [1].
CEiiA, an Engineering and Product Development Centre based in Portugal, is currently developing together with its partners a deep sea AUV, (Figure 1) [2]. This AUV follows a double-hull configuration and is capable of reaching a Nominal Diving Depth (NDD) of 3000 meters. Control is achieved via two horizontal and two vertical thrusters. The main goal of this vehicle is to reinforce the national capacity for mobile autonomous deep-sea exploration and monitoring. However, the absence of a human operator narrows down the AUV operations to its control system, computing, and sensing capabilities.
The AUV's dynamics is inherently nonlinear and time-variant. The uncertain external disturbances difficult controller design. Nonetheless, there are many successfully implemented controllers in this nonlinear environment. Over the years linear theory has evolved to meet control robustness and stability requirements.
This paper proposes two linear control designs that could eventually be implemented on the AUV being developed. First the AUV's dynamic model, derived in [3], is briefly described. After, a waypoint following guidance solution [4] is introduced. As for controller design, PID and LQR methods are applied to the AUV's dynamic model and computationally tested. Then, the results are briefly discussed.

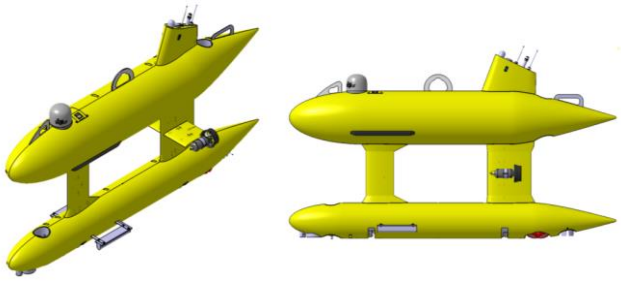

Figure 1 – 3D model of the AUV (courtesy of CEiiA).

Modelling the AUV

Coordinated Frames

To derive the equations of motion that describe the AUV's kinematics, first it is necessary to define two reference frames. The body-fixed $\{b\}$, which is the non-inertial frame, is composed of the axes $\{x_b, y_b, z_b\}$. The local NED (North-East-Down) $\{n\}$, the inertial reference frame, is composed of the orthonormal axes $\{x_n, y_n, z_n\}$.
The Centre of Gravity (CG) and the Centre of Buoyancy (CB) are defined with respect to the 0_b, and represented by $r_g^b = [x_g \quad y_g \quad z_g]^T$ and $r_g^b = [x_g \quad y_g \quad z_g]^T$, respectively.
The set of coordinates that expresses position and orientation of the vehicle are defined as:
$\eta = [x \quad y \quad z \quad \phi \quad \theta \quad \psi]^T$ expressed in the $\{n\}$ frame;
For linear velocities and angular velocities (surge, sway, heave, roll, pitch and yaw) the vector is:
$\nu = [u \quad v \quad w \quad p \quad q \quad r]^T$ expressed in the $\{b\}$ frame;
And finally, the control forces and moments vector is:
$\tau = [X \quad Y \quad Z \quad K \quad M \quad N]^T$ expressed in the $\{b\}$ frame;

The mathematical equation that represents the dynamics of the underwater vehicle can be derived by the Newton's second law. The resulting relation is given by [5]:

$$M\dot{v} + C(v)v + D(v)v + g(\eta) = \tau \tag{1}$$

where M is the inertia matrix including added mass, $C(v)$ is the Coriolis term including both rigid body and added mass term, $D(v)$ is the vector of hydrodynamic forces, and $g(\eta)$ is the vector of hydrostatic forces. The hydrodynamic data used was derived in [3]. For detailed description about the modeling process of this AUV please refer to [3].

Guidance

This section addresses an extension of the way*point guidance* algorithm of the one presented in [4].

Waypoint and Station-keeping Guidance

1) Steering Guidance by Line Of Sight:

The LOS guidance algorithm provides a reference angle ψ_r that will guide the AUV from its current position towards the waypoint (figure 2). The solution is [6]:

$$\psi_r = \arctan\left(\frac{y_k - y}{x_k - x}\right) \quad \in -\pi/2 \tag{2}$$

where ψ_r is calculated through the four-quadrant version of $\arctan(y/x) \in [-\pi, \pi]$, usually defined as $\mathrm{atan2}(y, x)$. The waypoint is reached if the vehicle lies inside a Circle Of Acceptance (COA) of radius (ρ_k), around the waypoint. That is [6]:

$$d_k = \sqrt{(x_k - x)^2 + (y_k - y)^2} \leq \rho_k \tag{3}$$

where d_k is the planar distance to the waypoint. Usually [7], ρ_k is $2 \times L$, where L stands for vehicle's length.

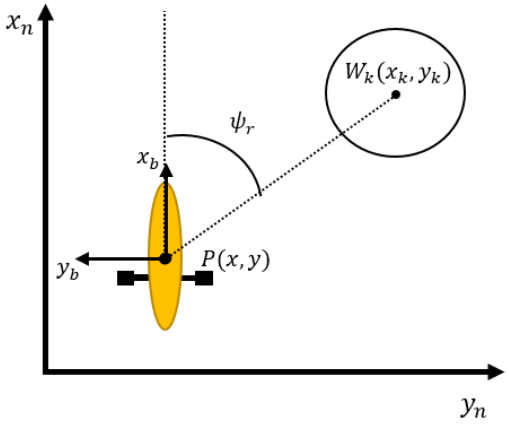

Figure 2 – Line Of Sight guidance in the steering plane

2) Reference speed law:

The speed reference is calculated as a function of the distance to the waypoint, d_k, by [4]:

$$u_d = k_u \sin^{-1}\left(\frac{d_k}{|d_k| + k_s}\right)\frac{2}{\pi} \tag{4}$$

where k_u is the upper limit of the reference speed and $k_s > 0$ a parameter for tuning that adjusts the reference speed value according to the distance error. The reference speed never reaches zero because the guidance block will switch for the next waypoint as soon as $d_k \leq \rho_k$.

3) Diving by Line Of Sight:

Underwater vehicles often control the movement in depth by adjusting pitch. In this case, the vertical common mode can be added to improve depth precision [6]. The reference pitch angle θ_r is given by:

$$\theta_r = \arctan\left(\frac{z_k - z}{x_k - x}\right) \quad \in [-\pi/2, \pi/2] \tag{5}$$

Since the hydrodynamic data is only valid for θ values between $20°$ to $-20°$ [3], the value of θ_r follows the same constrains. Special attention to the case where $x_k - x = 0$, which corresponds to the case that the vehicle is already on the planar position $(x = x_k)$. In this case, the vertical common will bring the AUV to the desired depth. The waypoint acceptance check is now done for both horizontal and vertical coordinates. Therefore, the condition for acceptance becomes:

$$| z - z_r | < \rho_x \quad \wedge \quad d_k = \sqrt{(x_k - x)^2 + (y_k - y)^2} \leq \rho_k \tag{6}$$

where ρ_x is the depth tolerance, which will be defined as equal to 1 meter.

4) Station-Keeping Mode:

For the final waypoint, the vehicle enters station-keeping mode. This is accomplished by defining the final planar distance as:

$$d_k = \sqrt{(x_k - x)^2 + (y_k - y)^2} - \rho_k \tag{7}$$

If $d_{kf} = 0$ means that the vehicle is inside the neighbourhood of the last waypoint and only heading control will work. On the other hand, if the vehicle is outside of this neighbourhood the heading and speed control will bring the AUV back.

Control Design

Linearization of the AUV Model

The linear equations can be formulated by linearizing about an equilibrium/operational point (v_0, η_0), as in [8]. Defining the state-space as $x = (x_1, x_2)^T$ where $x_1 = \Delta v = v - v_0$ and $x_2 = \Delta\eta = \eta - \eta_0$, the linear equations of motion are given by [8]:

$$\begin{bmatrix} \dot{x}_1 \\ \dot{x}_2 \end{bmatrix} = \begin{bmatrix} -M^{-1}[C + D] & -M^{-1}G \\ J & J^* \end{bmatrix} \begin{bmatrix} x_1 \\ x_2 \end{bmatrix} + \begin{bmatrix} -M^{-1} \\ 0 \end{bmatrix} \mathbf{u} \tag{8}$$

In many AUV applications, it is reasonable to assume that the AUV is moving with nonzero surge speed, u_0 [8]. It is assumed that the rest of steady state linear and angular velocities are zero, $w_0 = v_0 = p_0 = q_0 = r_0 = 0$. For this study, the operating point to be considered is $v_0 = (0.8,0,0,0,0,0)^T$.

PID - Proportional Integral Derivative

The Proportional Integral Derivative control will be applied to maximize the manoeuvrability of the AUV. For this AUV it is possible to actively control: surge u, heading ψ, pitch θ and heave w. For each, one controller is designed. The roll dynamic, ϕ, is passively controlled. The Matlab PID tuning tool, from the Control Systems Toolbox, was used for initial gain estimations. Then, by applying the controller to the nonlinear dynamic model, the gains were manually tuned to fit the desired performance. The process can be seen in Figure 3.

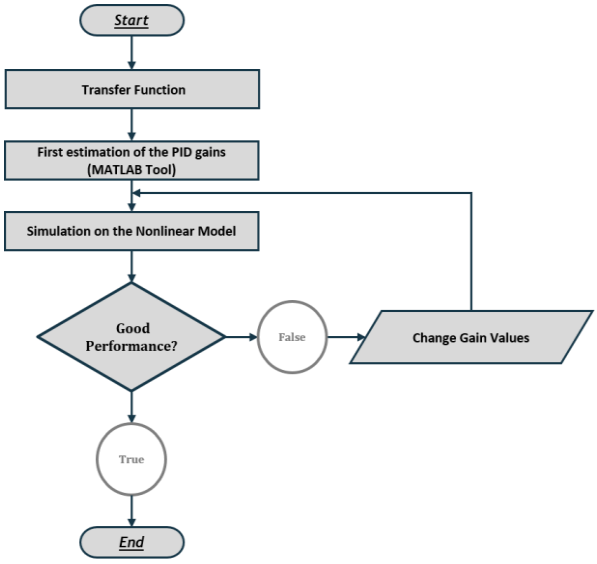

Figure 3 – PID design process.

1) Speed Controller:
The common mode (τ_1), i.e. equally dividing the required force by both thrusters, allows the vehicle to control motion in surge. Neglecting interaction with the remaining Degrees Of Freedom (DOFs) [1], the transfer function is given by:

$$\frac{u(s)}{\tau_1(s)} = \frac{0.0022}{s + 0.0544} \tag{9}$$

A PI control was applied to the transfer function and tuned. Therefore:

$$\tau_1 = K_{p\tilde{u}} + K_i \int_0^t \tilde{u}(\tau) d\,\tau \tag{10}$$

where $\tilde{u} = u_d - u$. To avoid integral windup, the back-calculation method is used. After tuning, since the resulting closed-loop poles are located in the Left Half Plane (LHP), the system is considered stable. The infinity gain margin and the $84.7°$ of phase margin, allied to the fact that the max sensitivity value is below 2 [9], makes the controller robust to disturbances (Figure 4). The respective tracking of a desired velocity can be seen in Figure 5.

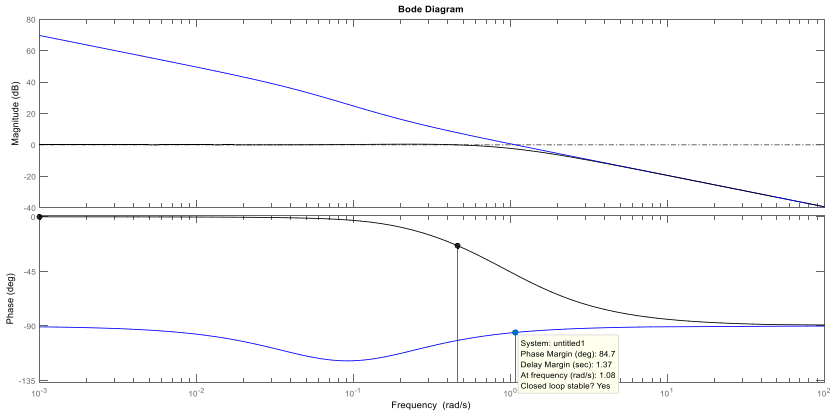

Figure 4 - Open- (blue) and closed-loop (black) bode plot for the speed controller.

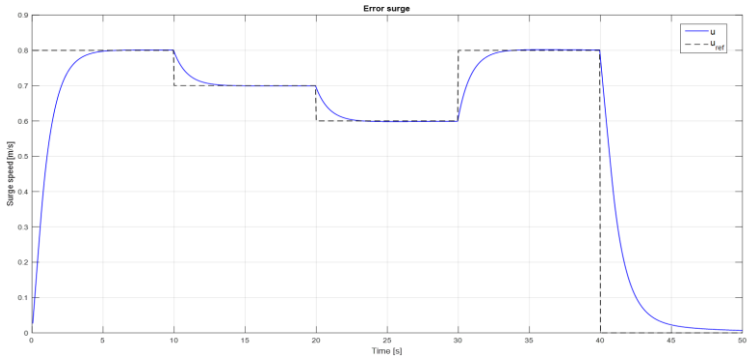

Figure 5 – Speed controller tracking a reference over time.

1) Heading Controller:

Heading control is accomplished through the differential mode (τ_6), i.e. dividing the required moment by both thrusters. For this subsystem, the state variables to account for are: $v(t), r(t)$ and $\psi(t)$. For the above mentioned operating point, the result is:

$$\begin{bmatrix} \dot{v} \\ \dot{r} \\ \dot{\psi} \end{bmatrix} = \begin{bmatrix} -0.3108 & -0.4037 & 0 \\ 0.4979 & -0.0441 & 0 \\ 0 & 1.0000 & 0 \end{bmatrix} \begin{bmatrix} v \\ r \\ \psi \end{bmatrix} + \begin{bmatrix} -0.0003 \\ 0.0037 \\ 0 \end{bmatrix} \tau_6 \tag{11}$$

The transfer function for this subsystem is:

$$\frac{\psi(s)}{\tau_6(s)} = \frac{0.003729s + 0.0009888}{s^3 + 0.3549s^2 + 0.2147s} \tag{12}$$

Heading measurements (ψ) may be given by compass readings and the yaw rate (r) by a gyroscope. A PD controller provides good performance. The derivative term provides additional phase margin, which increases robustness [1]. The control law yields:

$$\tau_6 = K_p\tilde{\psi} - K_d r \tag{13}$$

where $\tilde{\psi} = \psi_r - \psi$. Special attention to the yaw error. It must be redefined, as in [4]:

$$\begin{aligned} \text{if} \quad & \tilde{\psi} > \pi \quad (\text{right side}) \\ & \tilde{\psi} = \tilde{\psi} - 2\pi \\ \text{if} \quad & \tilde{\psi} < -\pi \quad (\text{left side}) \\ & \tilde{\psi} = \tilde{\psi} + 2\pi \end{aligned} \tag{14}$$

The closed-loop poles, for the closed-loop transfer function, are located in the LHP, meaning once more that that the controller is stable. The infinity gain margin and the $84.9°$ of phase margin of the open loop system translates into robustness to disturbances.

2) Depth Controller:

Depth control presents a common mode (τ_3) and a differential mode (τ_5). The associated state variables are: $w(t), q(t), \theta(t)$ and $z(t)$. Once more, for this operating point, the state-space form yields:

$$\begin{bmatrix} \dot{w} \\ \dot{q} \\ \dot{\theta} \\ \dot{z} \end{bmatrix} = \begin{bmatrix} -0.2604 & 0.4482 & 0.0974 & 0 \\ -0.7934 & -0.3070 & -1.0902 & 0 \\ 0 & 1.0000 & 0 & 0 \\ 1.0000 & 0 & 0 & 0 \end{bmatrix} \begin{bmatrix} w \\ q \\ \theta \\ z \end{bmatrix} + \begin{bmatrix} 0.0012 & -0.0003 \\ -0.0003 & 0.0034 \\ 0 & 0 \\ 0 & 0 \end{bmatrix} \begin{bmatrix} \tau_3 \\ \tau_5 \end{bmatrix} \tag{15}$$

The diving manoeuvre will be accomplished by adjusting pitch. Through the differential mode (τ_5) the controller will approach the θ_r angle. To maneuver/adjust the vehicle to the desired depth, as to cancel the residual buoyancy, the common mode (τ_3) is used. The transfer function of depth is:

$$\frac{z(s)}{\tau_3(s)} = \frac{0.00119s^2 + 0.0002308s + 0.001268}{s^4 + 0.5675s^3 + 1.526s^2 + 0.3612s} \tag{16}$$

The controller is designed without integral action according to:

$$\tau_3 = K_{p\tilde{z}} + K_d \frac{d\tilde{z}}{dt} \tag{17}$$

where $\tilde{z} = z_r - z$. Once more the infinity gain margin and the $82.2°$ of phase margin of the open loop system shows that the system is robust to disturbances.

The transfer function for pitch is:

$$\frac{\theta(s)}{\tau_5(s)} = \frac{0.003362s + 0.001114}{s^3 + 0.5675s^2 + 1.526s + 0.3612} \tag{18}$$

Implementing a PID controller:

$$\tau_5 = K_{p\tilde{\theta}} + K_i \int_0^t \tilde{\theta}(\tau)d\tau + K_d \frac{d\tilde{\theta}}{dt} \tag{19}$$

where $\tilde{\theta} = \theta_r - \theta$. An infinity gain margin and the $96.7°$ of phase margin shows robustness of the system.

LQR - Linear Quadratic Regulator

To derive the Linear Quadratic Regulator control law, *controllability* and *observability* need to be ensured [10]. Considering a linear model, $\dot{x} = Ax + B\mathbf{u}$, and that all states are available for the controller, the optimal control problem determines the feedback gain for the optimal control vector [11]:

$$\mathbf{u}(t) = -K(x - x_{desired}) \tag{20}$$

The process used to design the controllers is represented in Figure 6. The complete linear system is divided into two subsystems: lateral subsystem and longitudinal subsystem.

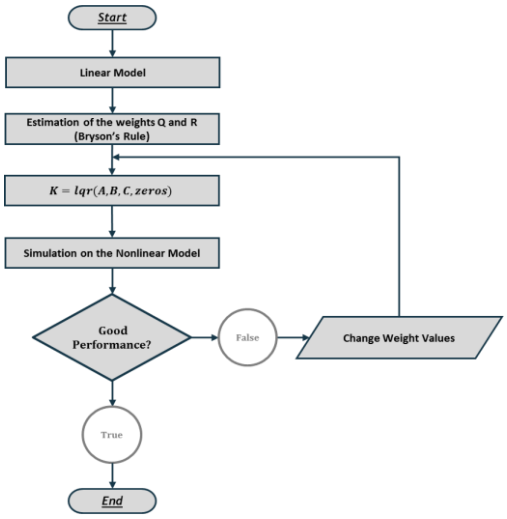

Figure 6 – LQR design process

1) Longitudinal Controller:
The longitudinal controller is dedicated to control the surge speed (τ_1) and depth (τ_3 for the common mode and τ_5 for the differential mode). The sate vector is constituted by the states: u, w, θ and z. For the longitudinal state vector x_L, the state and input matrices from the linearized model for the longitudinal controller are:

$$\begin{bmatrix} \Delta\dot{u} \\ \Delta\dot{w} \\ \Delta\dot{q} \\ \Delta\dot{\theta} \\ \Delta\dot{z} \end{bmatrix} = A_L x_l + B_L \mathbf{u}_L$$
$$= A_L \begin{bmatrix} u - u_0 - (u_d - u_0) \\ w - w_0 \\ q - q_0 \\ \theta - \theta_0 - (\theta_r - \theta_0) \\ z - z_0 - (z_d - z_0) \end{bmatrix} + B_L \mathbf{u}_L \tag{21}$$

To reduce the steady state values of u and θ, two integrative states were added to the state-space:

$$x_{\int u} = \int_0^t (u - u_d)d\tau\,; \tag{22}$$

$$x_{\int \theta} = \int_0^t (\theta - \theta_r)d\tau\,; \tag{23}$$

Therefore, the new state-space equation is:

$$\begin{bmatrix} \dot{x}_L \\ \dot{x}_{\int u} \\ \dot{x}_{\int \theta} \end{bmatrix} = \begin{bmatrix} & A_L & & & & 0_{5\times2} \\ \begin{bmatrix} 1 & 0 & 0 & 0 & 0 \\ 0 & 0 & 0 & 1 & 0 \end{bmatrix} & & & & & 0_{2\times2} \end{bmatrix} \begin{bmatrix} x_l \\ x_{\int u} \\ x_{\int \theta} \end{bmatrix} + \begin{bmatrix} B_L \\ 0_{1\times3} \\ 0_{1\times3} \end{bmatrix} \mathbf{u}_L \tag{24}$$

Because there is an output limitation, the actuators will most likely saturate, inducing once again integral windup. The anti-windup method described in [12] is applied.

2) Lateral Controller:

The main purpose of the lateral system is to control the yaw angle ψ. As in the PID heading control, the state vector is constituted by the states: v, r and ψ. Assuming the state-space vector of the lateral subsystem as x_H, the state and input matrices from the linearized model will be:

$$\begin{bmatrix} \Delta\dot{v} \\ \Delta\dot{r} \\ \Delta\dot{\psi} \end{bmatrix} = A_H x_H + B_H \mathbf{u}_H \; x_H = A_H \begin{bmatrix} v - v_0 \\ r - r_0 \\ \psi - \psi_0 - (\psi_d - \psi_0) \end{bmatrix} + B_H \mathbf{u}_H \tag{25}$$

The control input is defined as:

$$\mathbf{u}_H = -K_H x_H \tag{26}$$

The operating point is the same as in PID. By defining the performance index in terms of the output vector, the Q matrix will only contain the element that dictates the evolution of the output [5]. The resulting eigenvalues of the closed-loop systems $\left(eig(A_H - B_H K_H)\right)$ are negative which according, to Lyapunov [13], proves that the system is stable. With respect to stability margins, the LQR is known to have excellent stability characteristics with gains up to infinity and phase margin over $60°$ [14].

Control Allocation

Both of PID and LQR use a differential mode, τ_6, and a common mode, τ_3, through separate laws. This means that the two laws will compete for control authority. Without accounting for thrust constrains, this solution will lead to actuator saturation, resulting in poor performance and instability [15]. The control allocation law from [15] is adapted to solve this problem. Considering now the new common mode law, τ_1':

$$\tau_1' = \tau_1 e^{-\beta|\tau_6|} \tag{27}$$

where τ_1 is the control signal determined by the speed controller, β is user-set and dependent on the desired fraction of commanded surge, and τ_6 the control signal determined by the heading controller.

Simulation Results

Waypoint and Station-keeping

For simulation purposes, the selected waypoint coordinates are defined in table 1. The thrust output was limited at 120 N, in forward thrust, and 85 N in reverse thrust. Thruster dynamics were not considered. However, this should have an overall minor effect on the simulation results.

Table 1 – Waypoint coordinates.

	Waypoint 1	Waypoint 2	Waypoint 3	Waypoint 4
x [m]	10	40	50	80
y[m]	20	20	50	60
z[m]	10	20	10	0

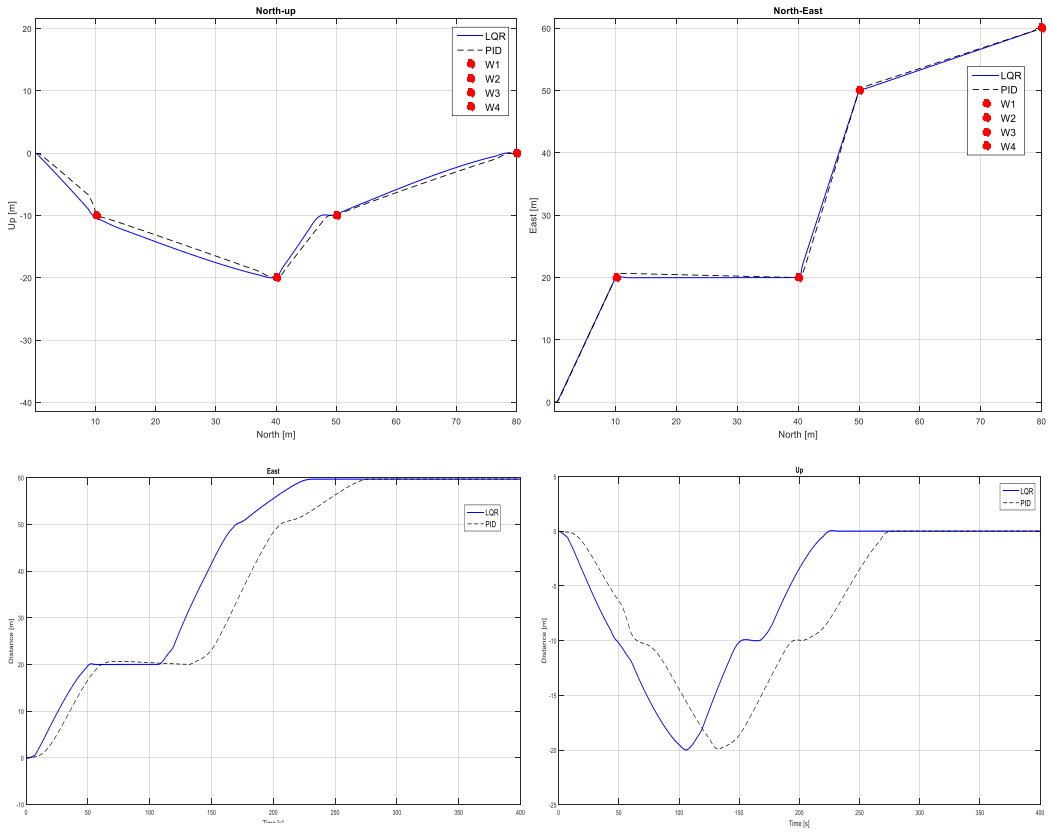

Figure 7 - LQR (full line) and PID (dashed line) results for the simulation. The top figures regard the spatial evolution of the vehicle in the vertical (left) and horizontal (right) planes. The bottom figures regard the evolution of the vehicle in the East (left) and Down (right) coordinates over time.

Conclusions

This paper briefly describes a guidance waypoint and station-keeping algorithm and two control solutions for three AUV autopilots: heading, speed and depth.

Both LQR and PID controllers proved robust for this operating point. For robustness and stability analysis bode was used. The phase margin above $60°$ and the gain margin up to infinity, allied to the maximum sensitivity values bellow 2, for all autopilots proved robustness of PID and LQR controllers.

Both controllers behaved satisfactorily. However, from the results in Figure 7, it is possible to conclude that the responsiveness of the LQR is greater than the PID's.

The control allocation law proved to reduce the overshoot on the waypoint, by prioritizing heading over velocity. For that reason, manoeuvrability was increased and COA had to be reduced to a minimum value. Otherwise the vehicle would switch to the next waypoint without reaching the current one.

It is intended, as a continuation of this work, to verify and validate the controllers through further analysis and tests. Further PID tuning could lead to a better performance. Also, the impact of ocean currents should be studied.

Acknowledgments

This research work was conducted at CEiiA and in the Laboratory of Avionics and Control (Department of Aerospace Sciences) of the University of Beira Interior. The underlying research activities were supported by CEiiA and by the Aeronautics and Astronautics Research Group (AeroG) of the Associated Laboratory for Energy, Transports and Aeronautics (LAETA).

References

[1] B. Jalving, "The ndre-auv flight control system," *IEEE Journal of Oceanic Engineering*, 2002.
[2] "Medusa deep sea." [Online]. Available: http://www.medusadeepsea.com/
[3] C. A. Bentes, "Modeling of an autonomous underwater vehicle," Master's thesis, University Of Beira Interior, 2016.
[4] J. Ribeiro, "Motion control of single and multiple autonomous marine vehicles," Master's thesis, Instituto Superior TÃ©cnico, 2011.
[5] T. I. Fossen, *Handbook of Marine Craft Hydrodynamics and Motion Control*. John Wiley & Sons, 2011.
[6] V. Bakaric, Z. Vukic, and R. Antonic, "Improved line-of-sight guidance for cruising underwater vehicles," *IFAC Proceeding Volumes*, vol. 37, pp. 447–452, 2004.
[7] A. J. Healey and D. Lienard, "Multivariable sliding mode control for autonomous diving and steering of unmanned underwater vehicles," *IEEE journal of Oceanic Engineering*, vol. 18, no. 3, pp. 327–339, 1993.
[8] L. Moreira and C. G. Soares, "H_2 and H_∞ designs for diving and course control of an autonomous underwater vehicle in presence of waves," *IEEE Journal of Oceanic Engineering*, 2008.
[9] K. J. Åström and T. Hägglund, *PID controllers: theory, design, and tuning*, vol. 2. Isa Research Triangle Park, NC, 1995.
[10] K. Ogata, *Modern Control Engineering*. Instrumentation and controls series, Prentice Hall, 2010.
[11] M. S. Triantafyllou and F. S. Hover, *Maneuvering and Control of Marine Vehicles*. Massachusetts Institute of Technology, 2003.
[12] C. M. R. Oliveira, M. L. Aguiar, W. C. A. Pereira, A. G. Castro, T. E. P. Almeida, and J. R. B. A. Monteiro, "Integral sliding mode controller with anti-windup method analysis in the vector control of induction motor," in *2016 12th IEEE International Conference on Industry Applications (INDUSCON)*, 2016.
[13] J. Slotine and W. Li, *Applied Nonlinear Control*. Prentice-Hall International Editions, Prentice-Hall, 1991.
[14] W. Naeem, *Guidance and Control of an Autonomous Underwater Vehicle*. phd, Univeristy of Plymouth, 2004.
[15] I. R. Bertaska and K. D. von Ellenrieder, "Supervisory switching control of an unmanned surface vehicle," in *OCEANS 2015 - MTS/IEEE Washington*, pp. 1–10, 2015.